Supporting Information For

A pyrazine core based luminescent Zr(IV) organic framework for specific sensing of Fe^{3+}, picric acid and $Cr_2O_7^{2-}$

Chiranjib Gogoi,[†] Helge Reinsch,[‡] and Shyam Biswas,[†]*

[†] *Department of Chemistry, Indian Institute of Technology Guwahati, Guwahati, 781039 Assam, India.*

[‡]*Institut für Anorganische Chemie, Christian-Albrechts-Universität, Max-Eyth-Strasse 2, 24118 Kiel, Germany*

* To whom correspondence should be addressed. E-mail: sbiswas@iitg.ernet.in; Tel: 91-3612583309.

Materials and Physical Methods. The 2,3,5,6-tetrakis(4-carboxyphenyl)pyrazine) (H_4**L**) ligand was synthesized by using previously reported procedure.[1] All other chemicals were purchased from chemical suppliers and used without any further purification. The Bruker D2 Phaser X-ray diffractometer was employed for X-ray powder diffraction (XRPD) measurements at 30 kV, 10 mA using Cu-Kα (λ = 1.5406 Å) radiation. The Fourier transform infrared (FT-IR) spectra were taken on a Perkin Elmer Spectrum Two FT-IR spectrometer with samples prepared on KBr pellets in the range of 4000-500 cm^{-1}. The characteristic peaks were mentioned using notation like very strong (vs), strong (s), medium (m), shoulder (sh), broad (br) and weak (w). Thermogravimetric analyses (TGA) of **1** and **1'** were carried out by using a SDT Q600 V20.9 Build 20 thermogravimetric analyzer from the temperature range 25 to 700 °C at a heating rate of 10 °C min^{-1} under argon atmosphere. The Brunauer−Emmett−Teller (BET) measurement of **1'** were recorded on a Quantachrome Autosorb iQ-MP volumetric gas adsorption equipment at -196 °C. The CO_2 gas adsorption experiment were carried out using Quantachrome iSorb-HP1 gas sorption analyzer at 0 °C and also at 25 °C. Prior to N_2 and CO_2 adsorption experiments, **1'** was degassed under dynamic vacuum condition for 6 h at 120 °C. The Zeiss (Gemini) SEM equipment and the Hitachi S3400N SEM-EDX instrument were used for the field emission-scanning electron microscopy (FE-SEM) images and the energy dispersive X-ray (EDX) experiment respectively. The fluorescence lifetime measurement was performed using Edinburgh Instrument Life-Spec II spectrometer. During lifetime measurement, the samples were excited at 295 nm and maintaining the emission wavelength at 410 nm. Caution! *NAEs like PA, 4-NP are highly explosive so should be handled very carefully and also used in small amounts.*

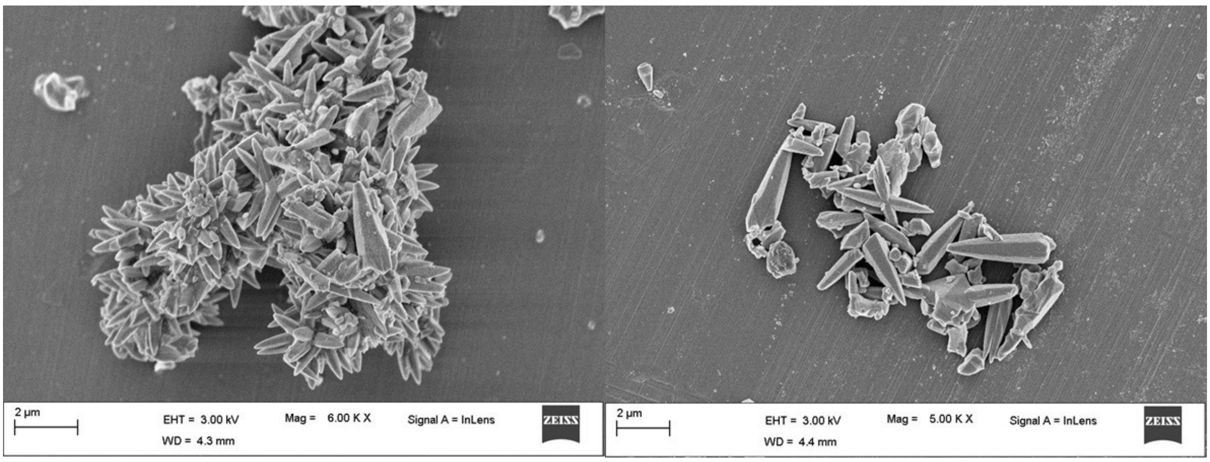

Figure S1. FE-SEM images of **1**.

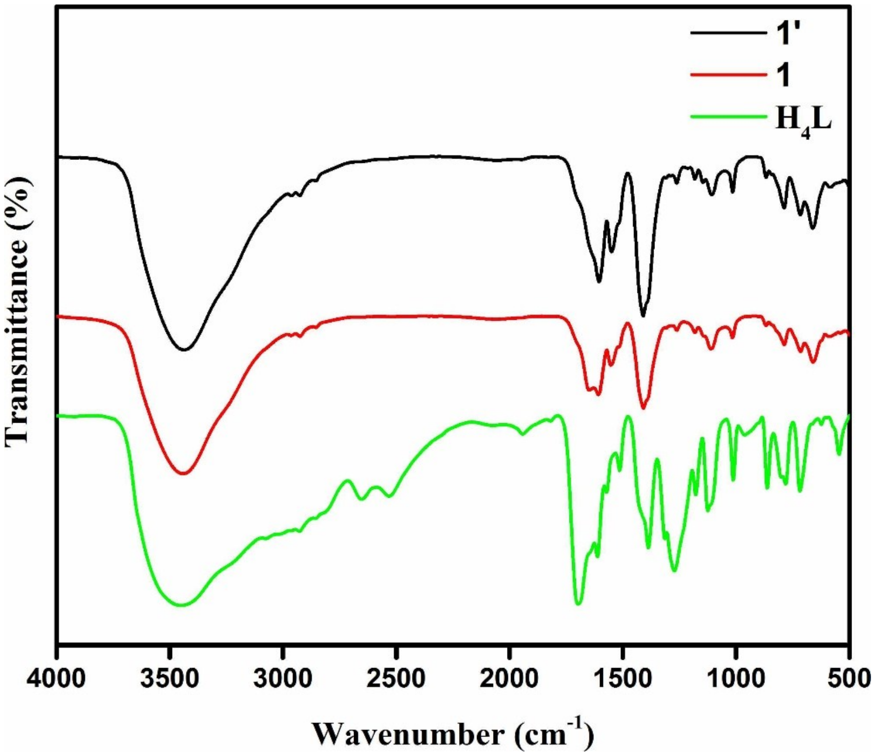

Figure S2. FT-IR spectra of H_4**L** ligand (green), compound **1** (red) and **1'** (black).

Table 1. Structural refinement parameters for compound **1** and **1'** obtained from Pawley fits.

Sample	Compound **1**	Compound **1'**
Crystal system	orthorhombic	orthorhombic
Space group	*Cmmm*	*Cmmm*
a / Å	19.375(12)	19.492(12)
b / Å	33.376(21)	33.489(20)
c / Å	12.712(12)	12.608(7)
$\alpha = \beta = \gamma$ / °	90	90
V/ Å^3	8220(10)	8230(8)
R_{wp} / %	3.5	4.9
GoF	3.0	2.0

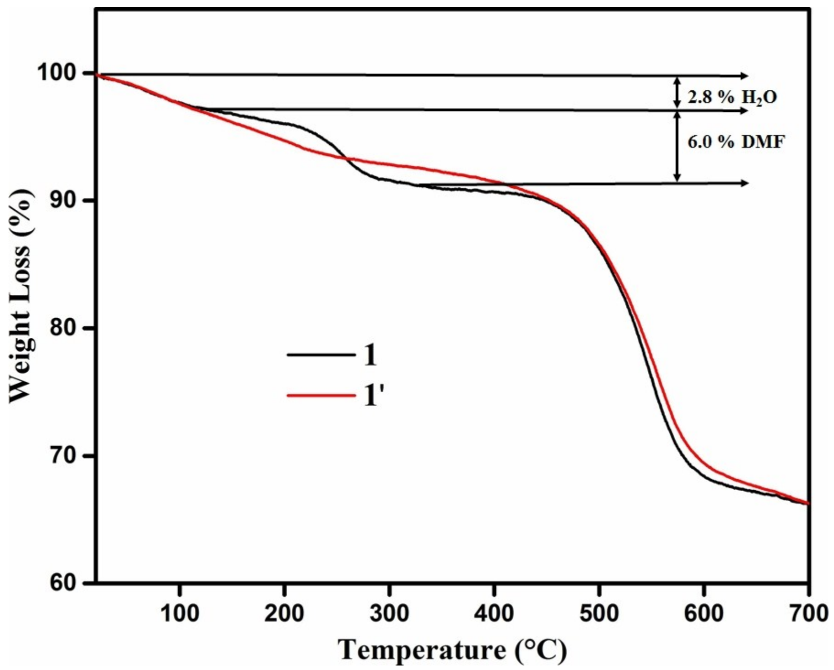

Figure S3. TG curves of **1** and **1'** recorded in an argon atmosphere in the temperature range of 25-700 °C with a heating rate of 10 °C/min.

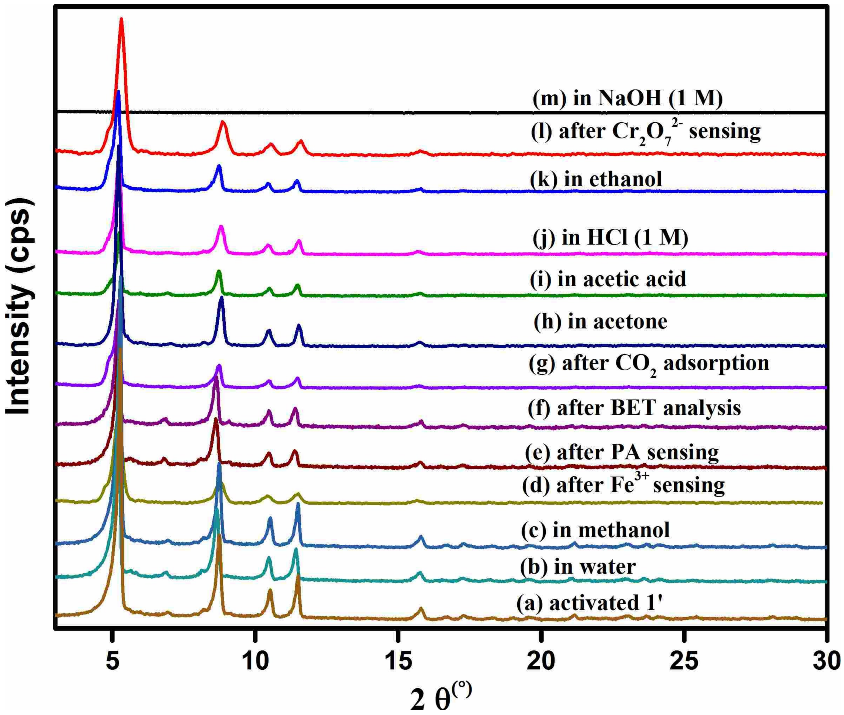

Figure S4. XRPD patterns of **1'** in different forms: (a) activated; (b) after treatment with water; (c) after treatment with methanol; (d) 5 cycles of fluorescence titration experiments with Fe^{3+} ions; (e) after 5 cycles of fluorescence titration experiments with PA; (f) after BET analysis; (g) after CO_2 adsorption; (h) after treatment with acetone; (i) after treatment with acetic acid; (j) after treatment with 1(M) HCl; (k) after treatment with ethanol; (l) after 5 cycles of fluorescence titration experiments with $Cr_2O_7^{2-}$ ions: (m) after treatment with 1(M) NaOH.

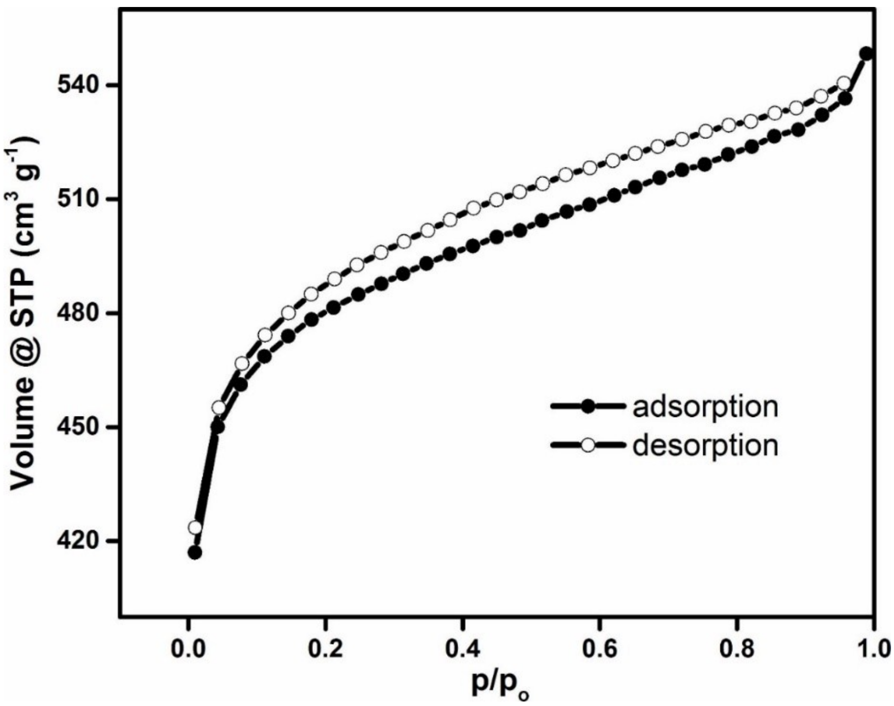

Figure S5. N_2 sorption isotherms of **1'** at -196 °C.

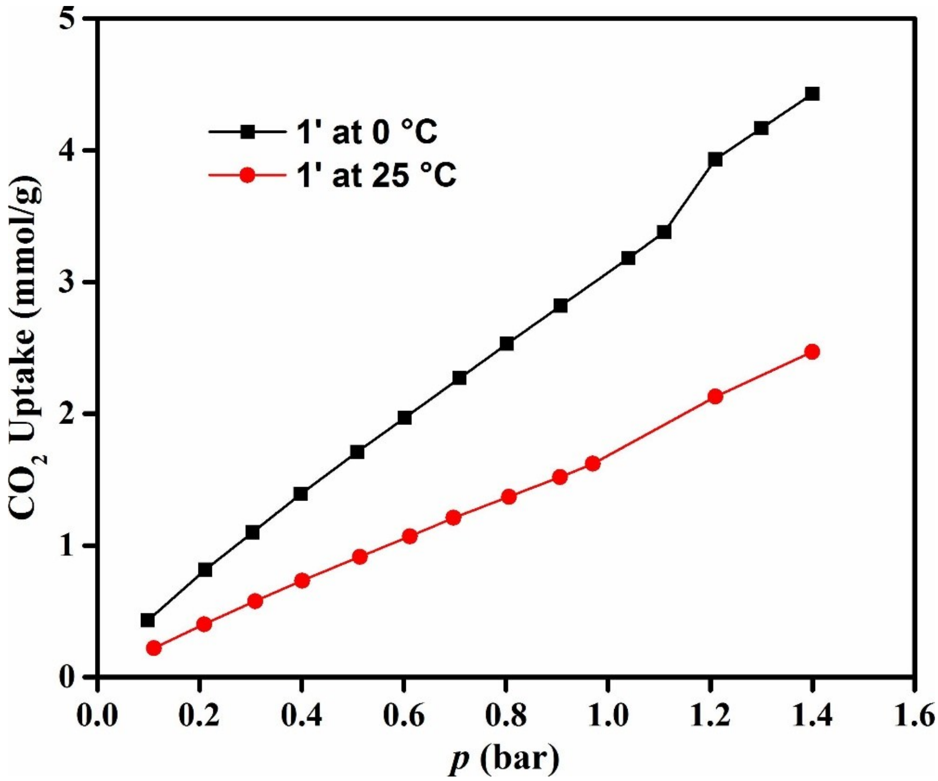

Figure S6. CO_2 sorption isotherms of **1'** at 0 °C and 25 °C.

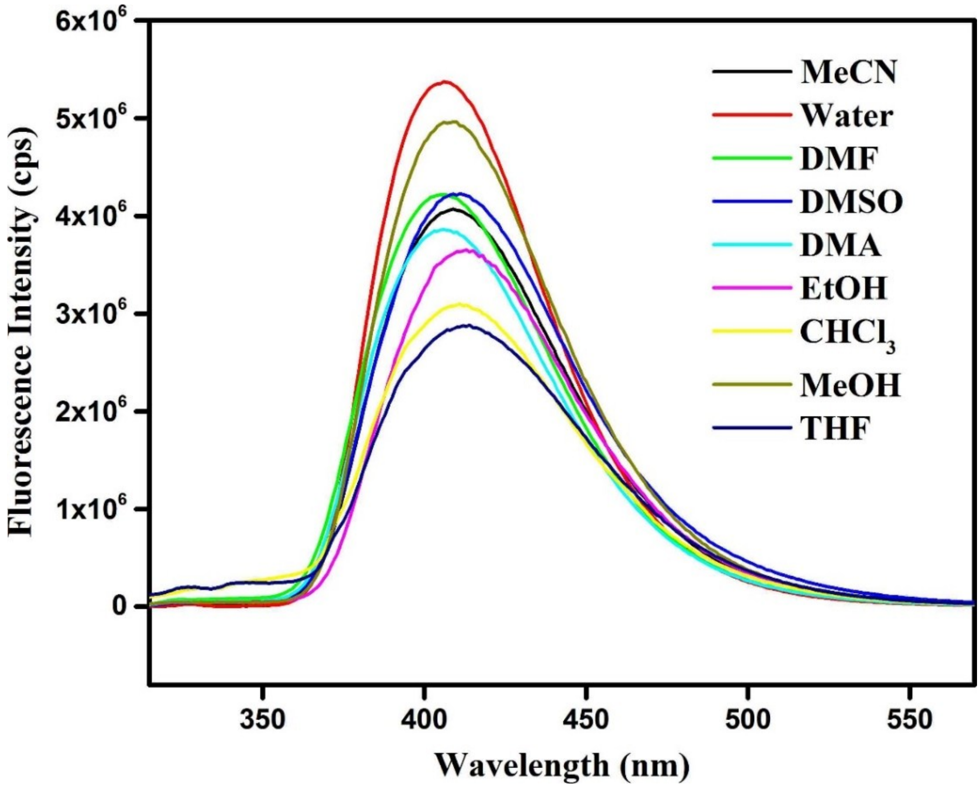

Figure S7. Fluorescence emission spectra of **1'** in water and common organic solvents (λ_{ex} = 295 nm).

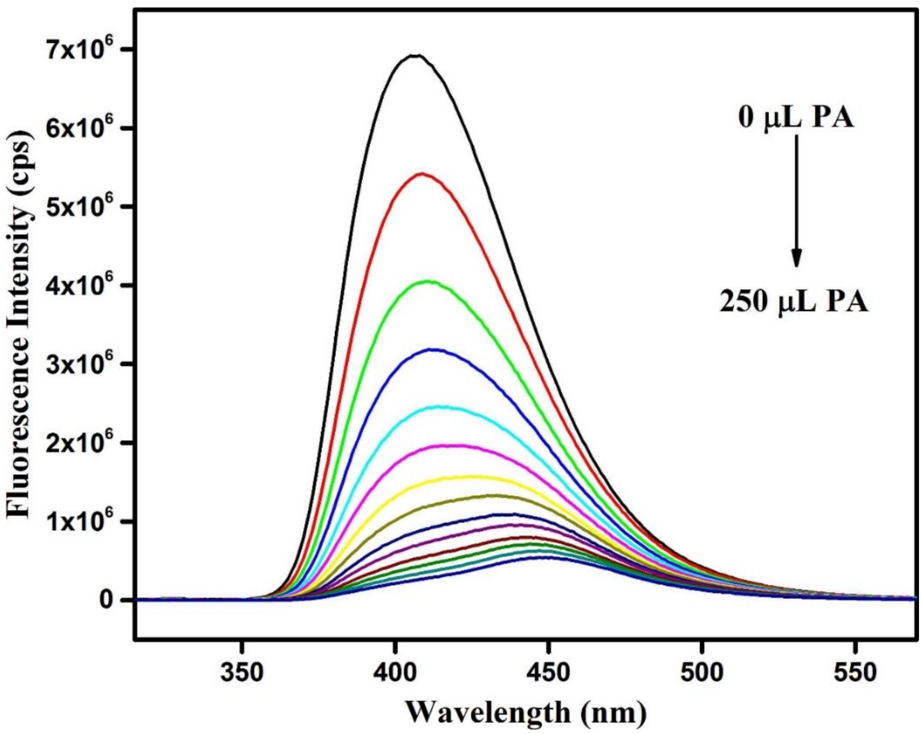

Figure S8. Luminescence quenching of **1'** dispersed in water after gradual addition of 3 mM solution of PA in water (250 μL).

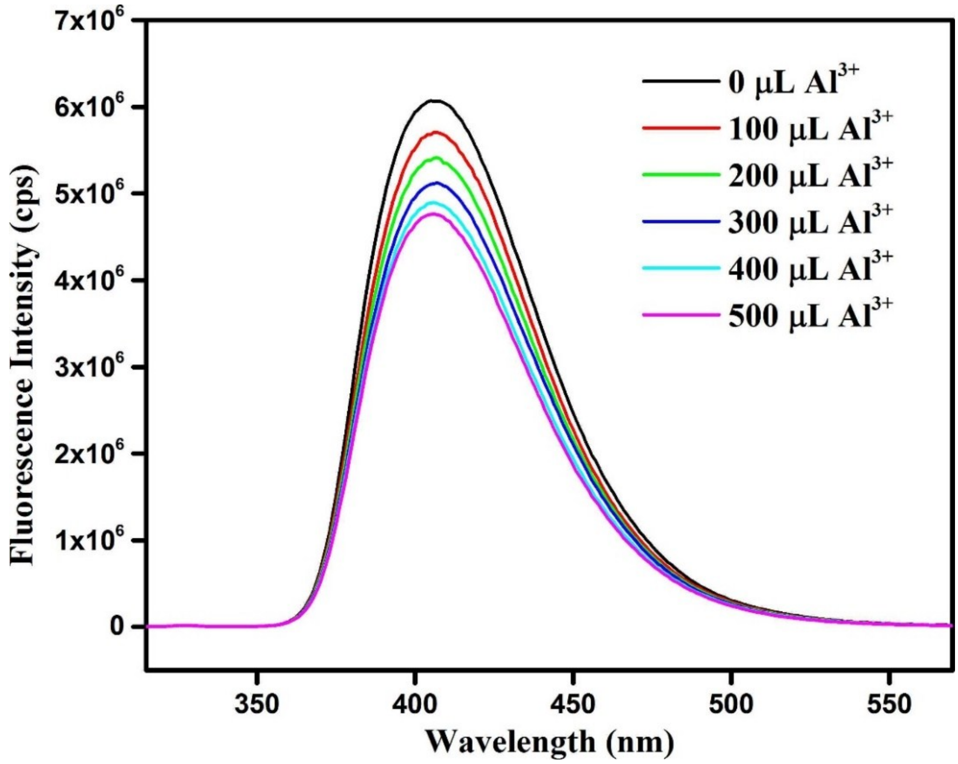

Figure S9. Luminescence quenching of **1'** dispersed in water after gradual addition of 10 mM solution of Al^{3+} in water.

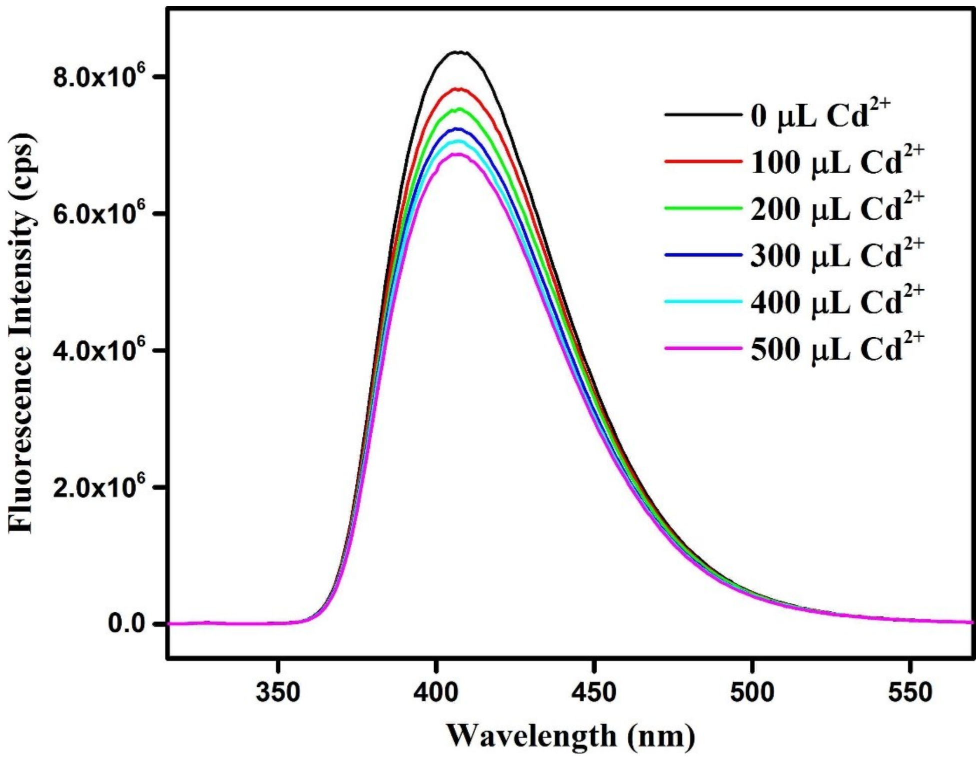

Figure S10. Luminescence quenching of **1'** dispersed in water after gradual addition of 10 mM solution of Cd^{2+} in water.

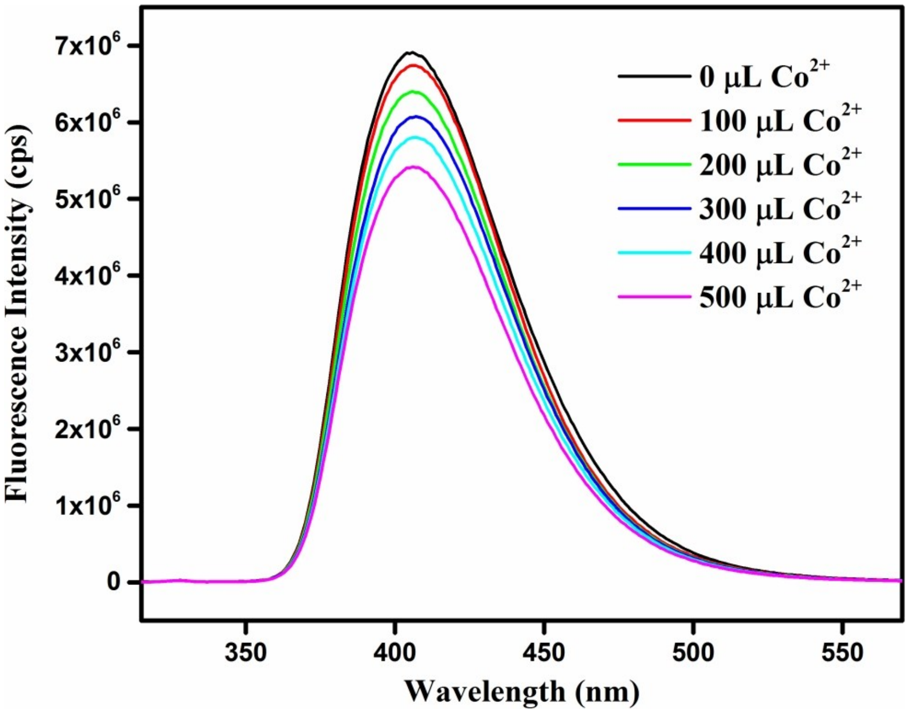

Figure S11. Luminescence quenching of **1'** dispersed in water after gradual addition of 10 mM solution of Co^{2+} in water.

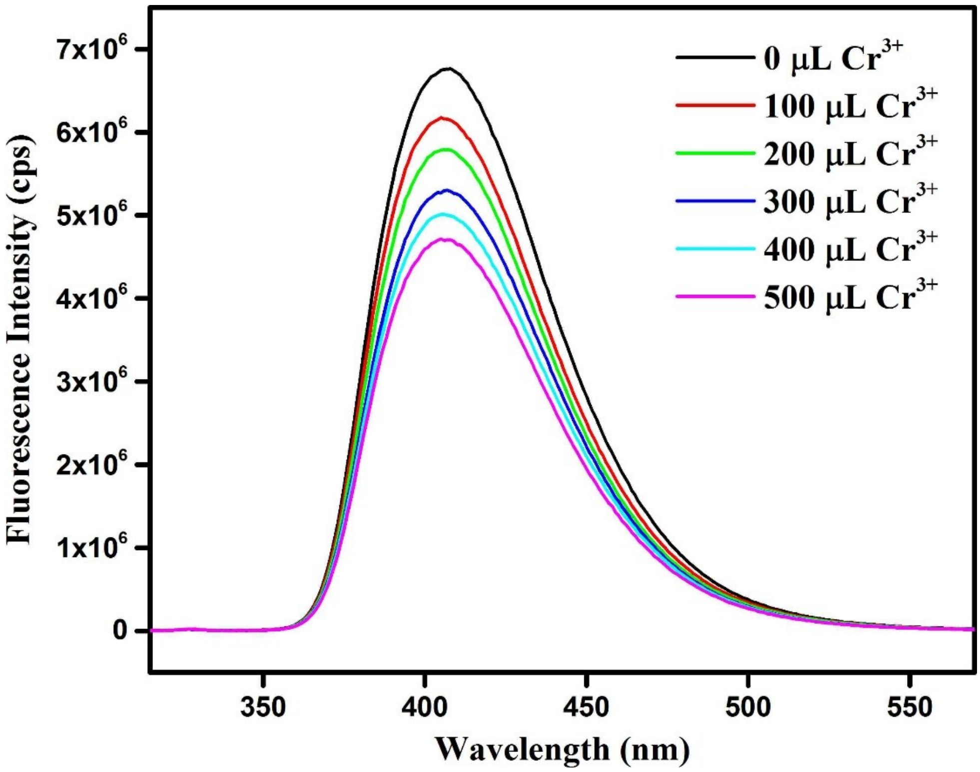

Figure S12. Luminescence quenching of **1'** dispersed in water after gradual addition of 10 mM solution of Cr^{3+} in water.

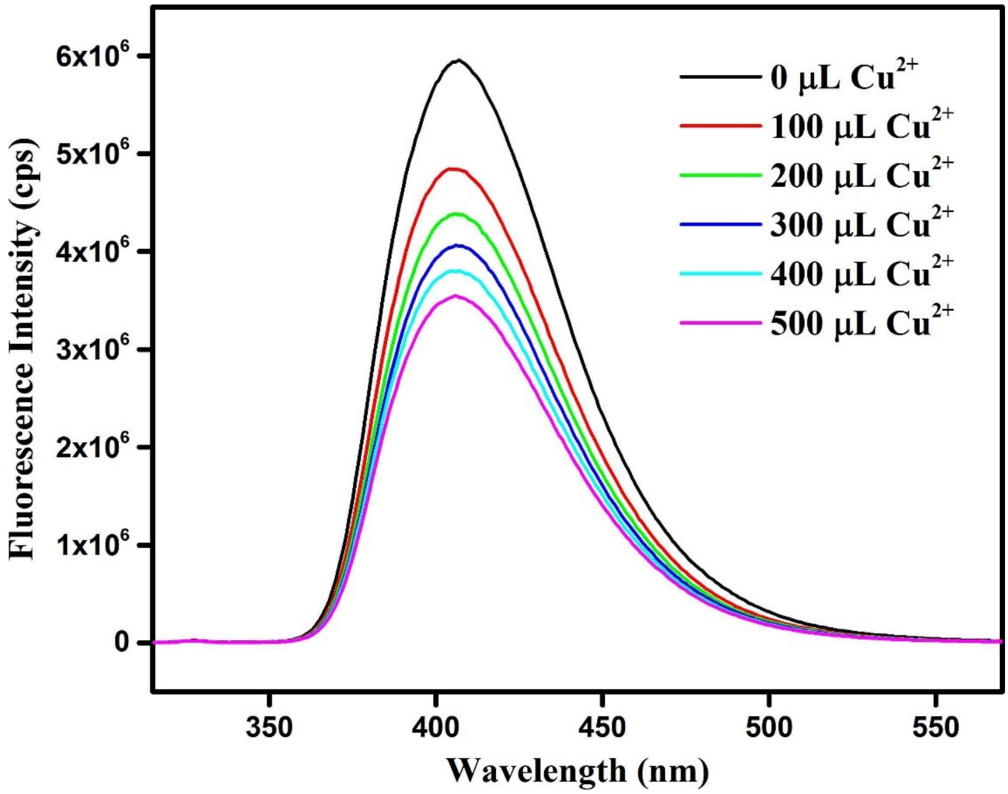

Figure S13. Luminescence quenching of **1'** dispersed in water after gradual addition of 10 mM solution of Cu^{2+} in water.

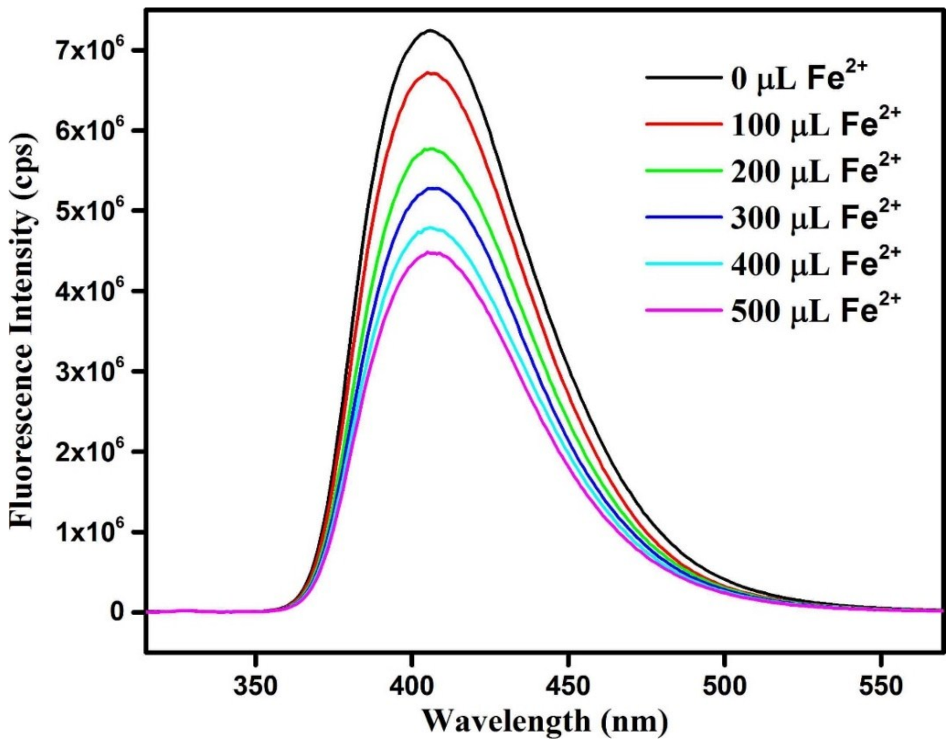

Figure S14. Luminescence quenching of **1'** dispersed in water after gradual addition of 10 mM solution of Fe^{2+} in water.

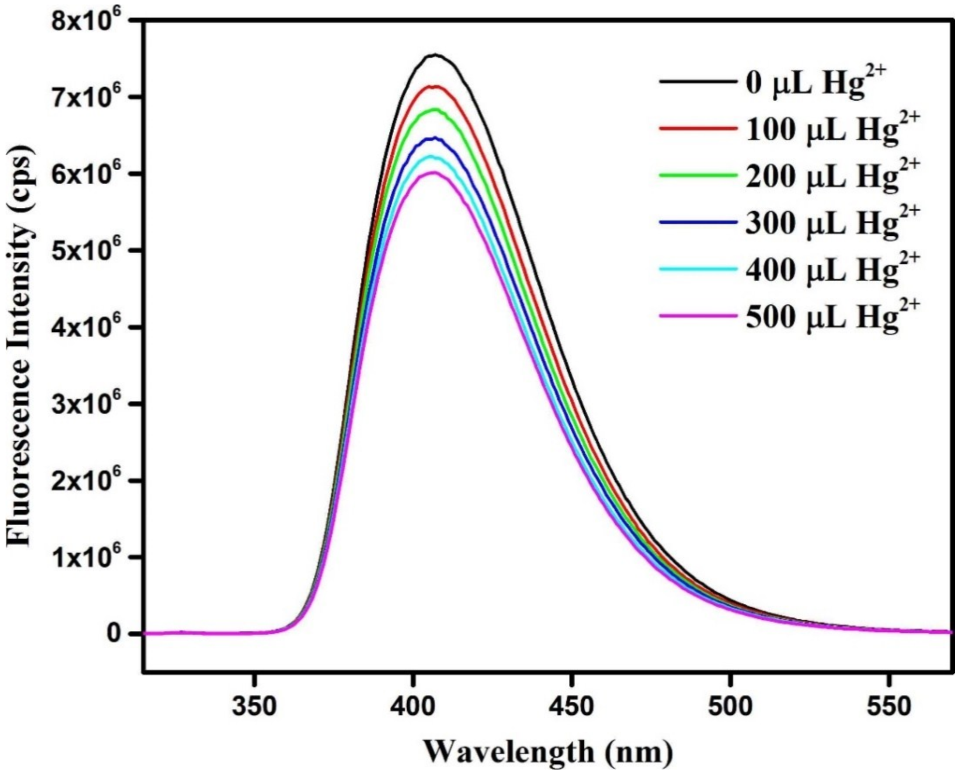

Figure S15. Luminescence quenching of **1'** dispersed in water after gradual addition of 10 mM solution of Hg^{2+} in water.

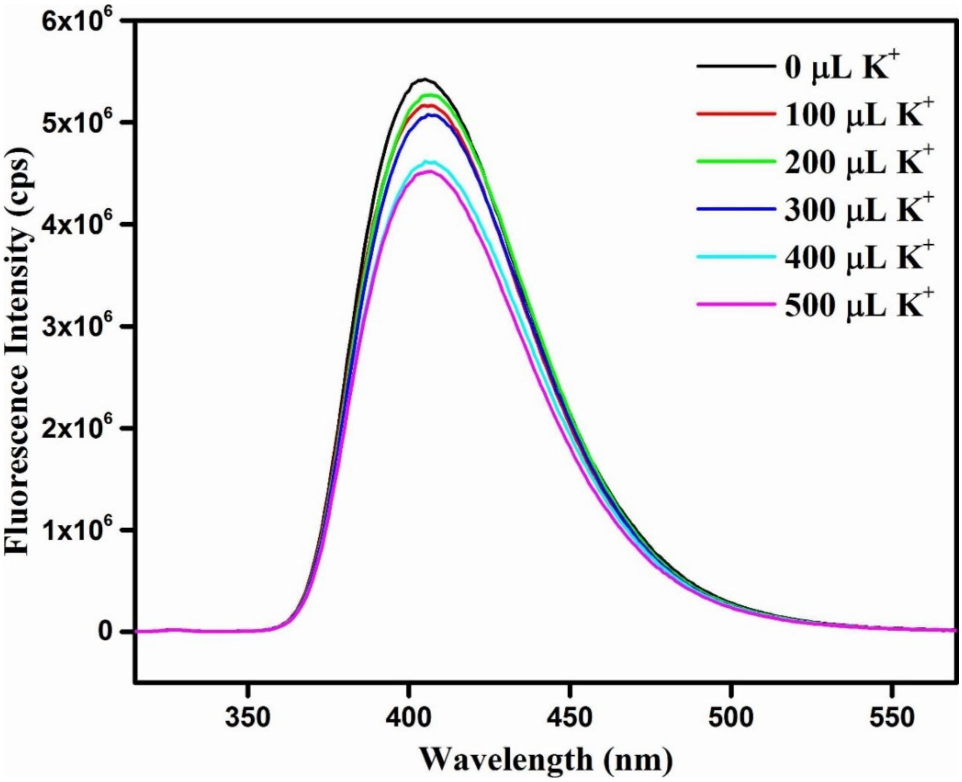

Figure S16. Luminescence quenching of **1'** dispersed in water after gradual addition of 10 mM solution of K^{+} in water.

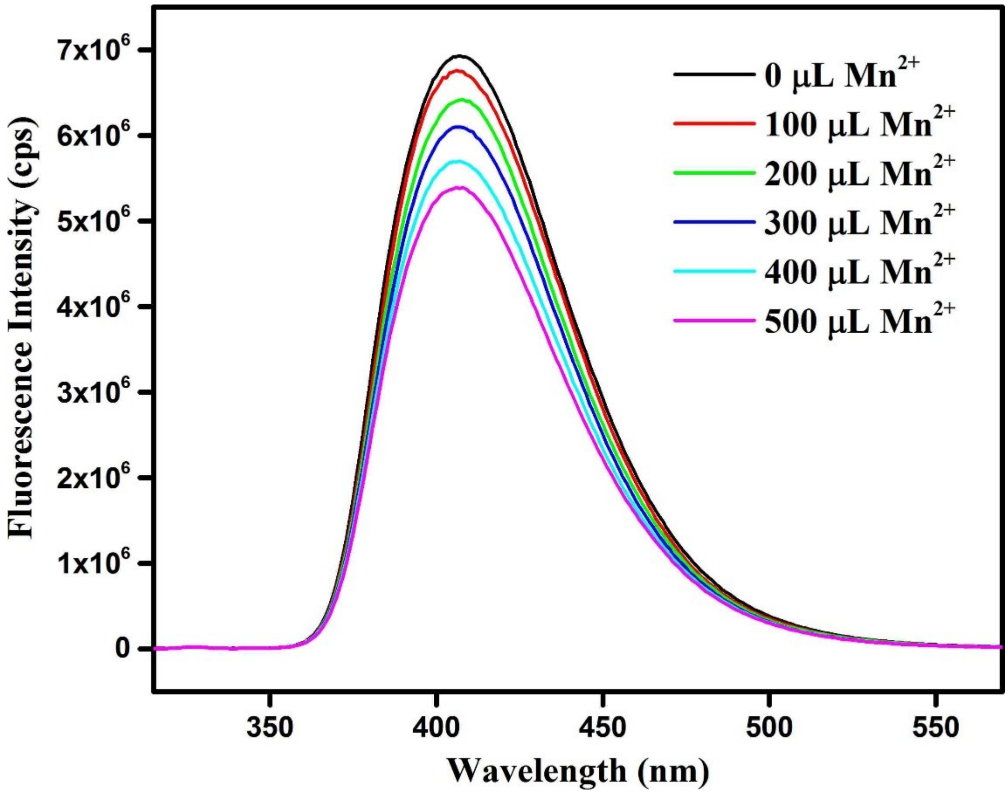

Figure S17. Luminescence quenching of **1'** dispersed in water after gradual addition of 10 mM solution of Mn^{2+} in water.

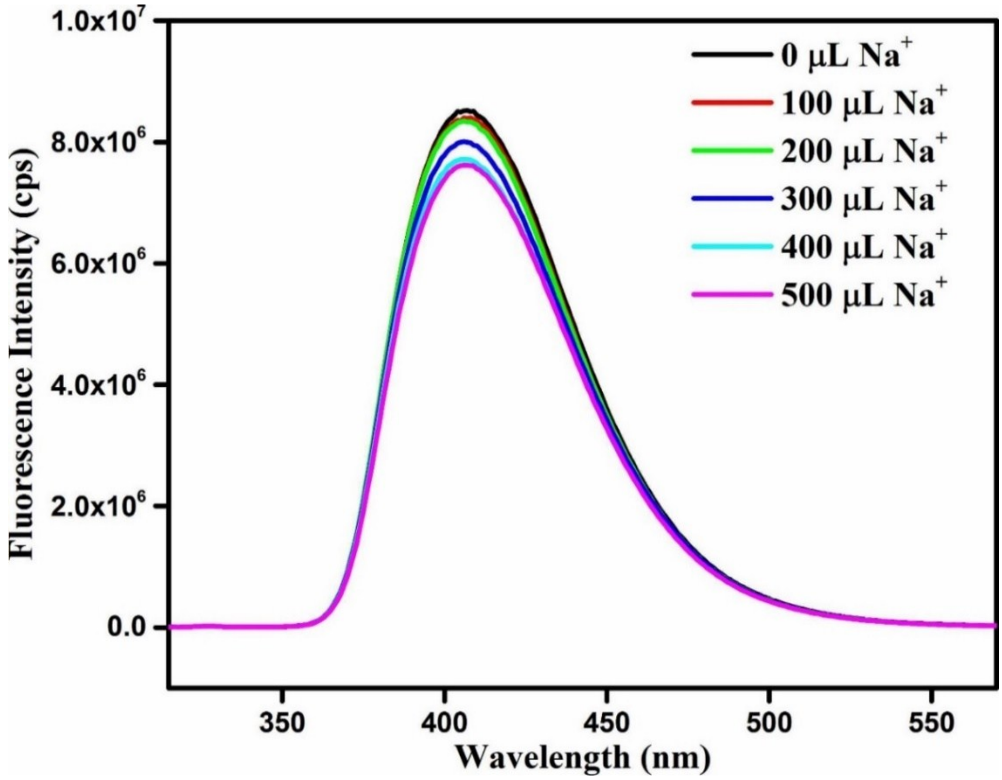

Figure S18. Luminescence quenching of **1'** dispersed in water after gradual addition of 10 mM solution of Na^{+} in water.

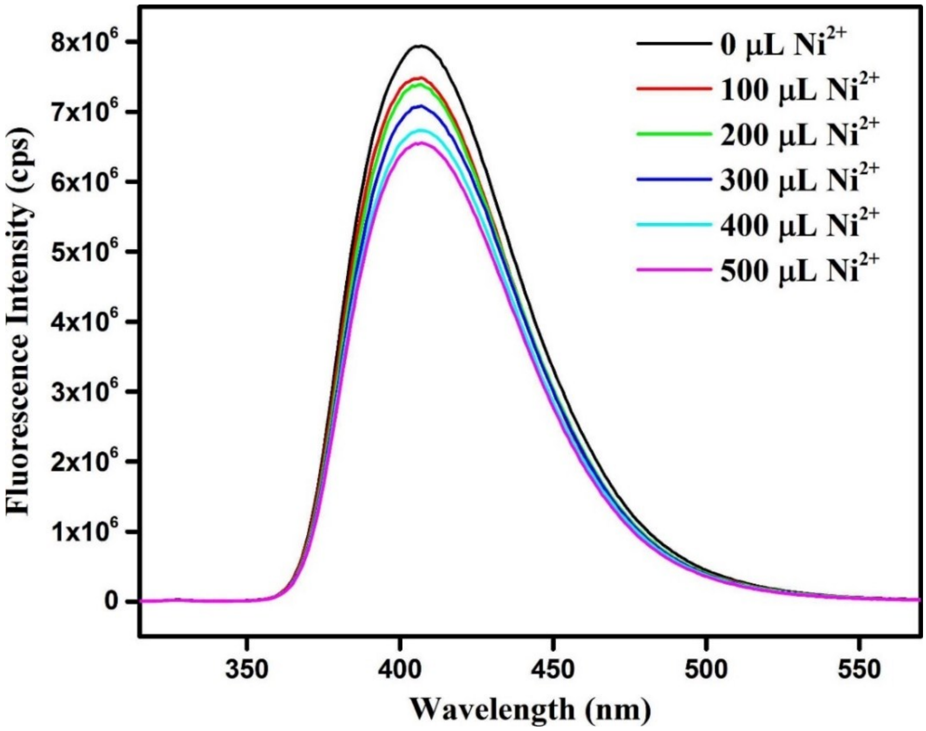

Figure S19. Luminescence quenching of **1'** dispersed in water after gradual addition of 10 mM solution of Ni^{2+} in water.

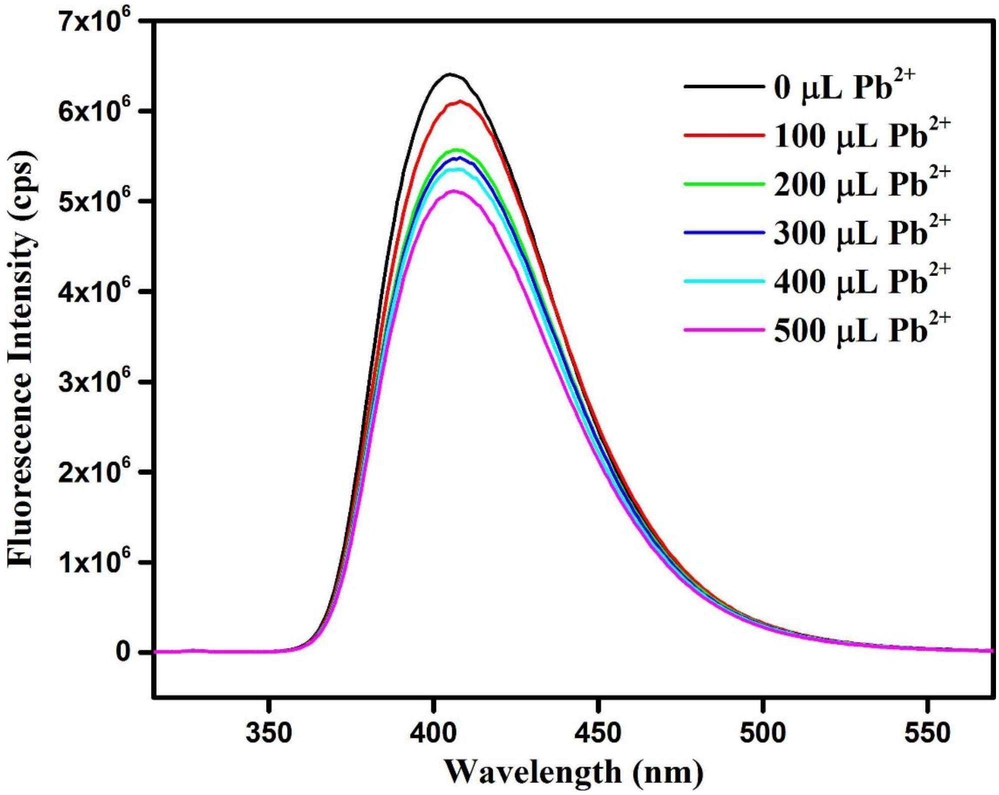

Figure S20. Luminescence quenching of **1'** dispersed in water after gradual addition of 10 mM solution of Pb^{2+} in water.

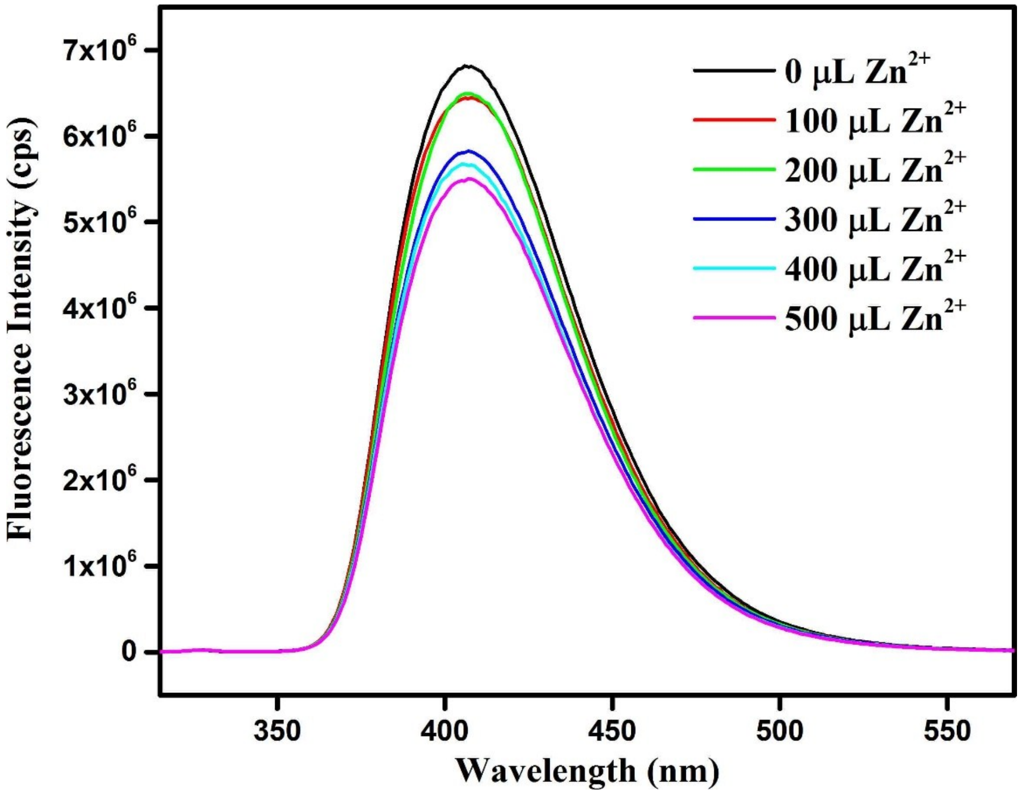

Figure S21. Luminescence quenching of **1'** dispersed in water after gradual addition of 10 mM solution of Zn^{2+} in water.

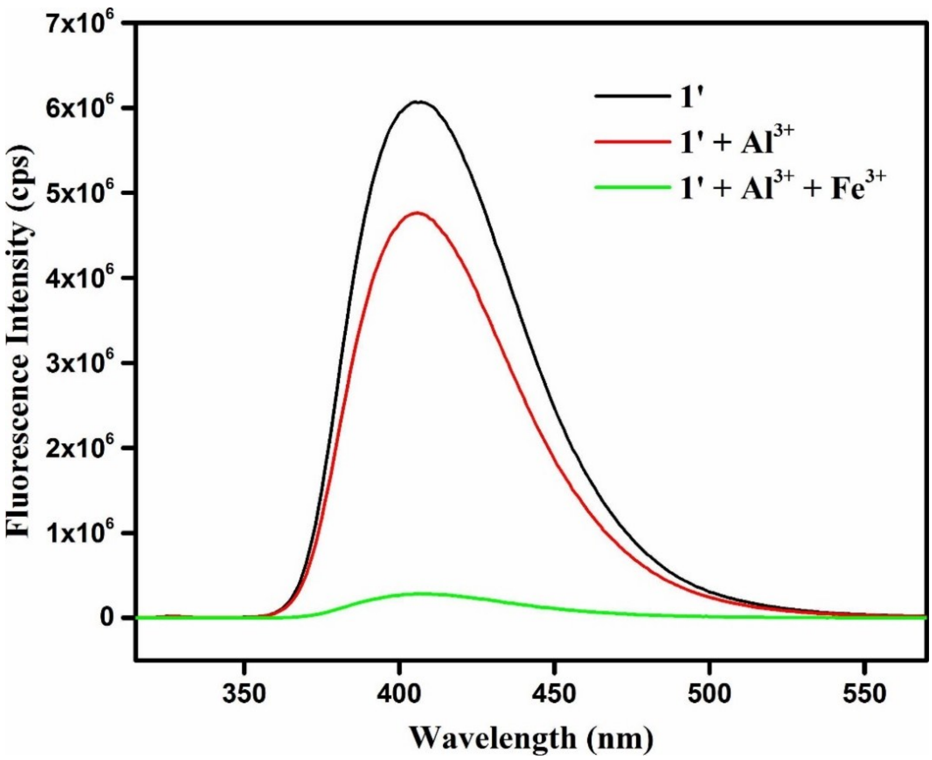

Figure S22. Luminescence quenching of **1'** dispersed in water after gradual addition of 10 mM solution of Al^{3+} in water (500 μL) in presence of 10 mM solution of Fe^{3+} in water (500 μL).

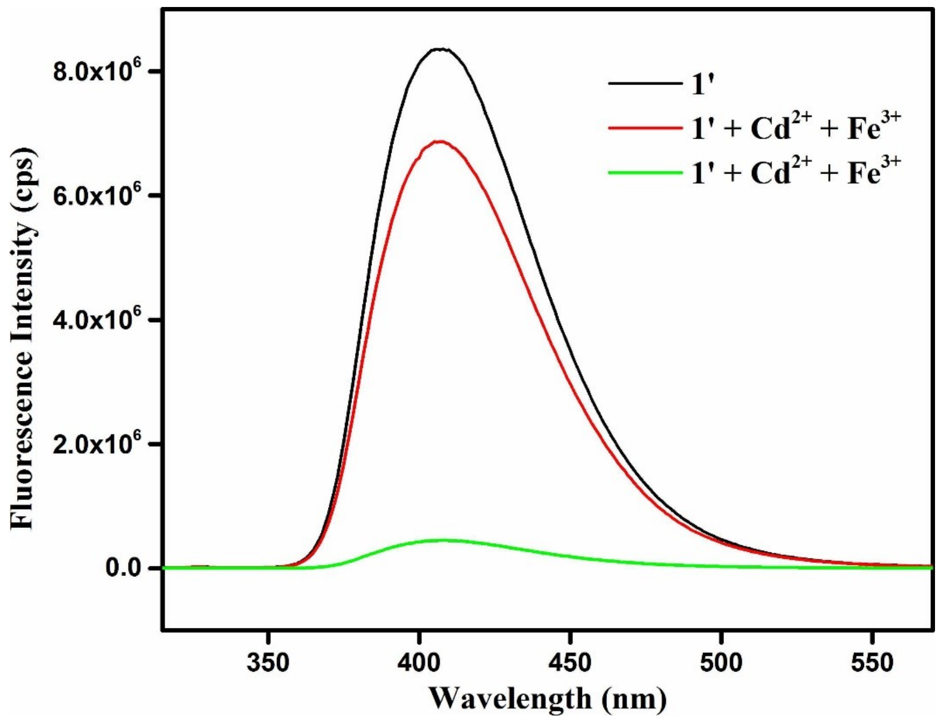

Figure S23. Luminescence quenching of **1'** dispersed in water after gradual addition of 10 mM solution of Cd^{2+} in water (500 μL) in presence of 10 mM solution of Fe^{3+} in water (500 μL).

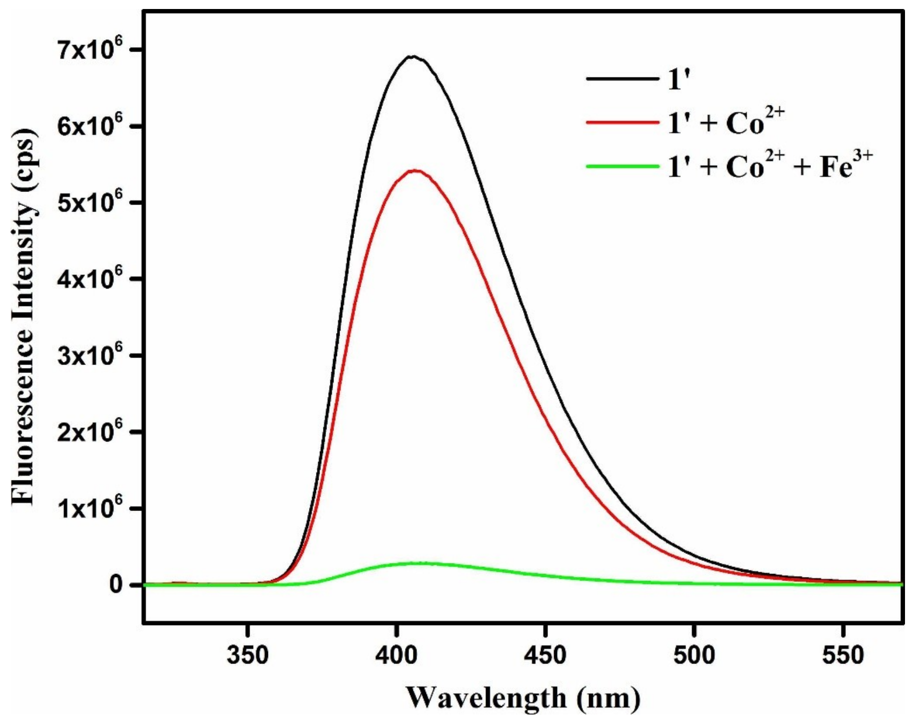

Figure S24. Luminescence quenching of **1'** dispersed in water after gradual addition of 10 mM solution of Co^{2+} in water (500 μL) in presence of 10 mM solution of Fe^{3+} in water (500 μL).

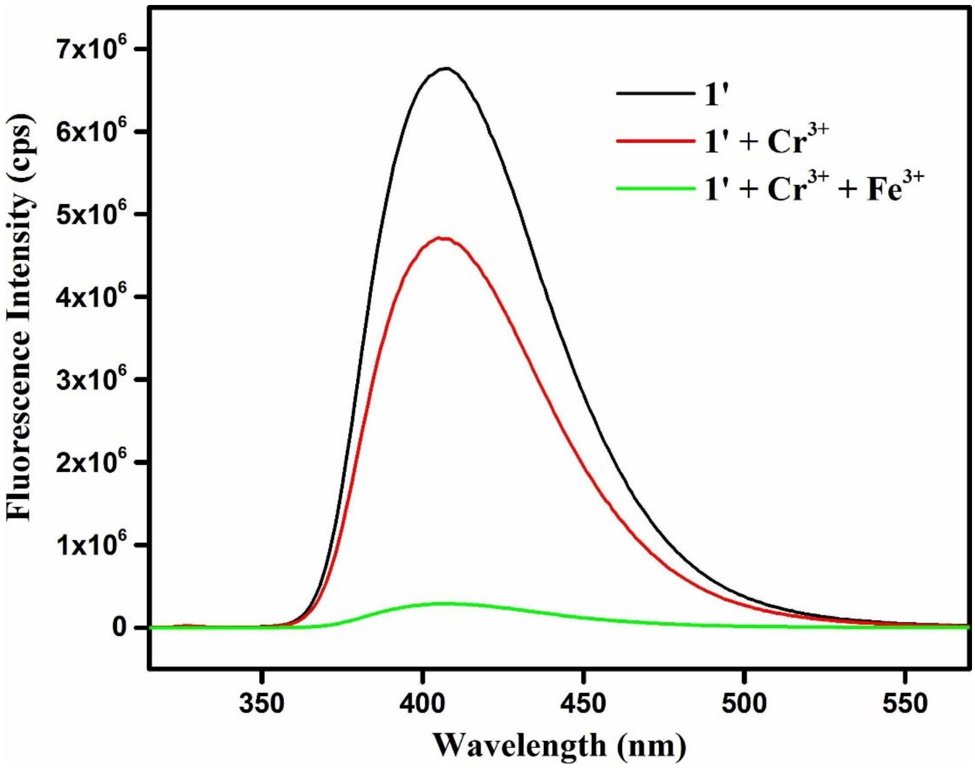

Figure S25. Luminescence quenching of **1'** dispersed in water after gradual addition of 10 mM solution of Cr^{3+} in water (500 μL) in presence of 10 mM solution of Fe^{3+} in water (500 μL).

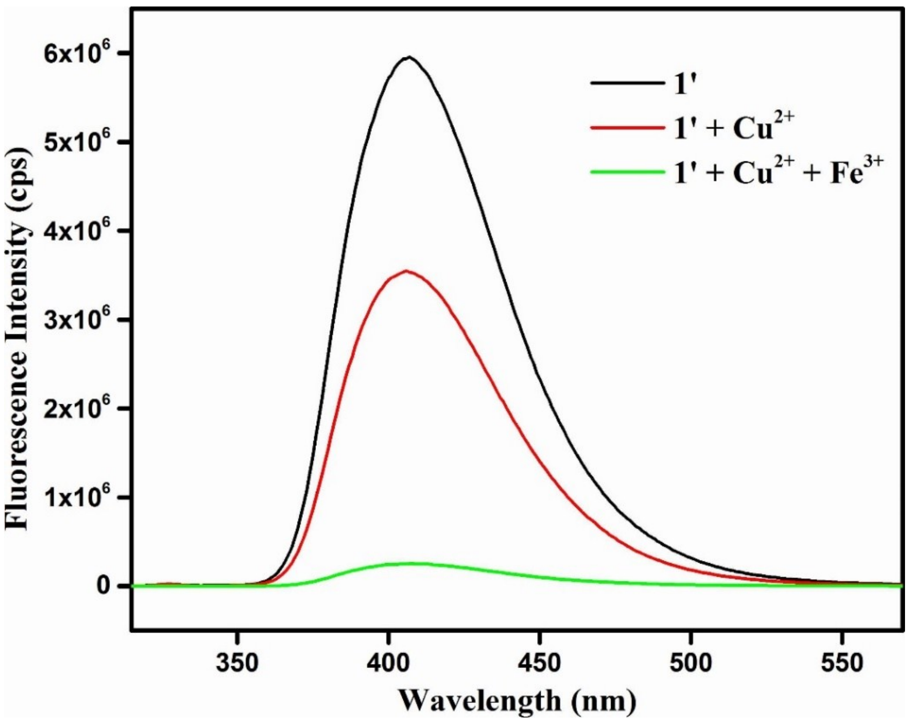

Figure S26. Luminescence quenching of **1'** dispersed in water after gradual addition of 10 mM solution of Cu^{2+} in water (500 μL) in presence of 10 mM solution of Fe^{3+} in water (500 μL).

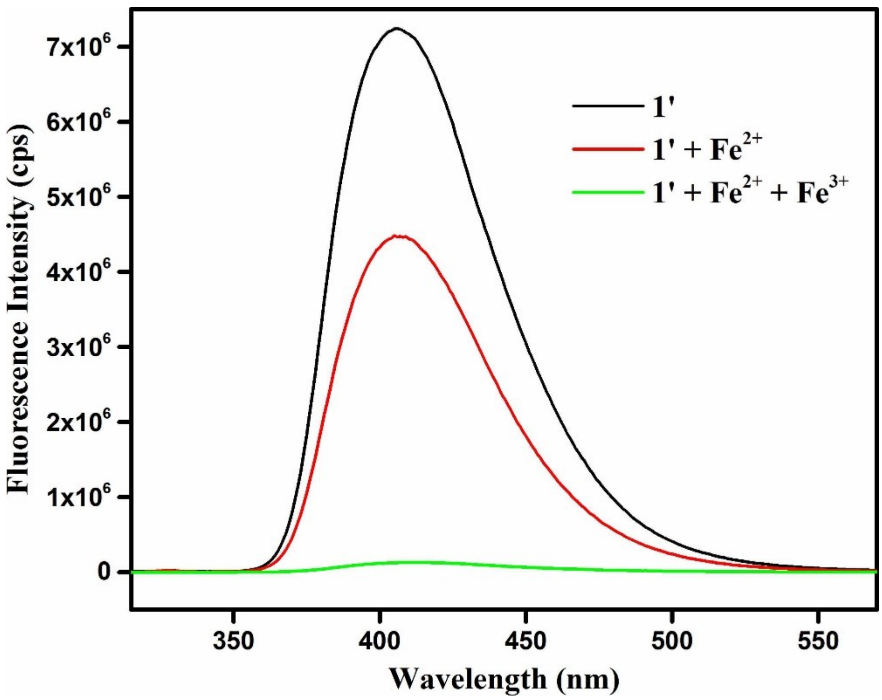

Figure S27. Luminescence quenching of **1'** dispersed in water after gradual addition of 10 mM solution of Fe^{2+} in water (500 μL) in presence of 10 mM solution of Fe^{3+} in water (500 μL).

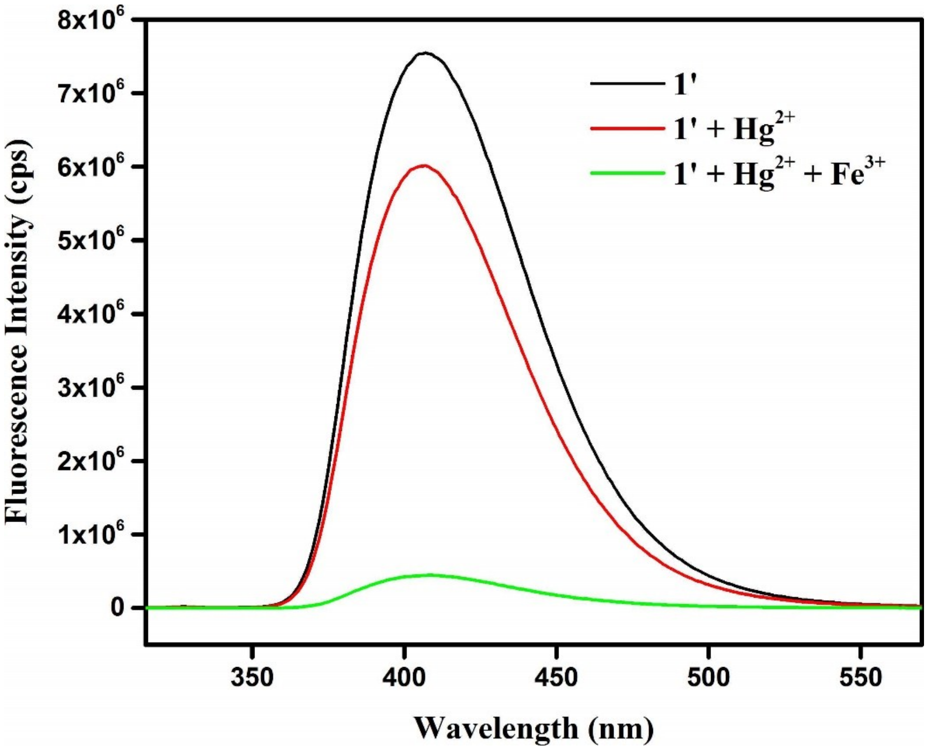

Figure S28. Luminescence quenching of **1'** dispersed in water after gradual addition of 10 mM solution of Hg^{2+} in water (500 μL) in presence of 10 mM solution of Fe^{3+} in water (500 μL).

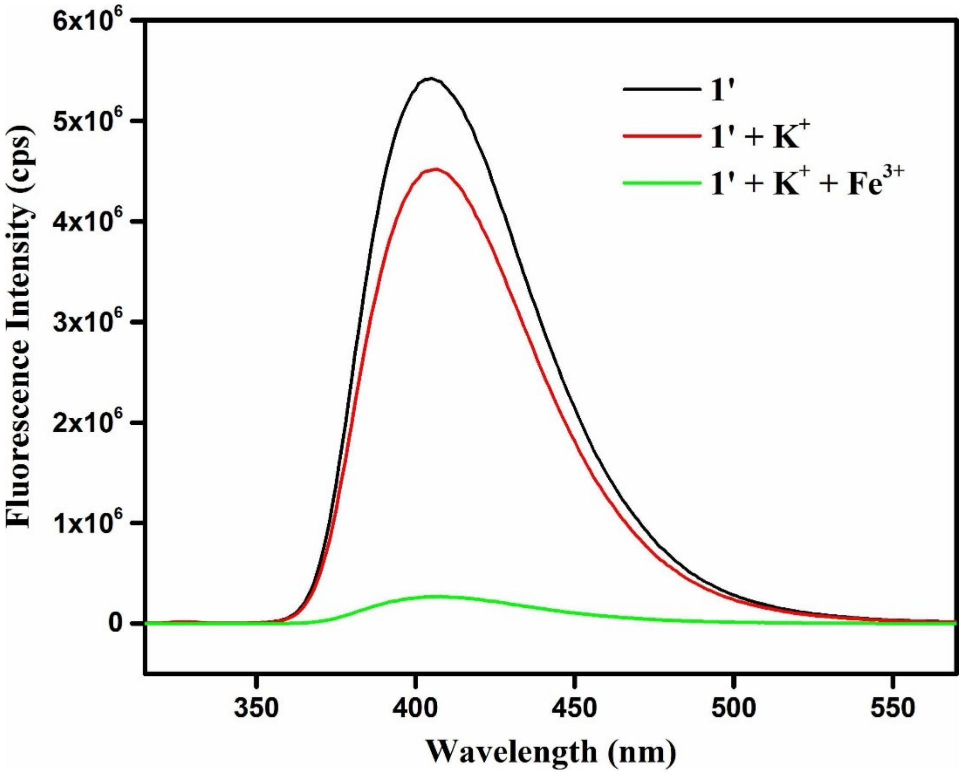

Figure S29. Luminescence quenching of **1'** dispersed in water after gradual addition of 10 mM solution of K^{+} in water (500 μL) in presence of 10 mM solution of Fe^{3+} in water (500 μL).

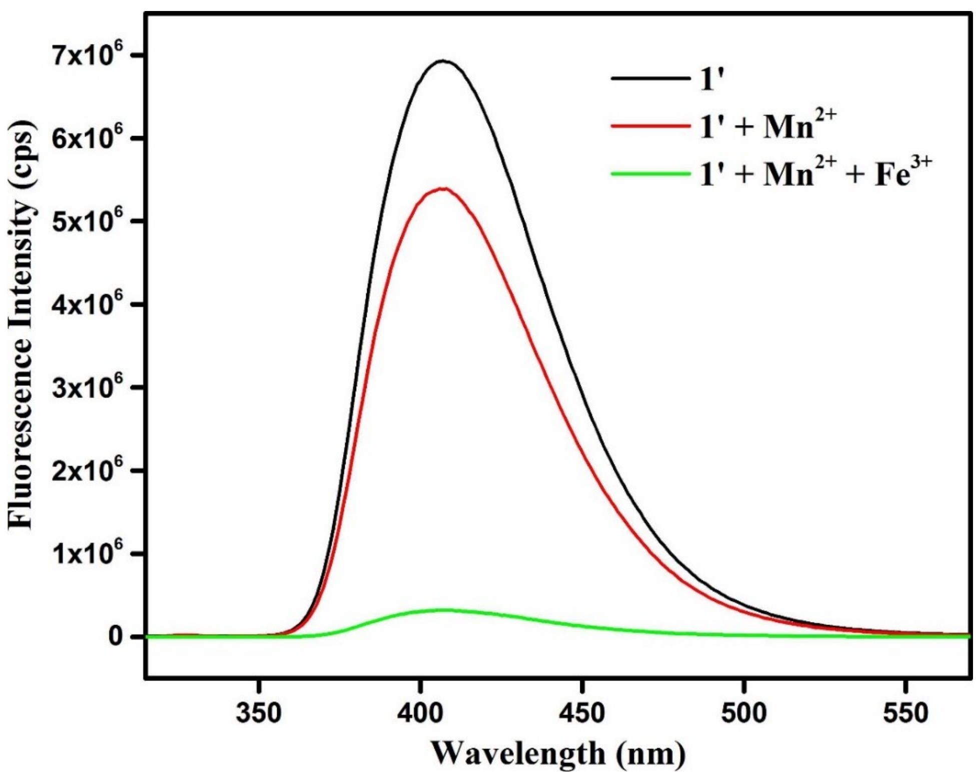

Figure S30. Luminescence quenching of **1'** dispersed in water after gradual addition of 10 mM solution of Mn^{2+} in water (500 μL) in presence of 10 mM solution of Fe^{3+} in water (500 μL).

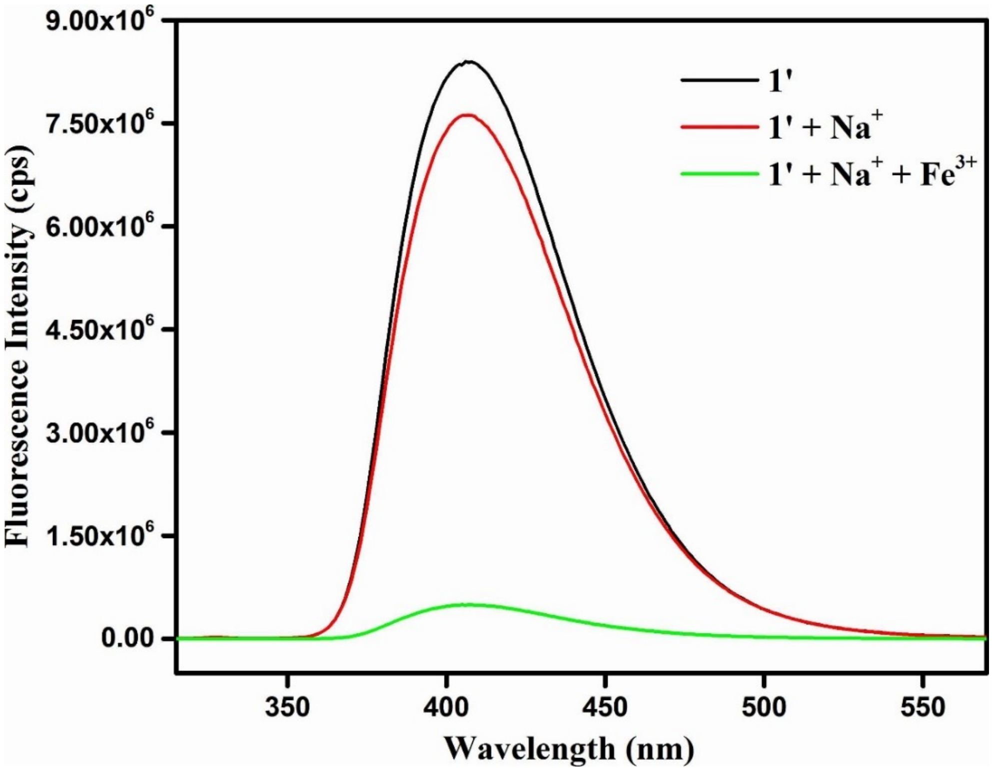

Figure S31. Luminescence quenching of **1'** dispersed in water after gradual addition of 10 mM solution of Na^{+} in water (500 μL) in presence of 10 mM solution of Fe^{3+} in water (500 μL).

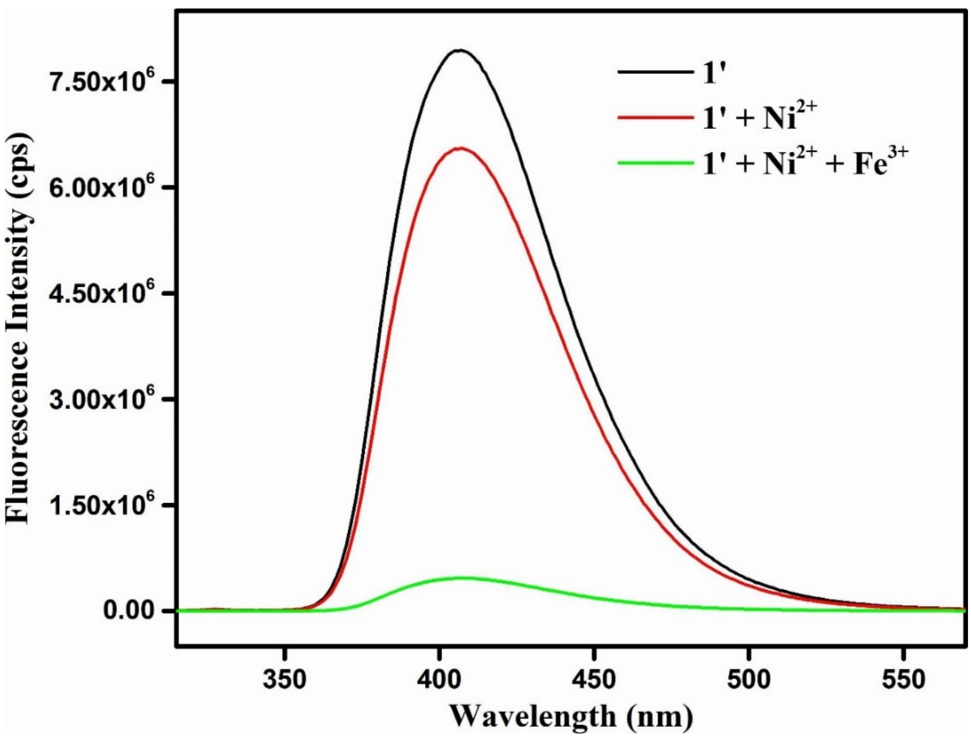

Figure S32. Luminescence quenching of **1'** dispersed in water after gradual addition of 10 mM solution of Ni^{2+} in water (500 μL) in presence of 10 mM solution of Fe^{3+} in water (500 μL).

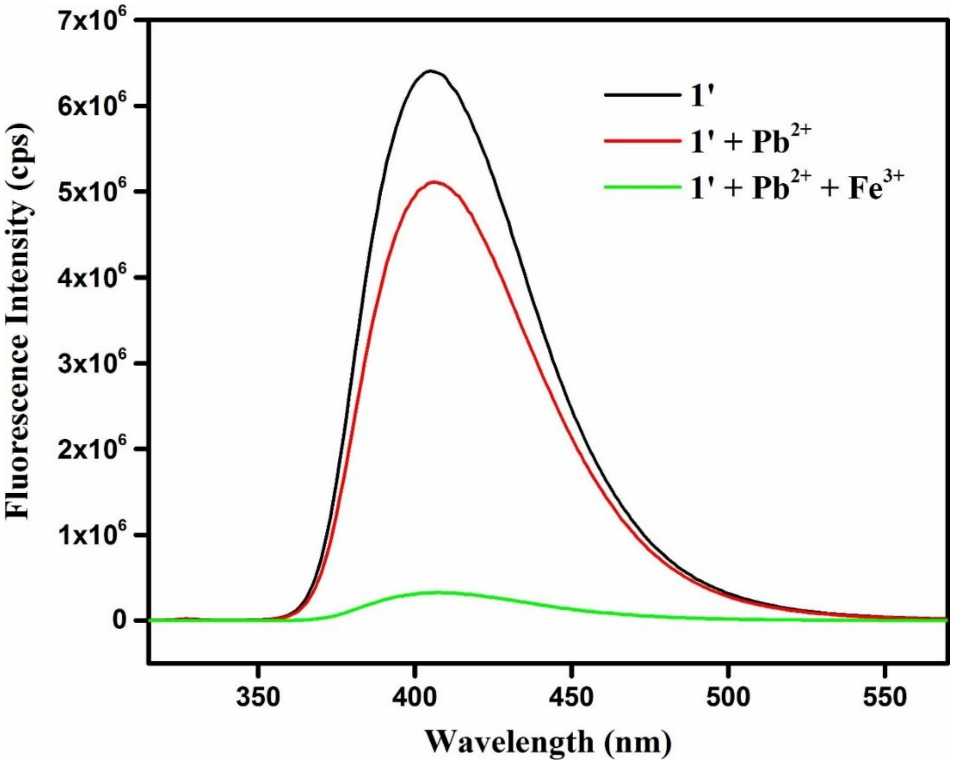

Figure S33. Luminescence quenching of **1'** dispersed in water after gradual addition of 10 mM solution of Pb^{2+} in water (500 μL) in presence of 10 mM solution of Fe^{3+} in water (500 μL).

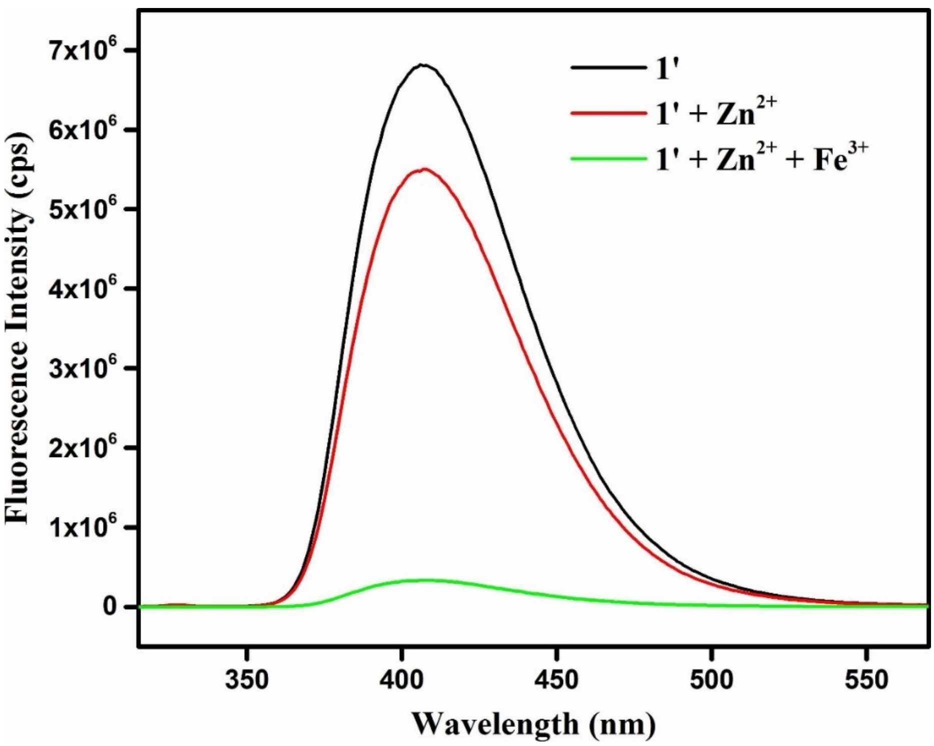

Figure S34. Luminescence quenching of **1'** dispersed in water after gradual addition of 10 mM solution of Zn^{2+} in water (500 μL) in presence of 10 mM solution of Fe^{3+} in water (500 μL).

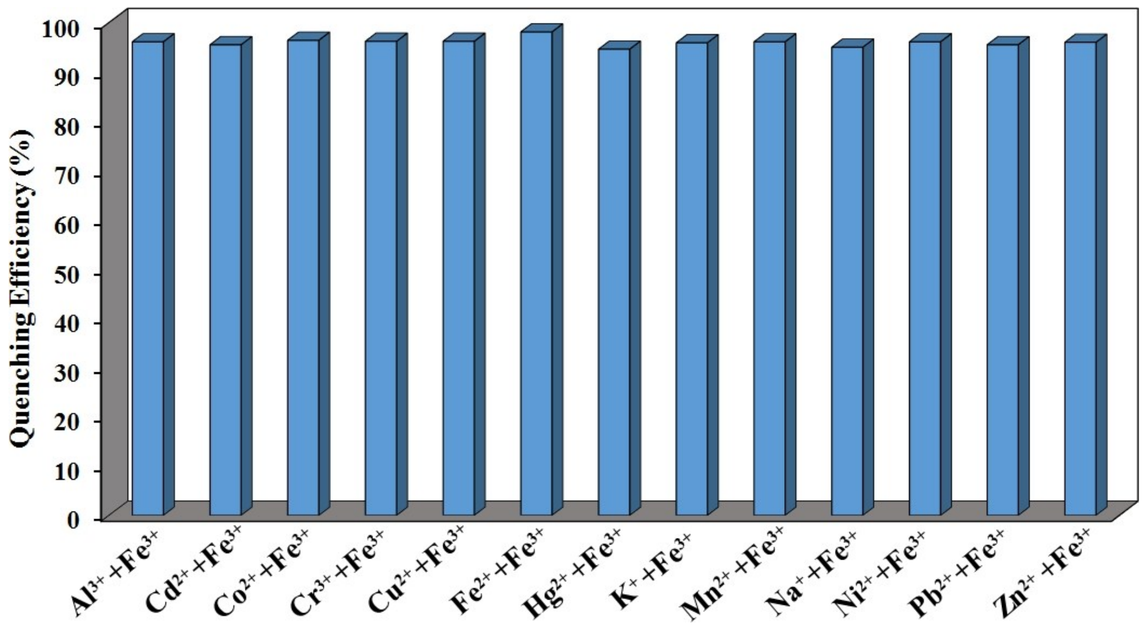

Figure S35. Quenching efficiencies of **1'** after addition of equal amounts of other cations and Fe^{3+} ion.

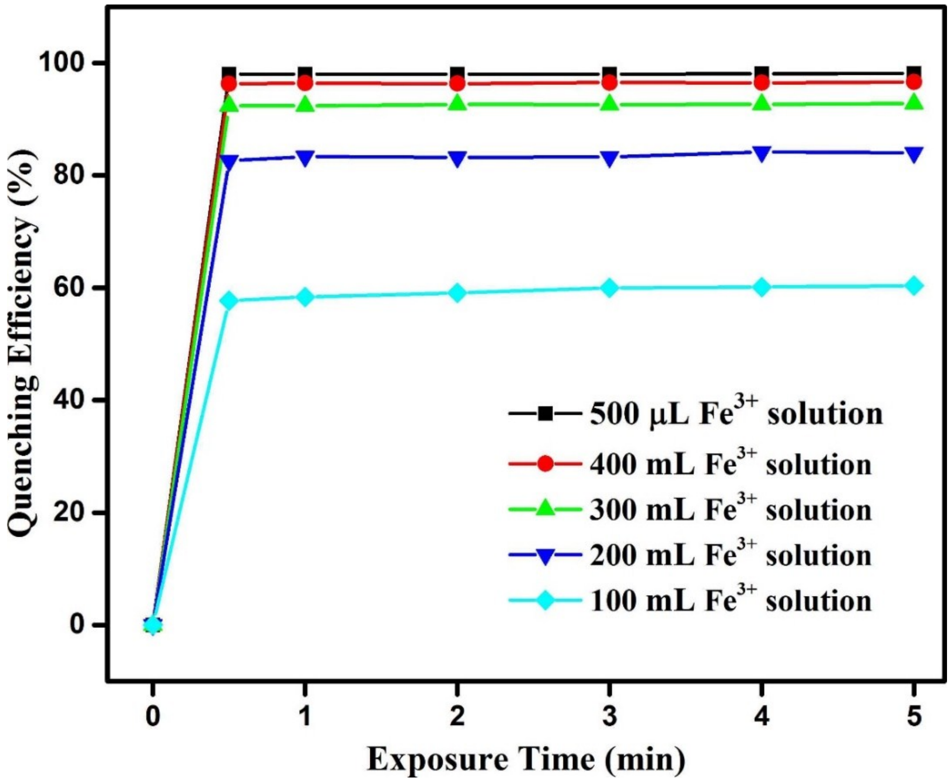

Figure S36. Quenching efficiencies of **1'** after addition of 10 mM Fe^{3+} solution as a function of exposure time in water.

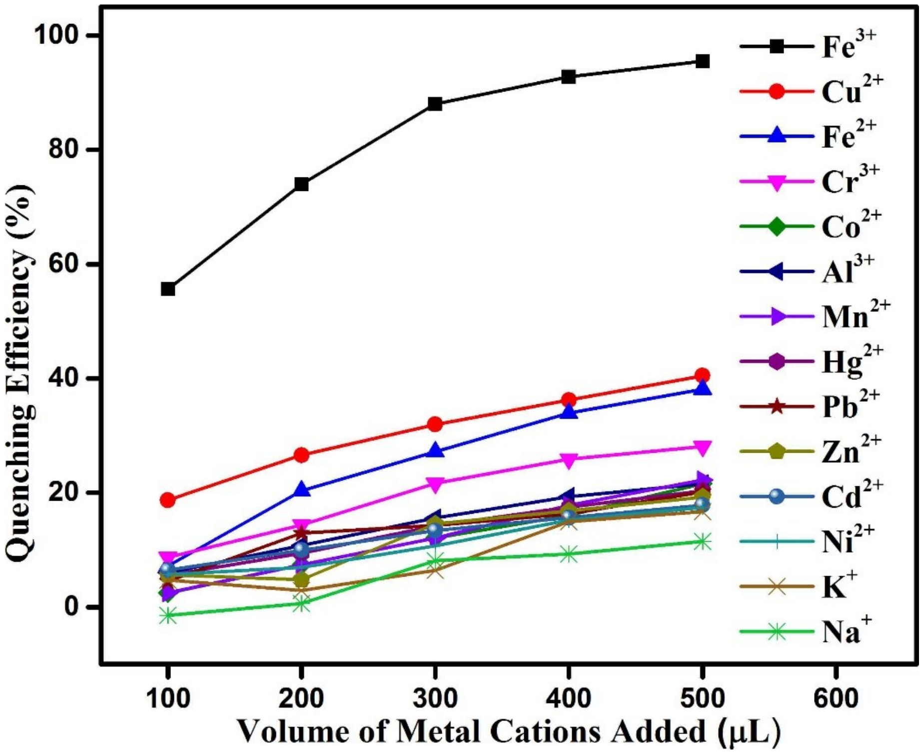

Figure S37. Change of quenching efficiency (%) after addition of different volumes of 10 mM different metal cations.

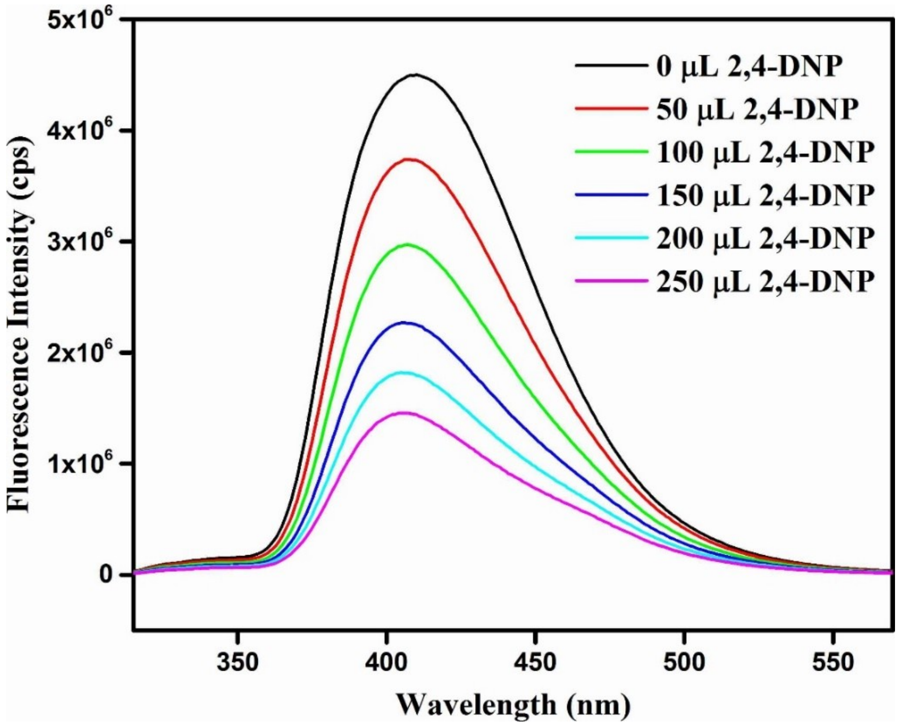

Figure S38. Luminescence quenching of **1'** dispersed in DMSO after gradual addition of 3 mM solution of 2,4-DNP in DMSO.

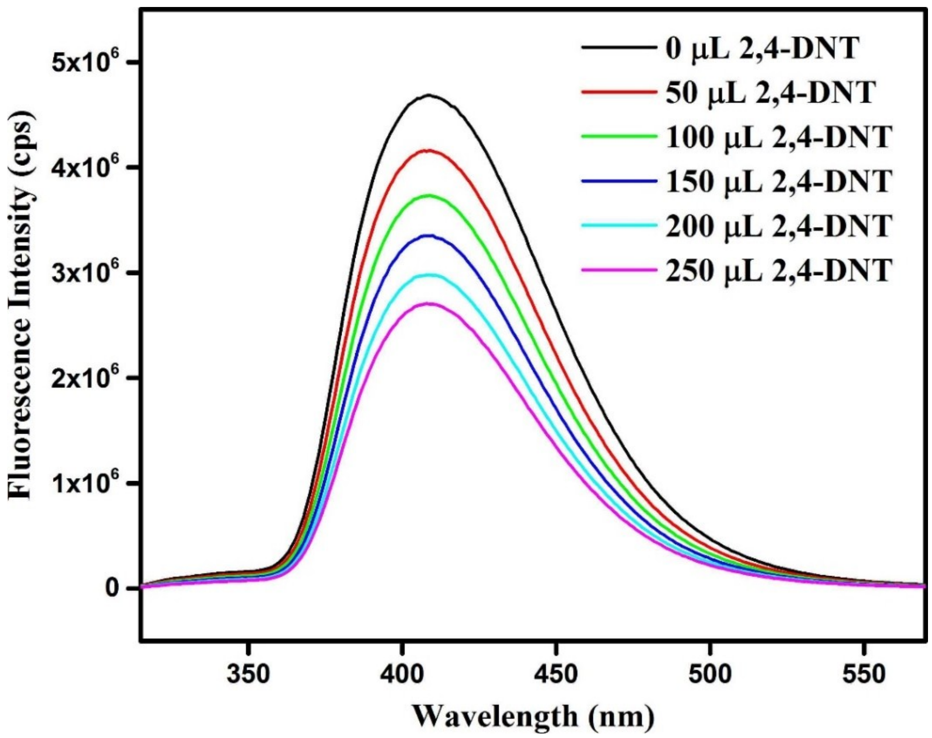

Figure S39. Luminescence quenching of **1'** dispersed in DMSO after gradual addition of 3 mM solution of 2,4-DNT in DMSO.

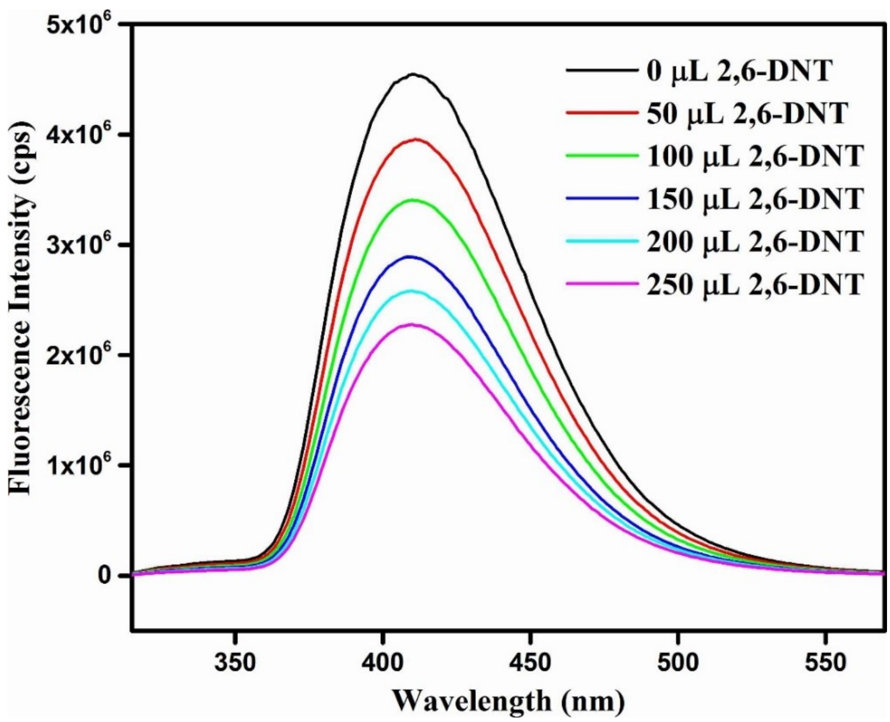

Figure S40. Luminescence quenching of **1'** dispersed in DMSO after gradual addition of 3 mM solution of 2,6-DNT in DMSO.

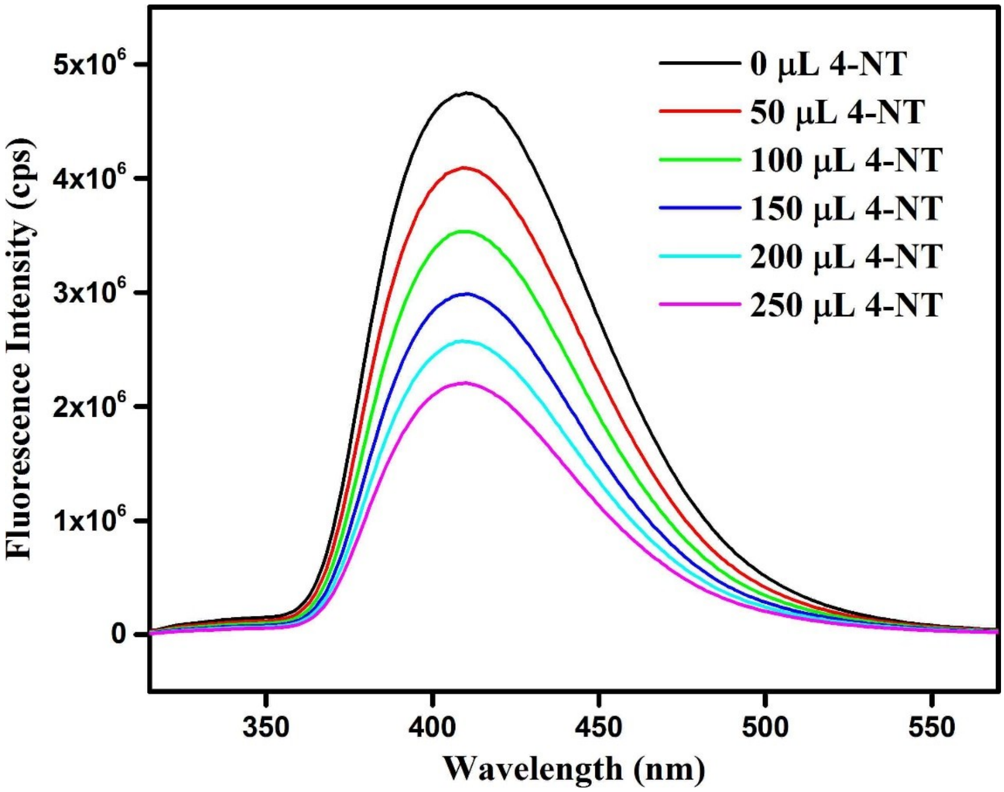

Figure S41. Luminescence quenching of **1'** dispersed in DMSO after gradual addition of 3 mM solution of 4-NT in DMSO.

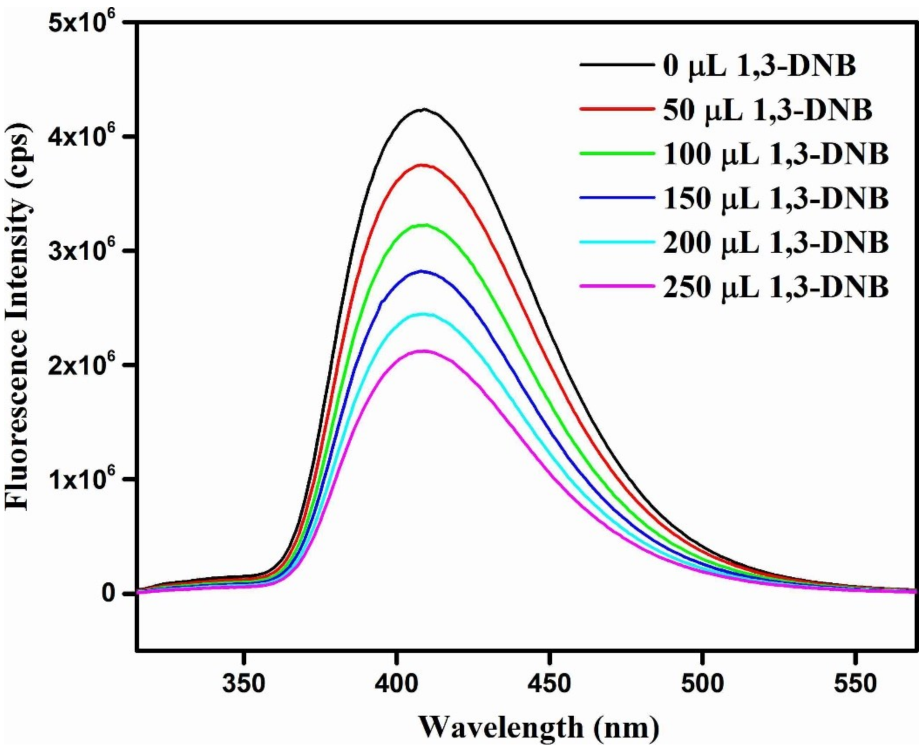

Figure S42. Luminescence quenching of **1'** dispersed in DMSO after gradual addition of 3 mM solution of 1,3-DNB in DMSO.

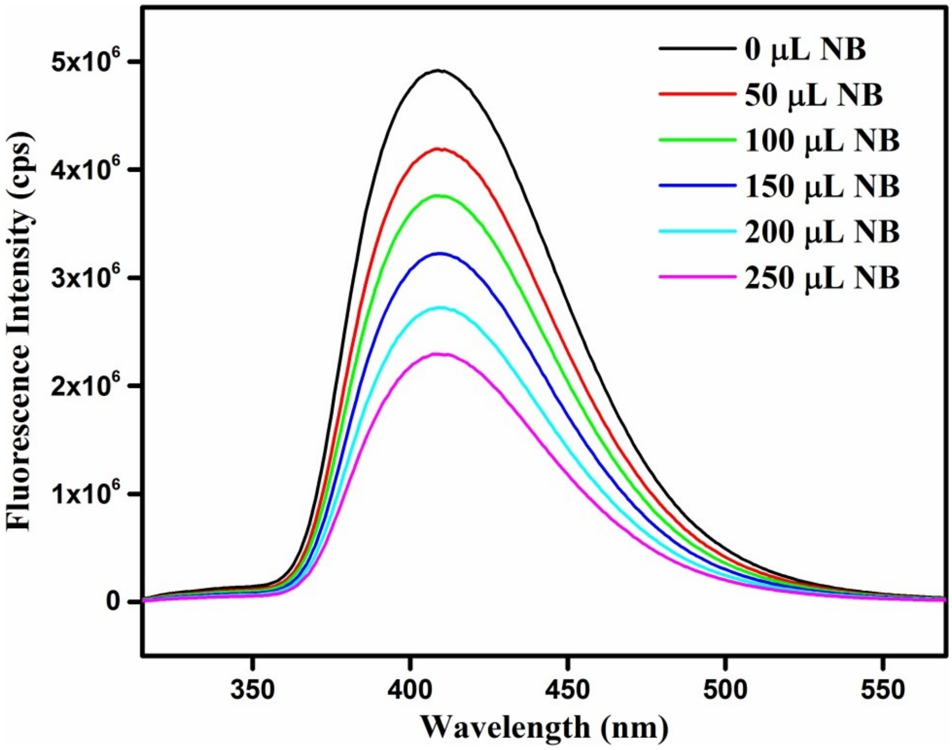

Figure S43. Luminescence quenching of **1'** dispersed in DMSO after gradual addition of 3 mM solution of NB in DMSO.

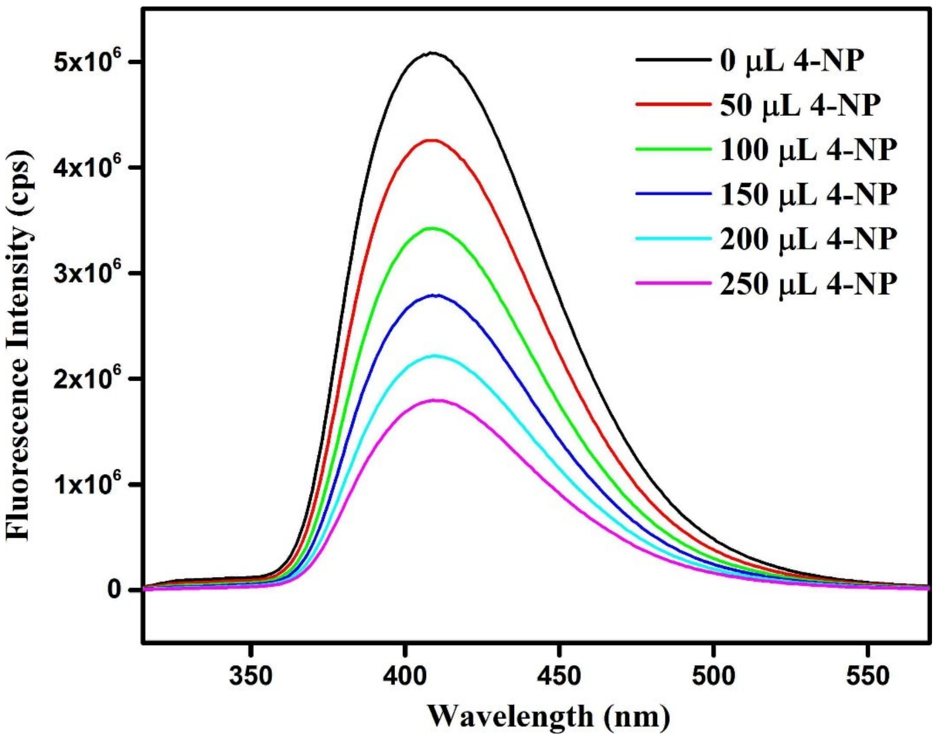

Figure S44. Luminescence quenching of **1'** dispersed in DMSO after gradual addition of 3 mM solution of 4-NP in DMSO.

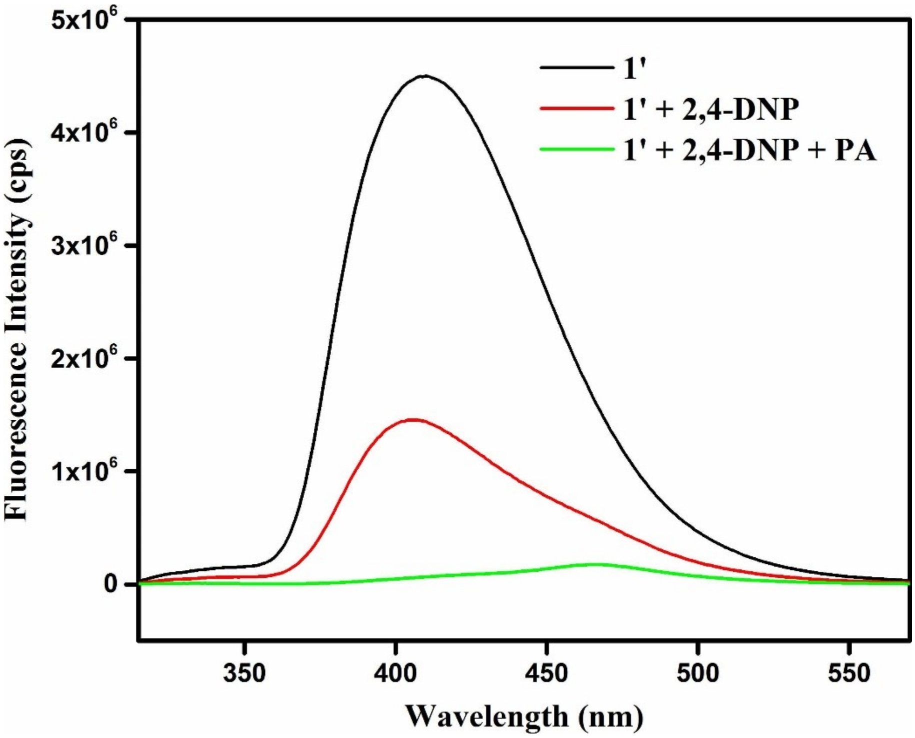

Figure S45. Luminescence quenching of **1'** dispersed in DMSO after gradual addition of 3 mM solution of 2,4-DNP in DMSO (250 μL) in presence of 3 mM solution of PA in DMSO (250 μL).

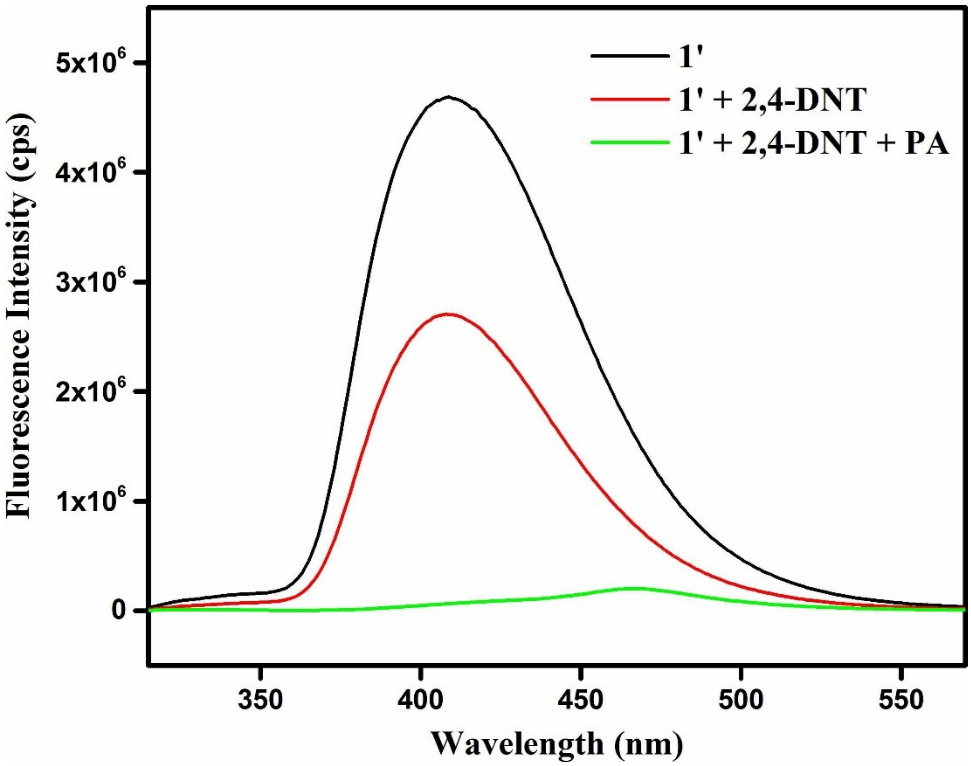

Figure S46. Luminescence quenching of **1'** dispersed in DMSO after gradual addition of 3 mM solution of 2,4-DNP in DMSO (250 μL) in presence of 3 mM solution of PA in DMSO (250 μL).

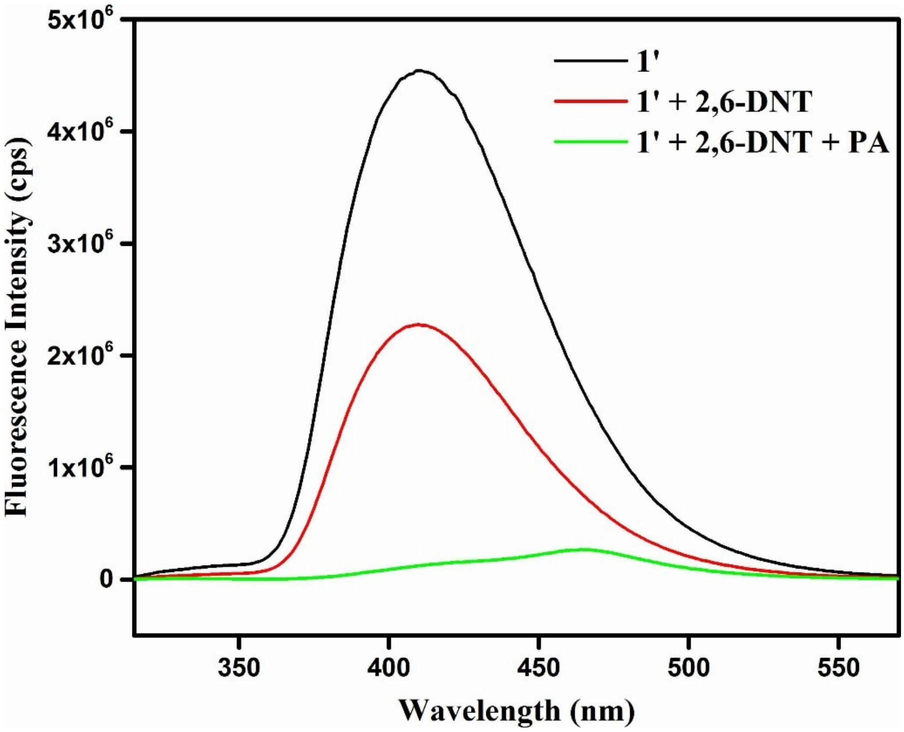

Figure S47. Luminescence quenching of **1'** dispersed in DMSO after gradual addition of 3 mM solution of 2,6-DNT in DMSO (250 μL) in presence of 3 mM solution of PA in DMSO (250 μL).

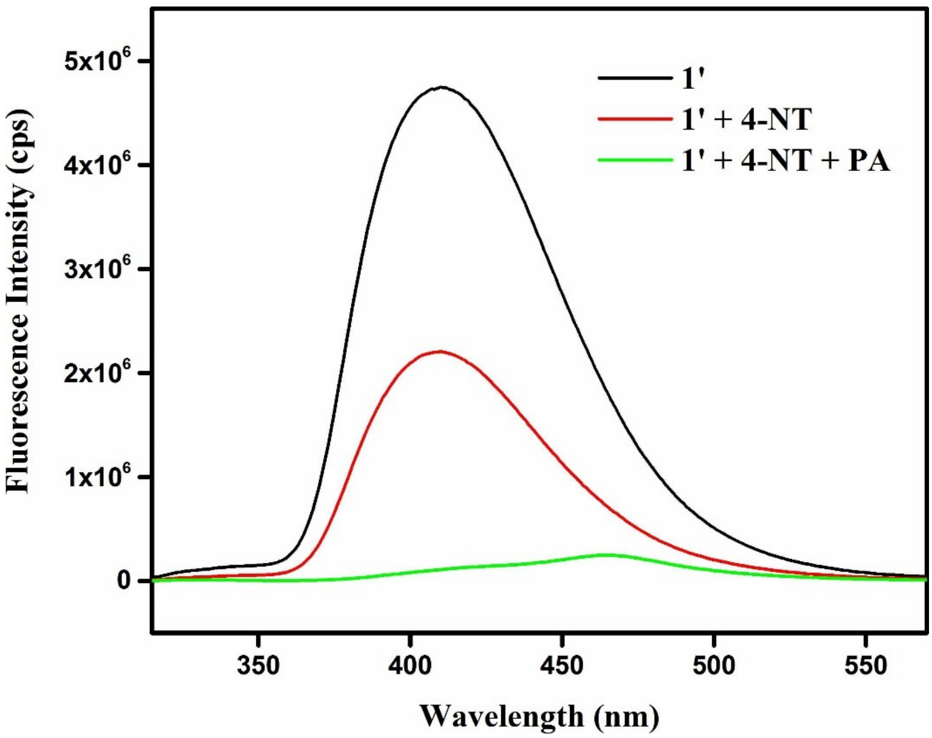

Figure S48. Luminescence quenching of **1'** dispersed in DMSO after gradual addition of 3 mM solution of 4-NT in DMSO (250 μL) in presence of 3 mM solution of PA in DMSO (250 μL).

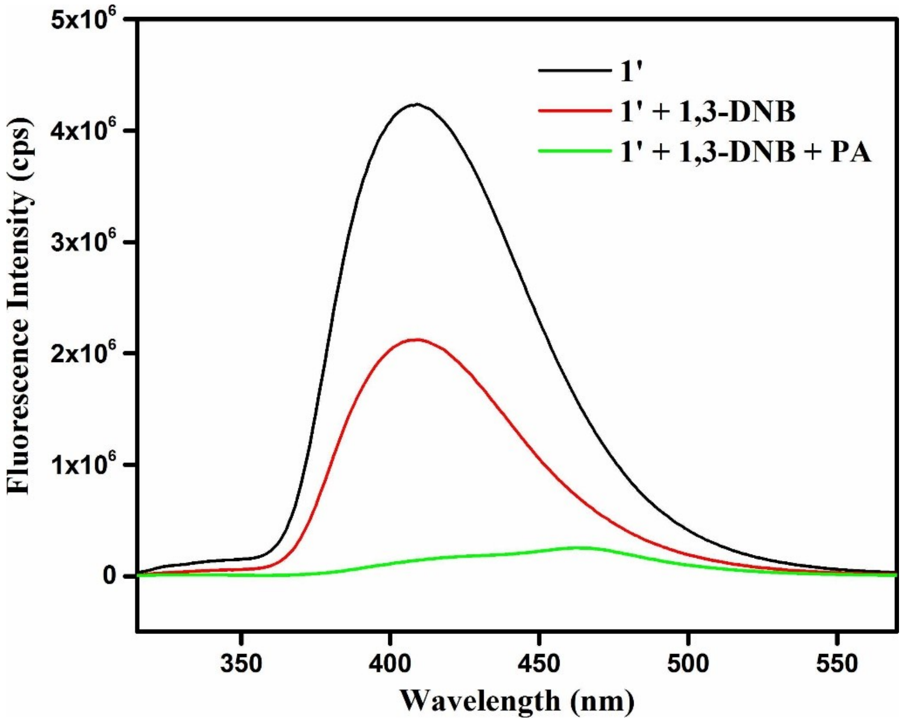

Figure S49. Luminescence quenching of **1'** dispersed in DMSO after gradual addition of 3 mM solution of 1,3-DNB in DMSO (250 μL) in presence of 3 mM solution of PA in DMSO (250 μL).

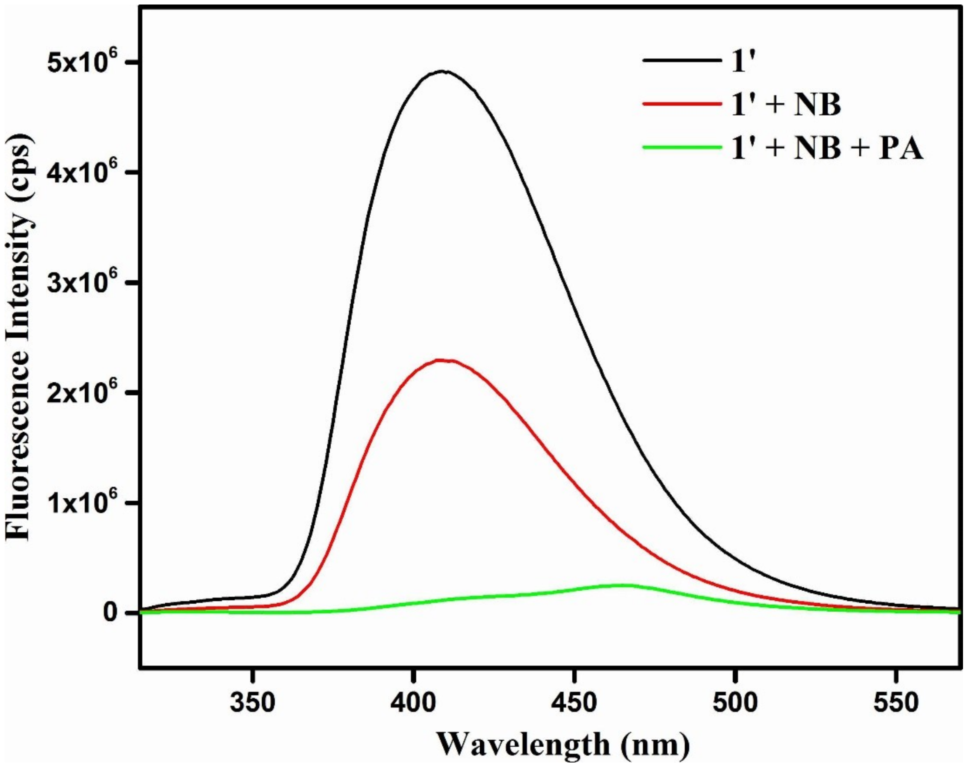

Figure S50. Luminescence quenching of **1'** dispersed in DMSO after gradual addition of 3 mM solution of NB in DMSO (250 μL) in presence of 3 mM solution of PA in DMSO (250 μL).

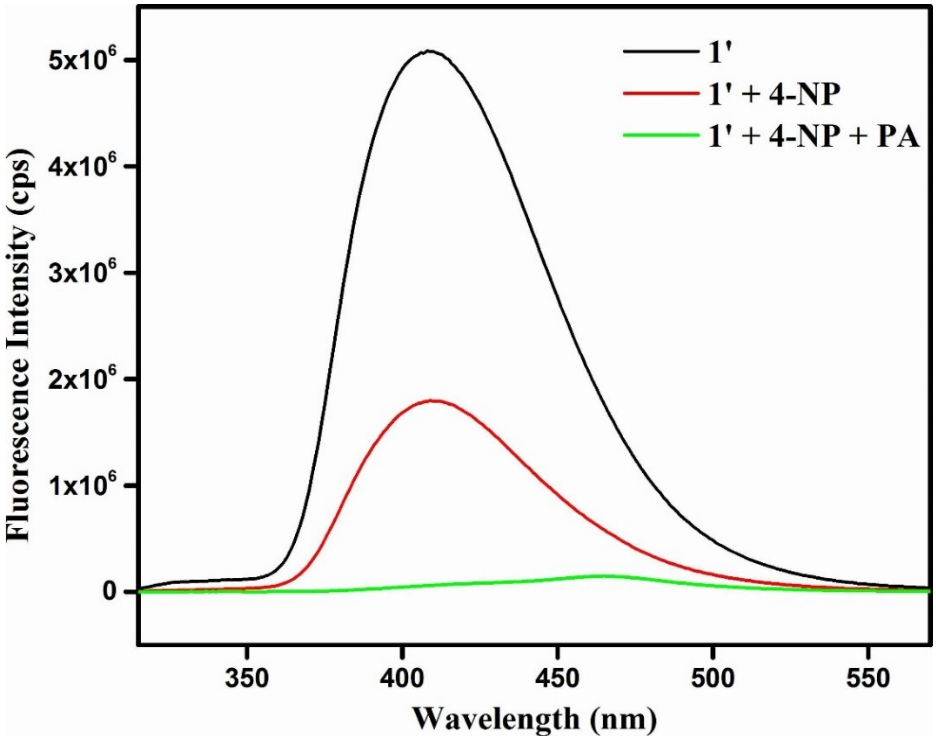

Figure S51. Luminescence quenching of **1'** dispersed in DMSO after gradual addition of 3 mM solution of 4-NP in DMSO (250 μL) in presence of 3 mM solution of PA in DMSO (250 μL).

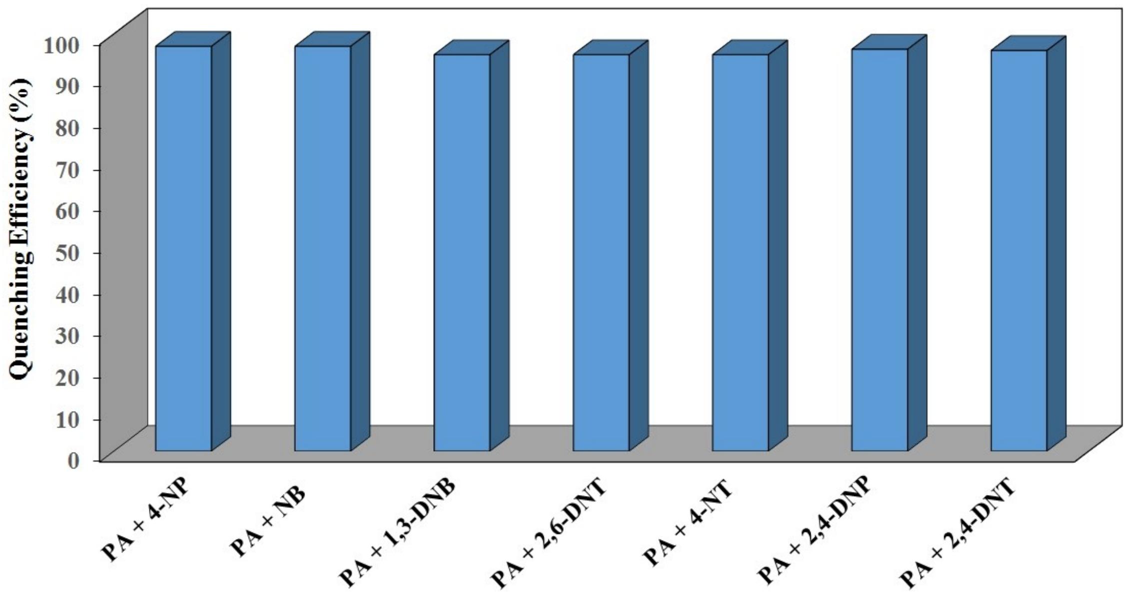

Figure S52. Quenching efficiencies of **1'** after addition of equal amounts of different NAEs and PA in DMSO.

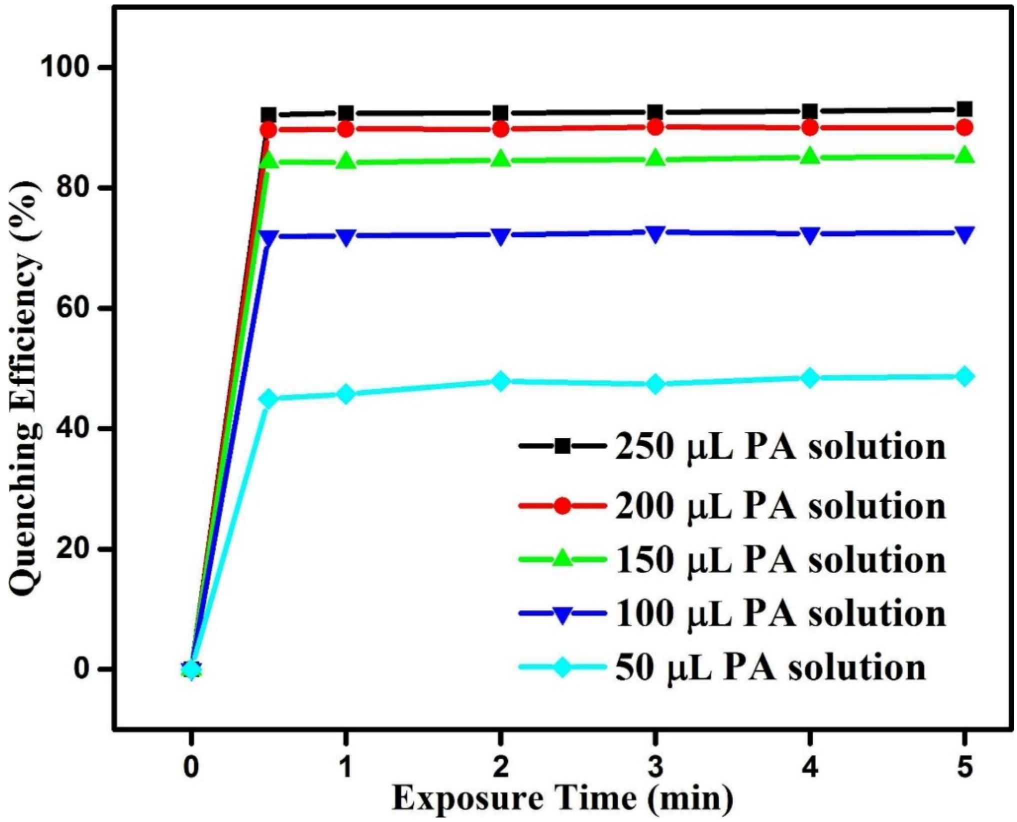

Figure S53. Quenching efficiencies of **1'** after addition of 3 mM PA as a function of exposure time in DMSO solvent.

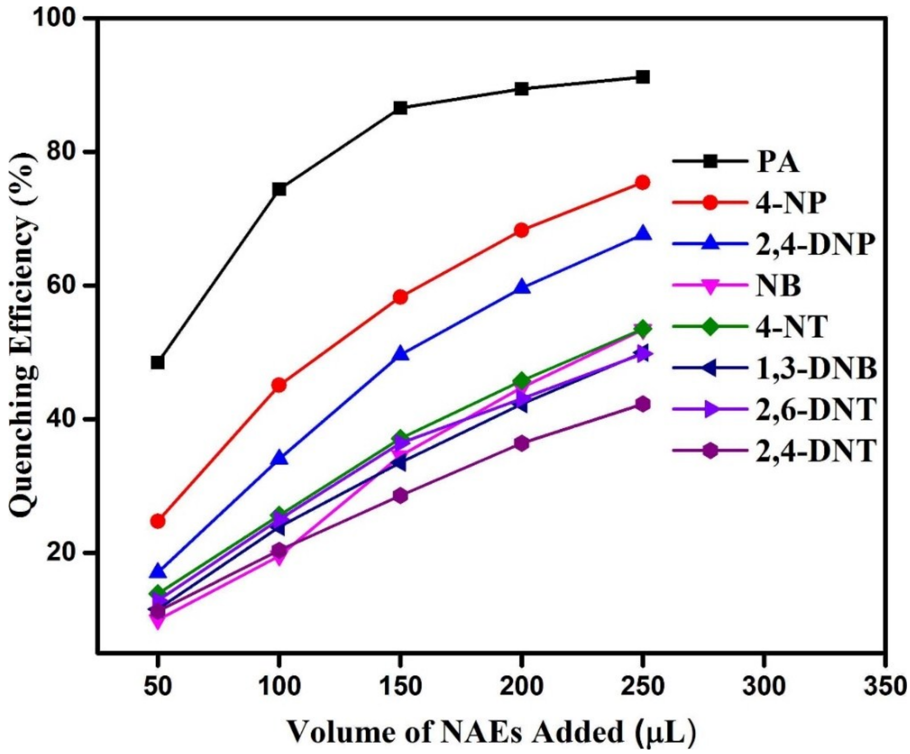

Figure S54. Change of quenching efficiency (%) after addition of different volumes of 3 mM solutions of different NAEs.

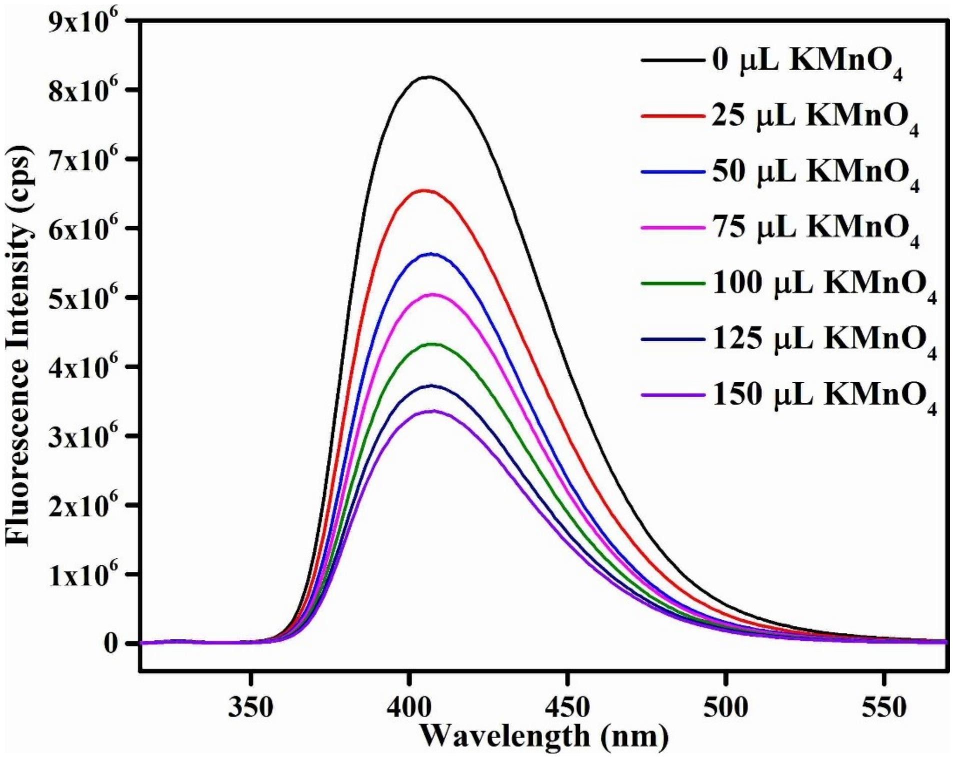

Figure S55. Luminescence quenching of **1'** dispersed in water after gradual addition of 3 mM solution of $KMnO_4$ in water.

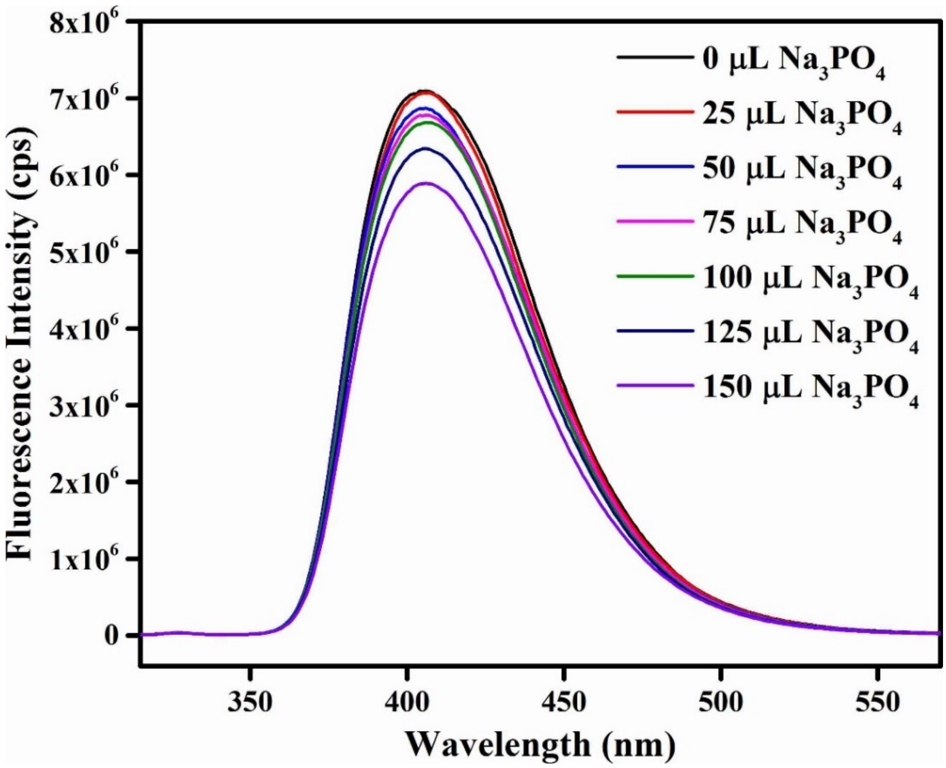

Figure S56. Luminescence quenching of **1'** dispersed in water after gradual addition of 3 mM solution of $Na_3PO_4{\cdot}12H_2O$ in water.

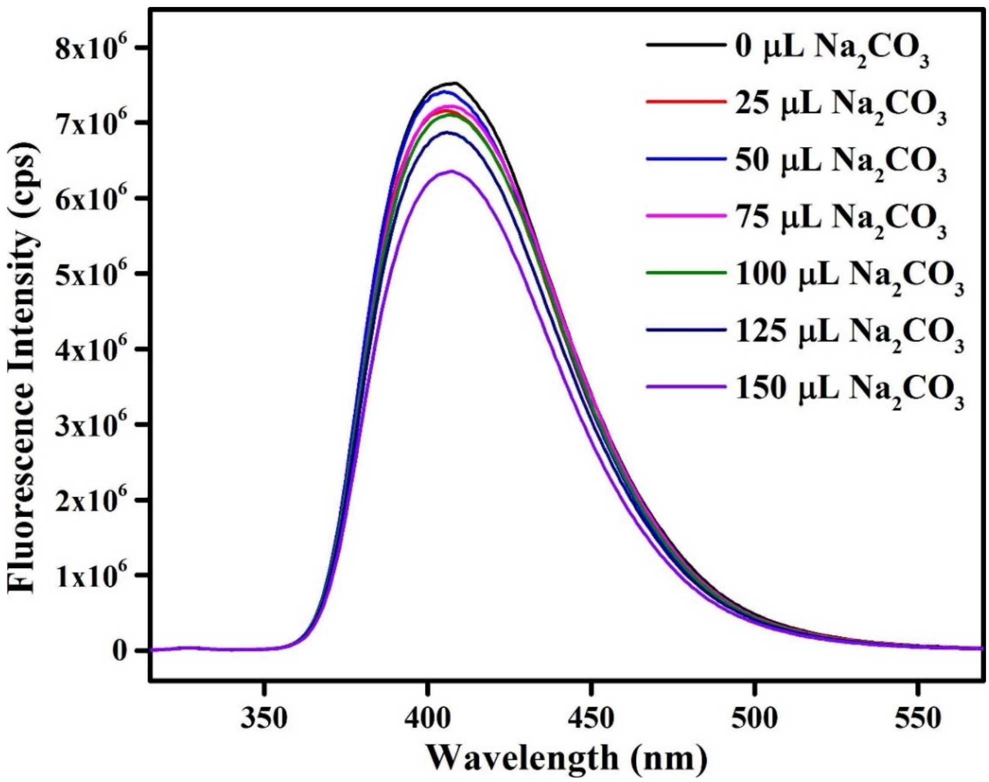

Figure S57. Luminescence quenching of **1'** dispersed in water after gradual addition of 3 mM solution of Na_2CO_3 in water.

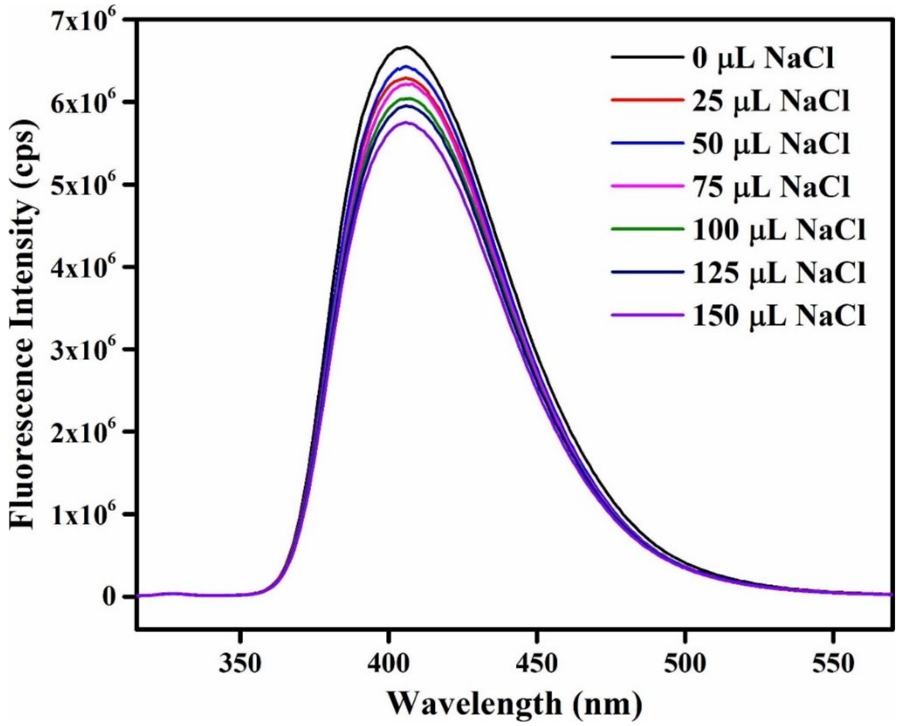

Figure S58. Luminescence quenching of **1'** dispersed in water after gradual addition of 3 mM solution of NaCl in water.

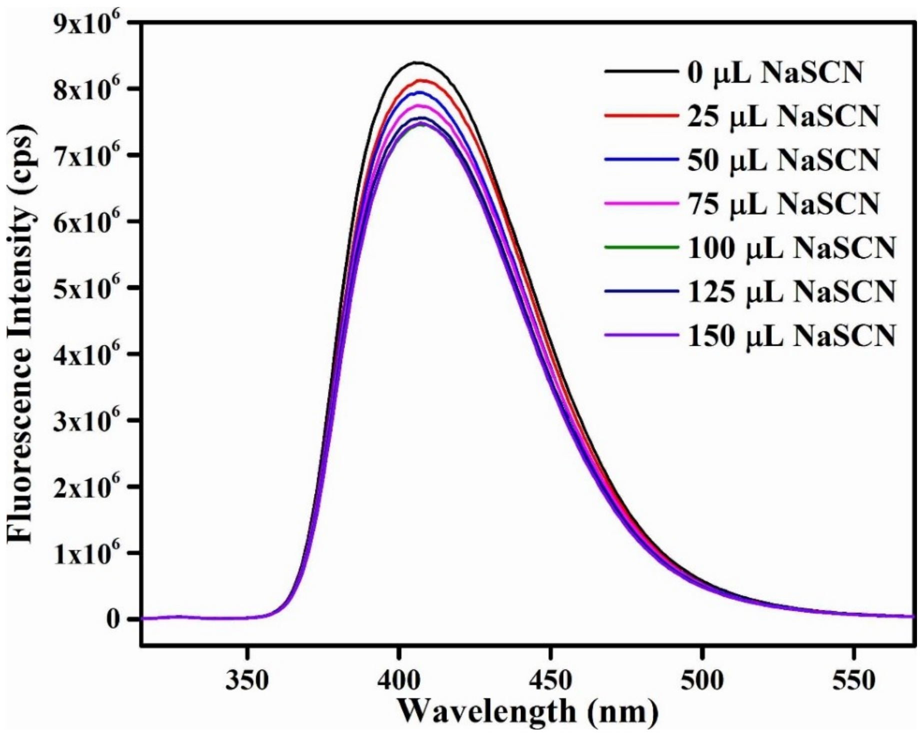

Figure S59. Luminescence quenching of **1'** dispersed in water after gradual addition of 3 mM solution of NaSCN in water.

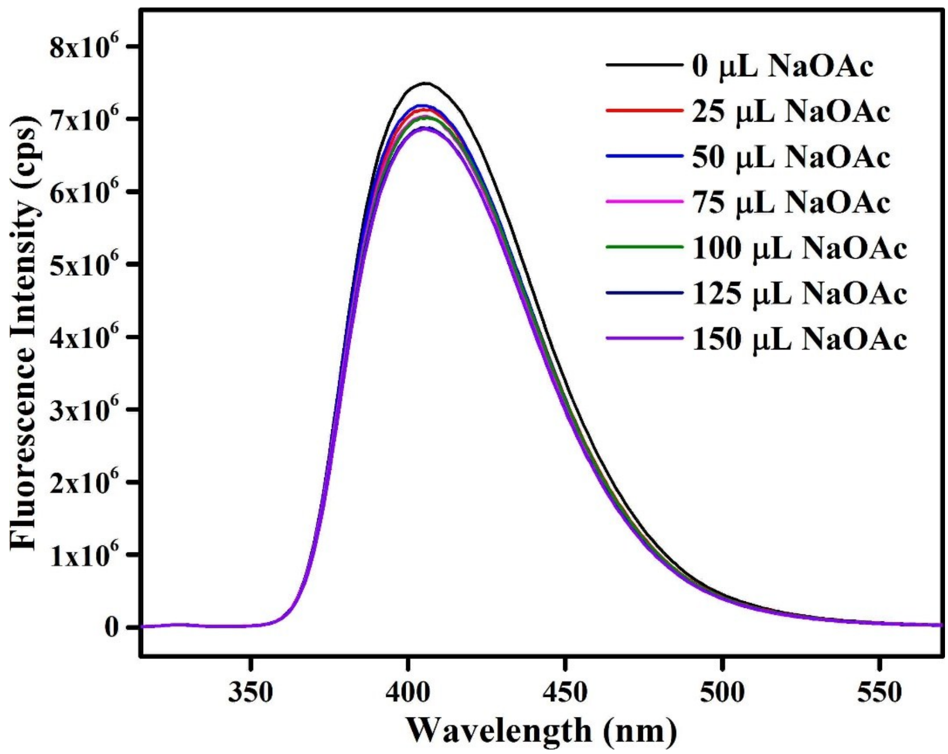

Figure S60. Luminescence quenching of **1'** dispersed in water after gradual addition of 3 mM solution of NaOAc in water.

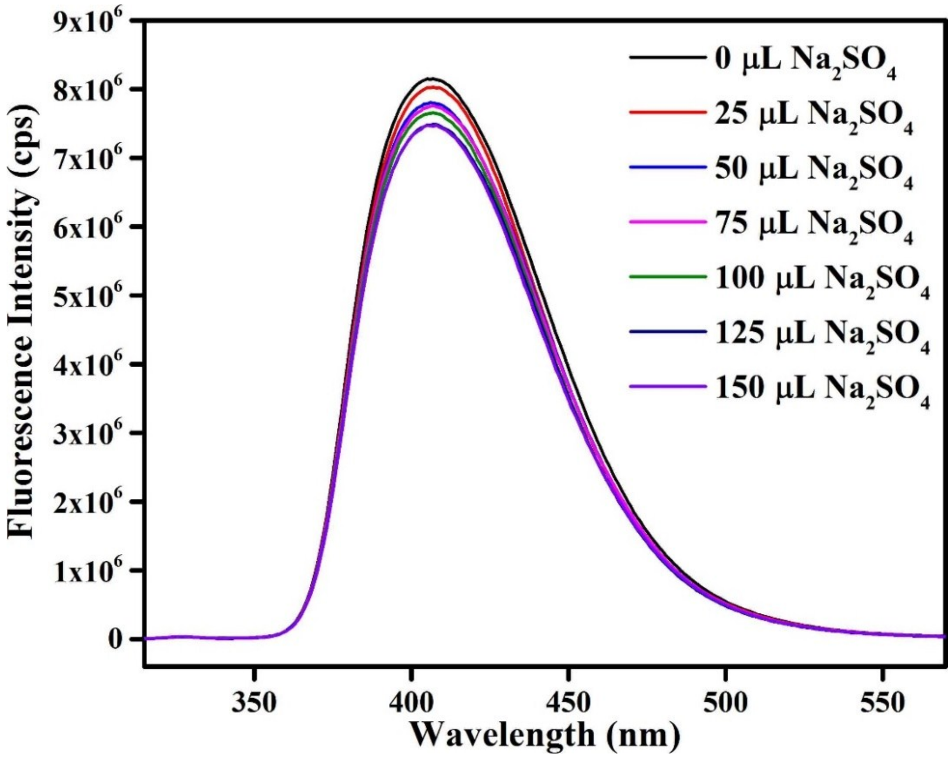

Figure S61. Luminescence quenching of **1'** dispersed in water after gradual addition of 3 mM solution of Na_2SO_4 in water.

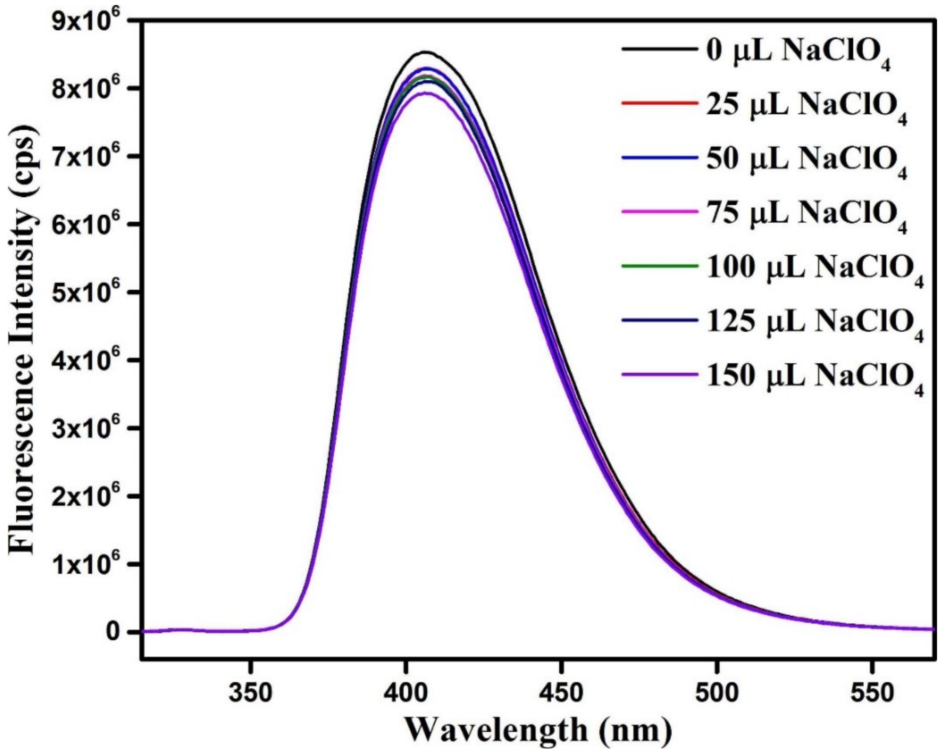

Figure S62. Luminescence quenching of **1'** dispersed in water after gradual addition of 3 mM solution of $NaClO_4{\cdot}H_2O$ in water.

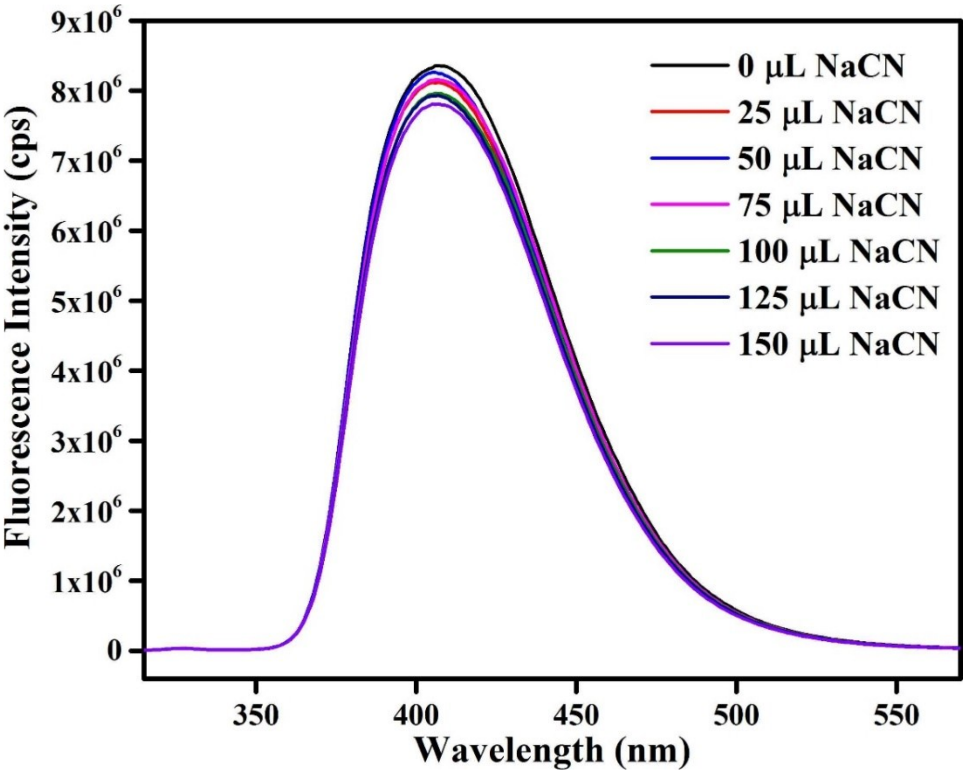

Figure S63. Luminescence quenching of **1'** dispersed in water after gradual addition of 3 mM solution of NaCN in water.

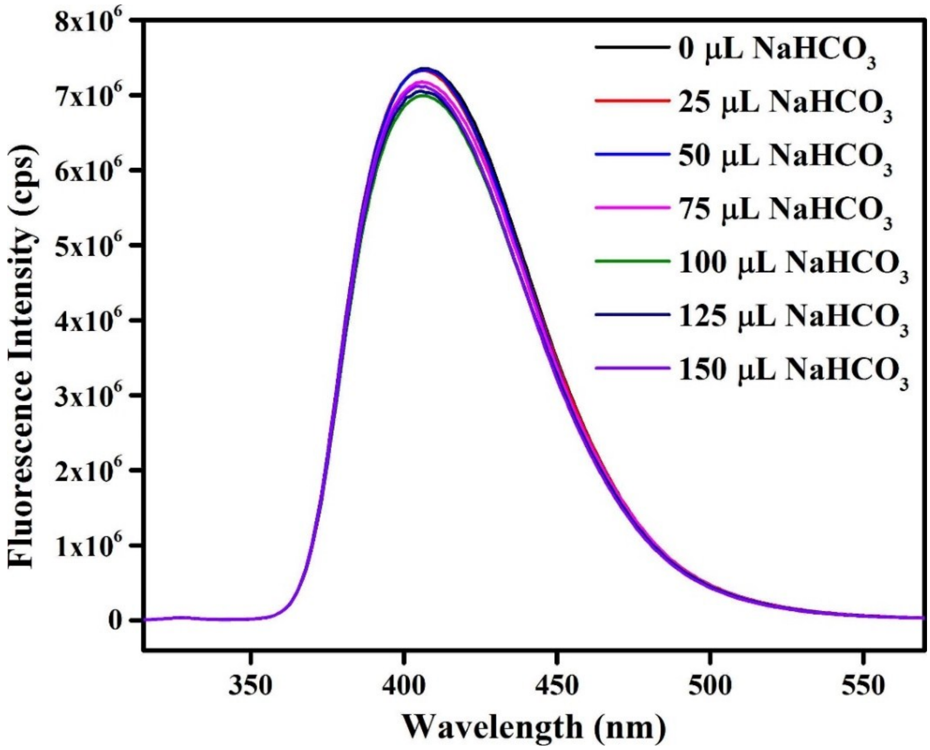

Figure S64. Luminescence quenching of **1'** dispersed in water after gradual addition of 3 mM solution of $NaHCO_3$ in water.

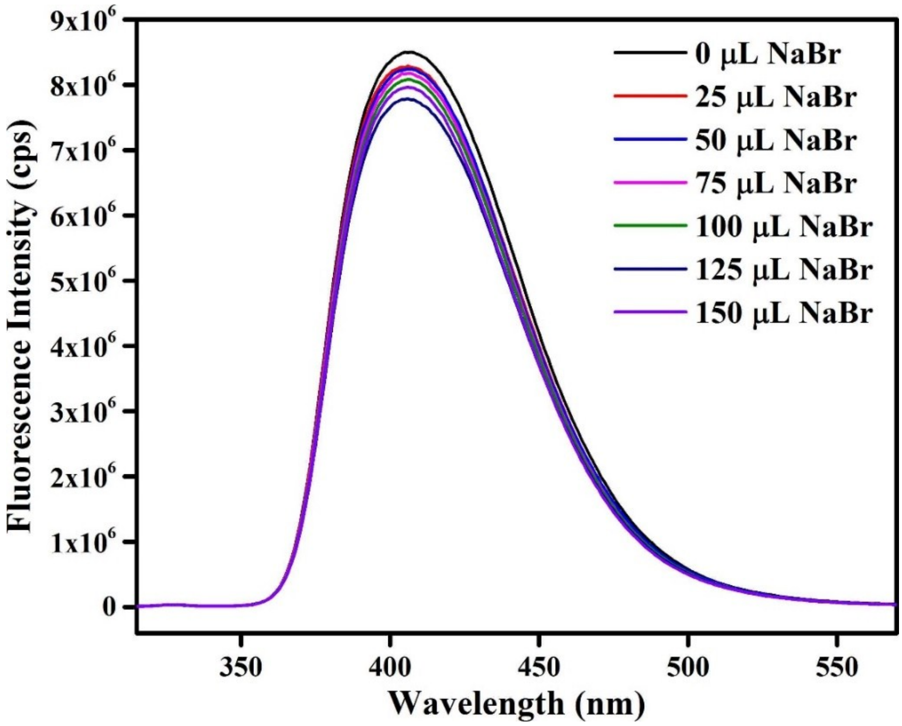

Figure S65. Luminescence quenching of **1'** dispersed in water after gradual addition of 3 mM solution of NaBr in water.

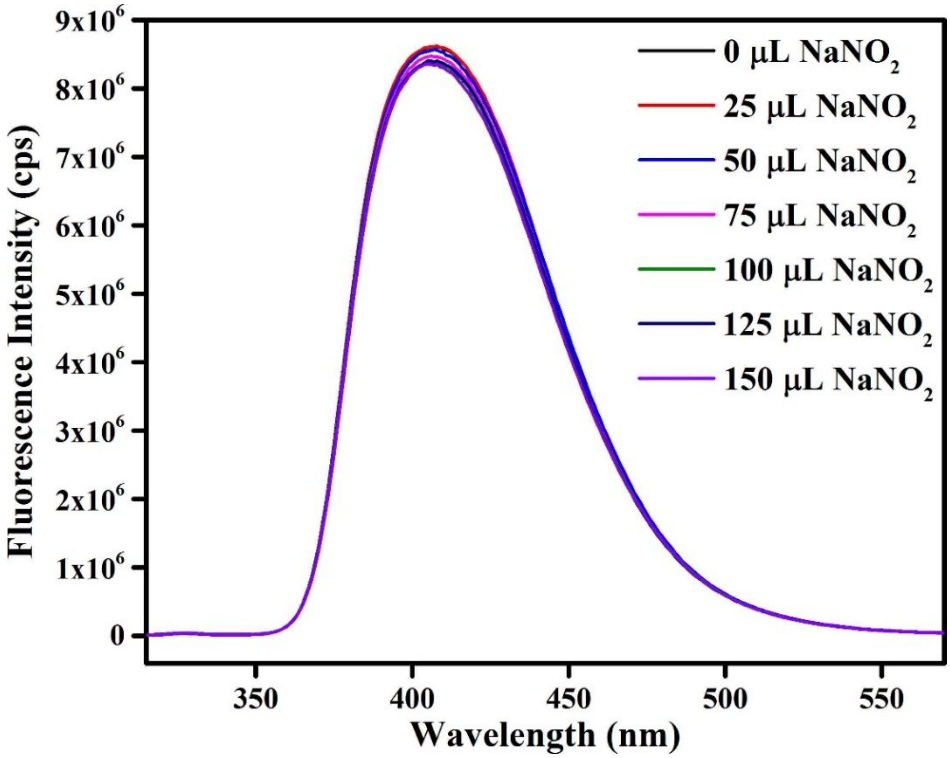

Figure S66. Luminescence quenching of **1'** dispersed in water after gradual addition of 3 mM solution of $NaNO_2$ in water.

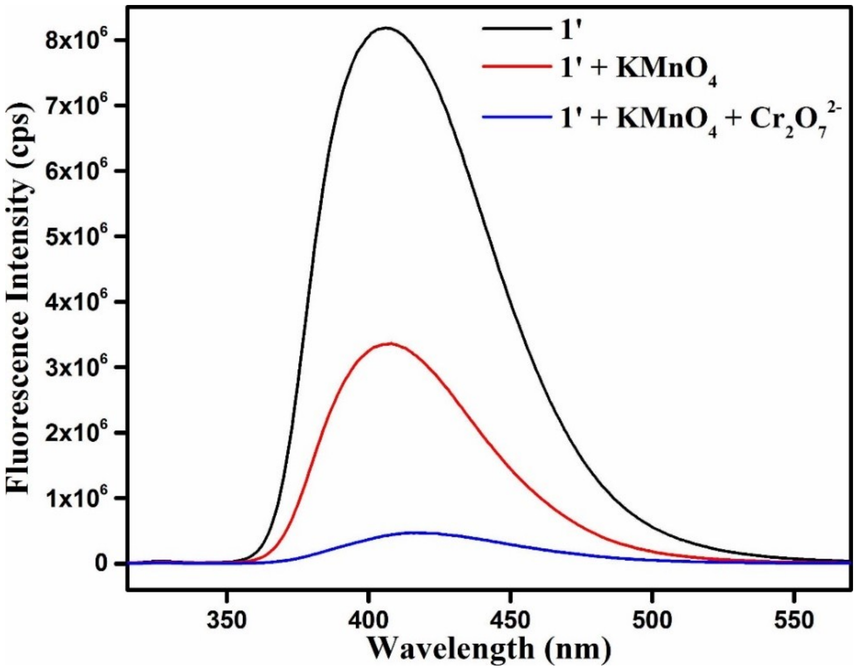

Figure S67. Luminescence quenching of **1'** dispersed in water after gradual addition of 3 mM solution of $KMnO_4$ in water (150 μL) in presence of 3 mM solution of $Cr_2O_7^{2-}$ in water (150 μL).

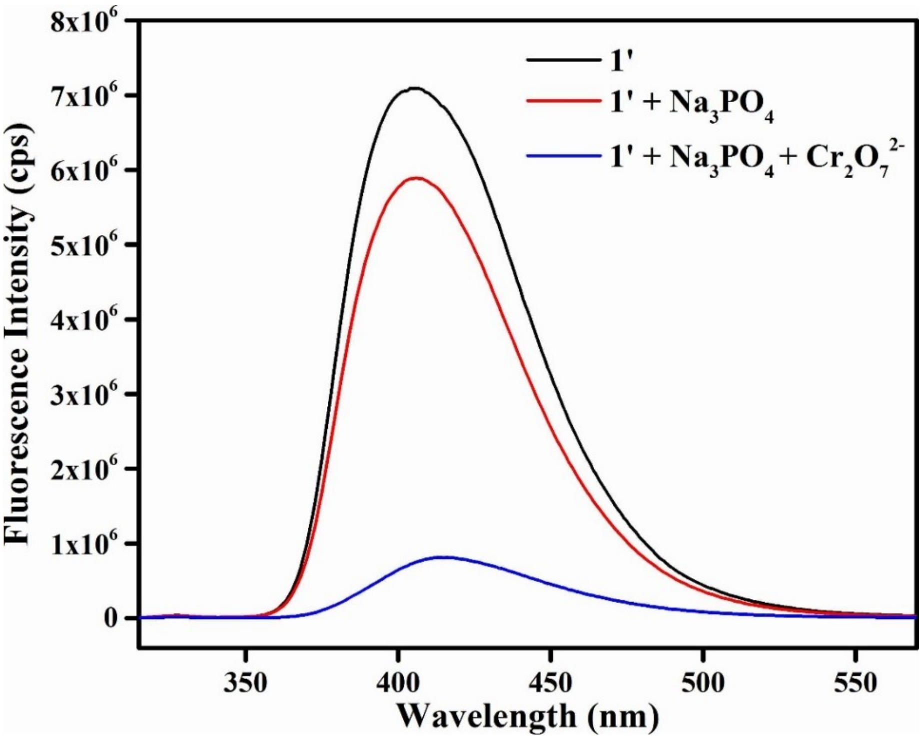

Figure S68. Luminescence quenching of **1'** dispersed in water after gradual addition of 3 mM solution of $Na_3PO_4 \cdot 12H_2O$ in water (150 μL) in presence of 3 mM solution of $Cr_2O_7^{2-}$ in water (150 μL).

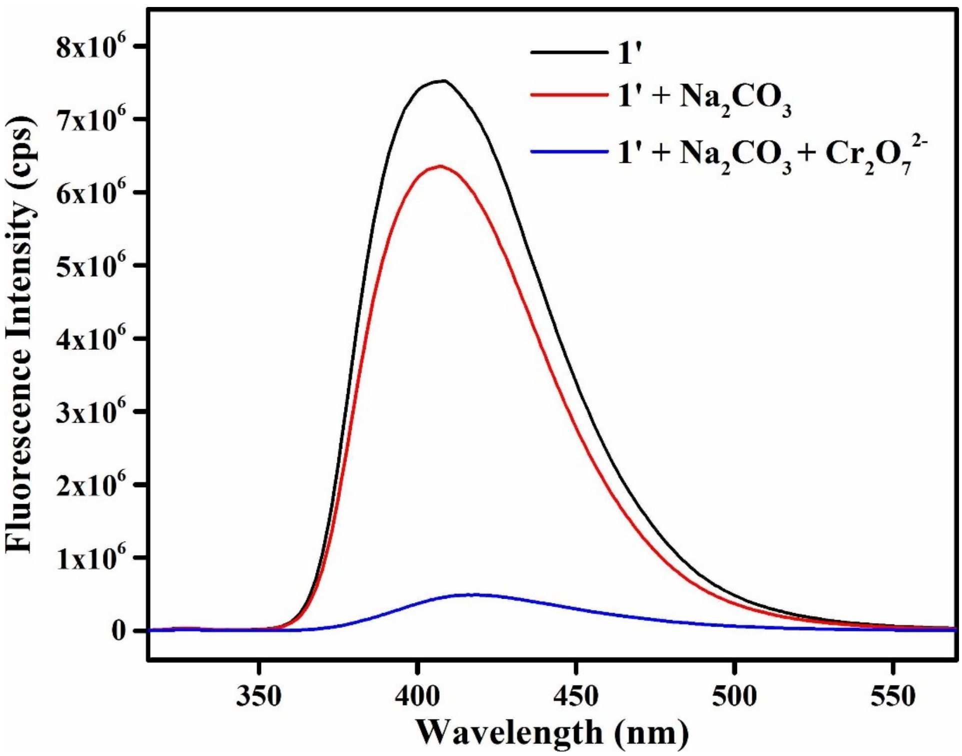

Figure S69. Luminescence quenching of **1'** dispersed in water after gradual addition of 3 mM solution of Na_2CO_3 in water (150 μL) in presence of 3 mM solution of $Cr_2O_7^{2-}$ in water (150 μL).

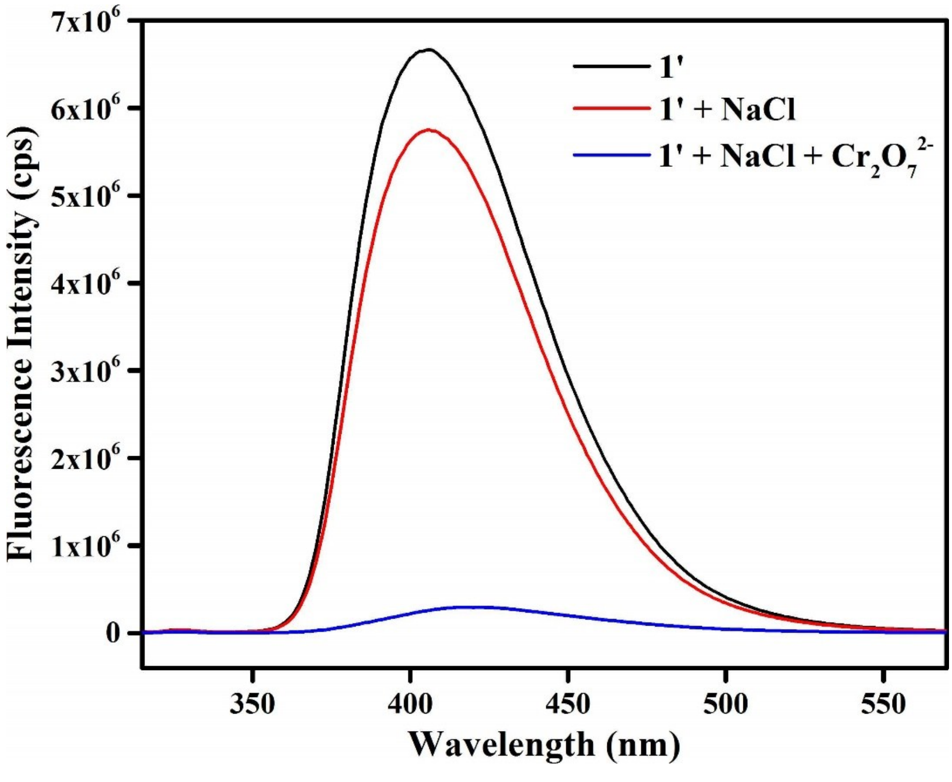

Figure S70. Luminescence quenching of **1'** dispersed in water after gradual addition of 3 mM solution of NaCl in water (150 μL) in presence of 3 mM solution of $Cr_2O_7^{2-}$ in water (150 μL).

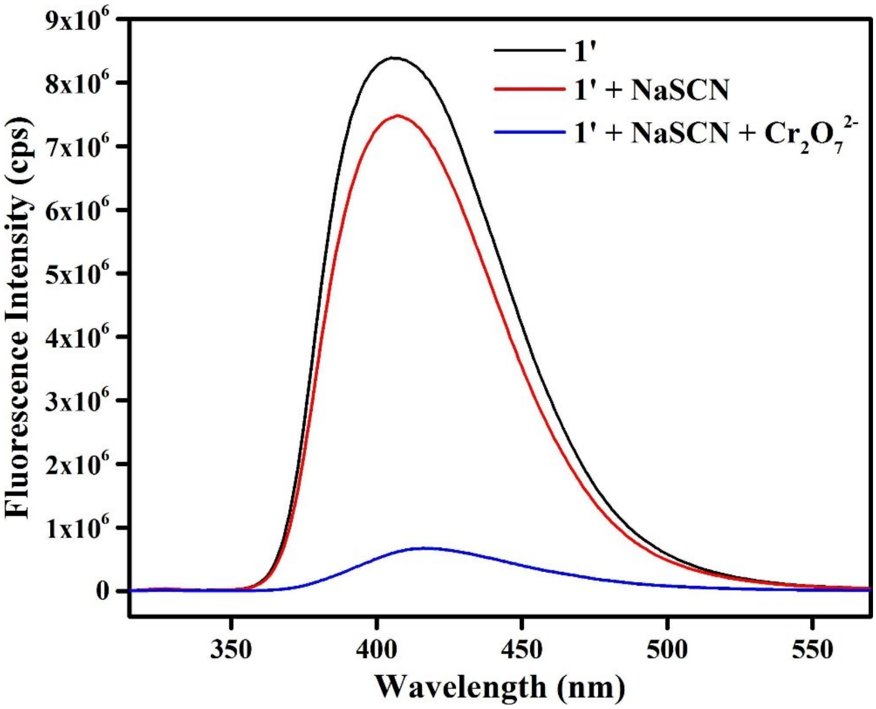

Figure S71. Luminescence quenching of **1'** dispersed in water after gradual addition of 3 mM solution of NaSCN in water (150 μL) in presence of 3 mM solution of $Cr_2O_7^{2-}$ in water (150 μL).

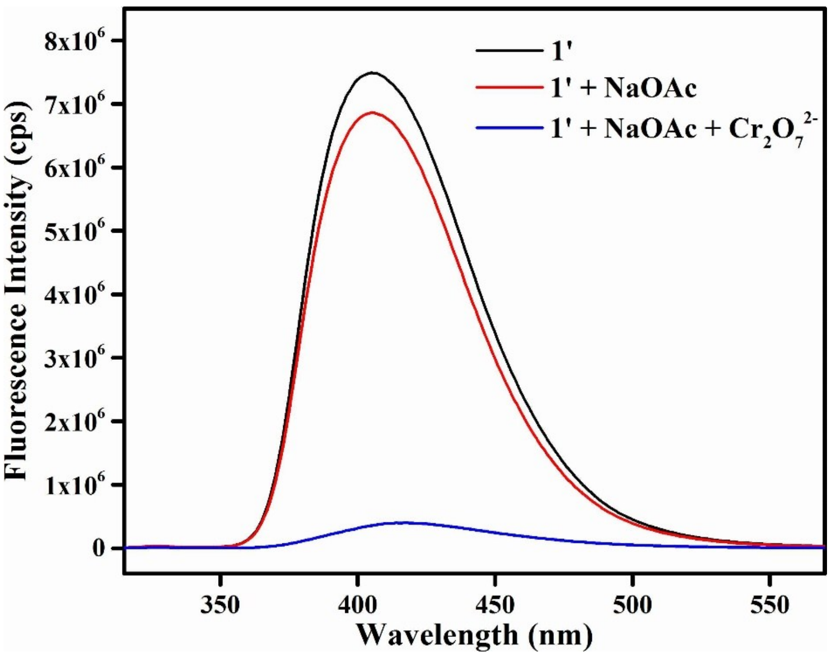

Figure S72. Luminescence quenching of **1'** dispersed in water after gradual addition of 3 mM solution of NaOAc in water (150 μL) in presence of 3 mM solution of $Cr_2O_7^{2-}$ in water (150 μL).

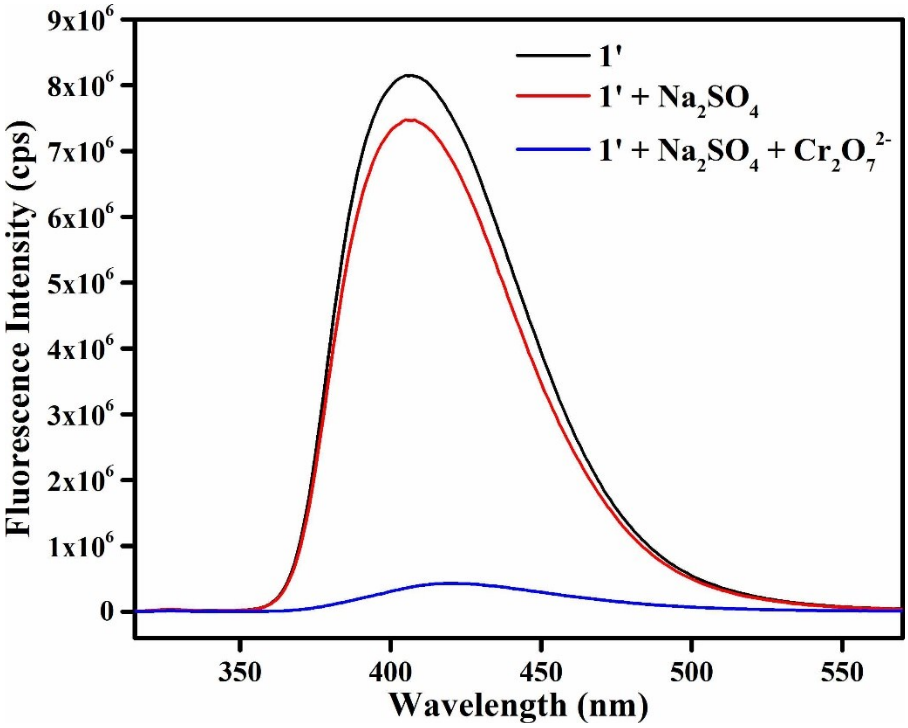

Figure S73. Luminescence quenching of **1'** dispersed in water after gradual addition of 3 mM solution of Na_2SO_4 in water (150 μL) in presence of 3 mM solution of $Cr_2O_7^{2-}$ in water (150 μL).

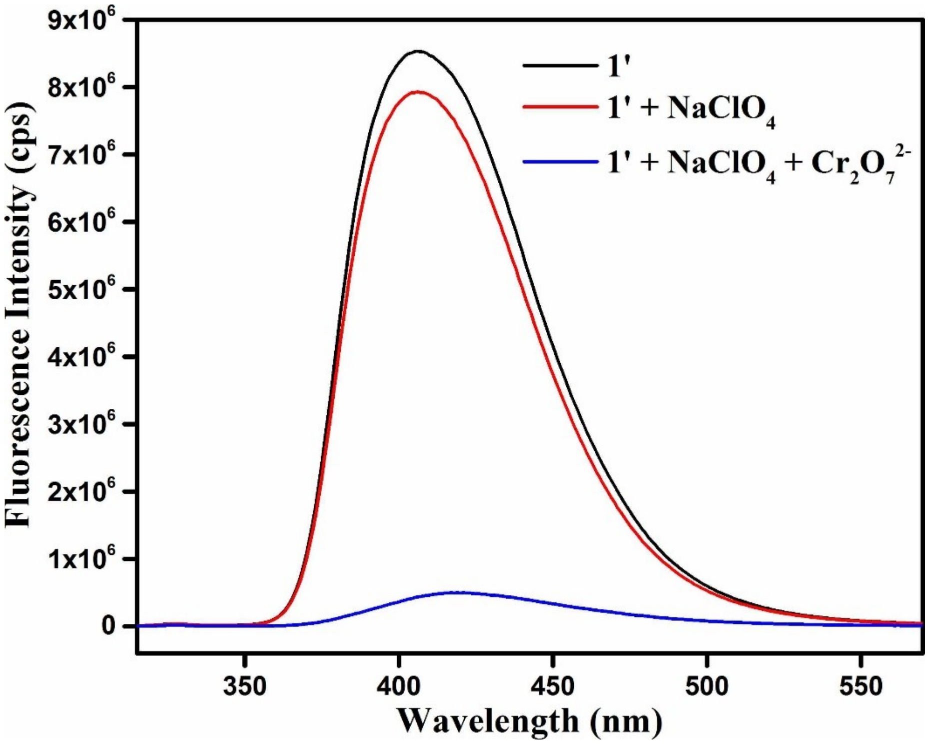

Figure S74. Luminescence quenching of **1'** dispersed in water after gradual addition of 3 mM solution of $NaClO_4 \cdot H_2O$ in water (150 μL) in presence of 3 mM solution of $Cr_2O_7^{2-}$ in water (150 μL).

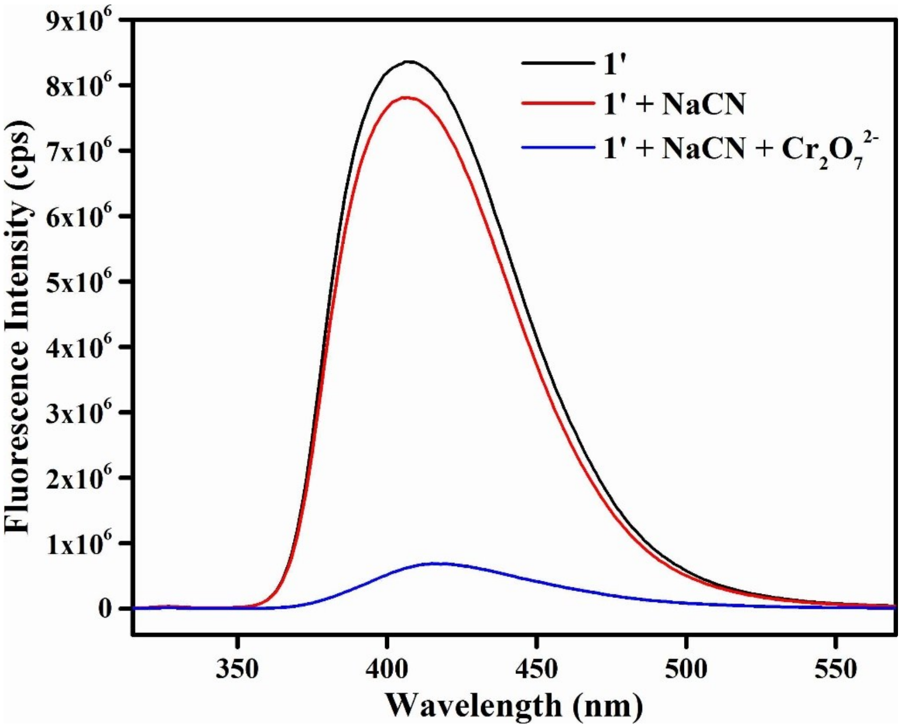

Figure S75. Luminescence quenching of **1'** dispersed in water after gradual addition of 3 mM solution of NaCN in water (150 μL) in presence of 3 mM solution of $Cr_2O_7^{2-}$ in water (150 μL).

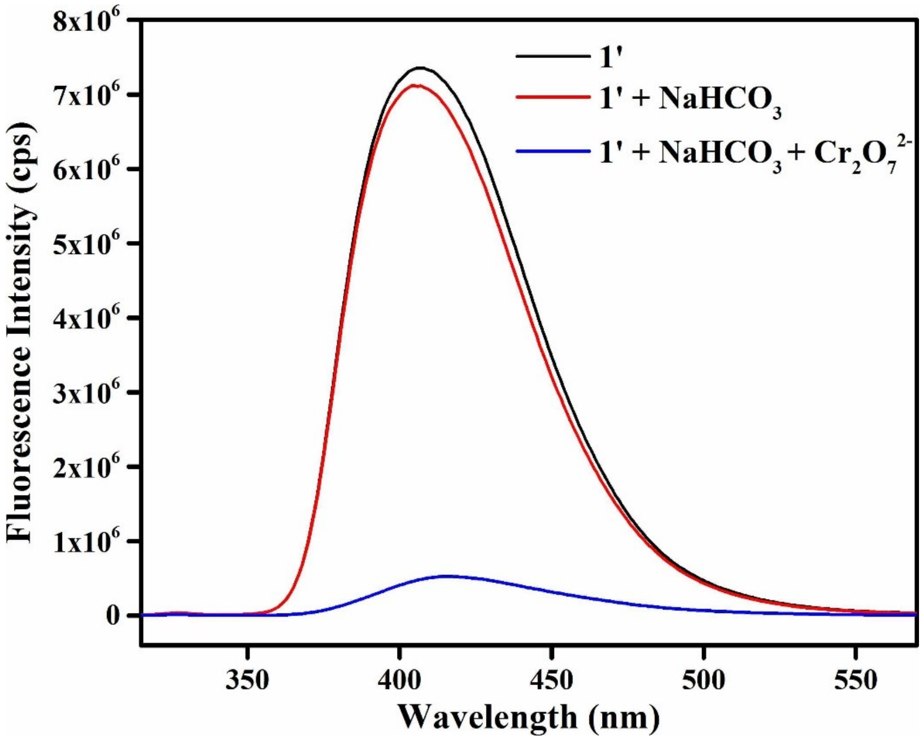

Figure S76. Luminescence quenching of **1'** dispersed in water after gradual addition of 3 mM solution of $NaHCO_3$ in water (150 μL) in presence of 3 mM solution of $Cr_2O_7^{2-}$ in water (150 μL).

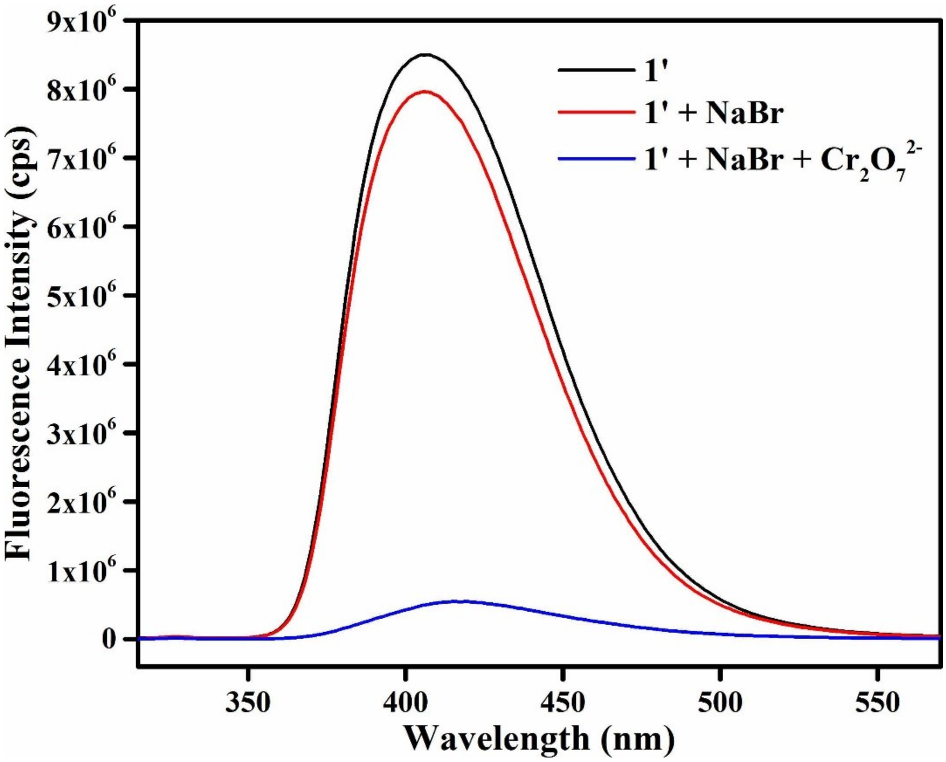

Figure S77. Luminescence quenching of **1'** dispersed in water after gradual addition of 3 mM solution of NaBr in water (150 μL) in presence of 3 mM solution of $Cr_2O_7^{2-}$ in water (150 μL).

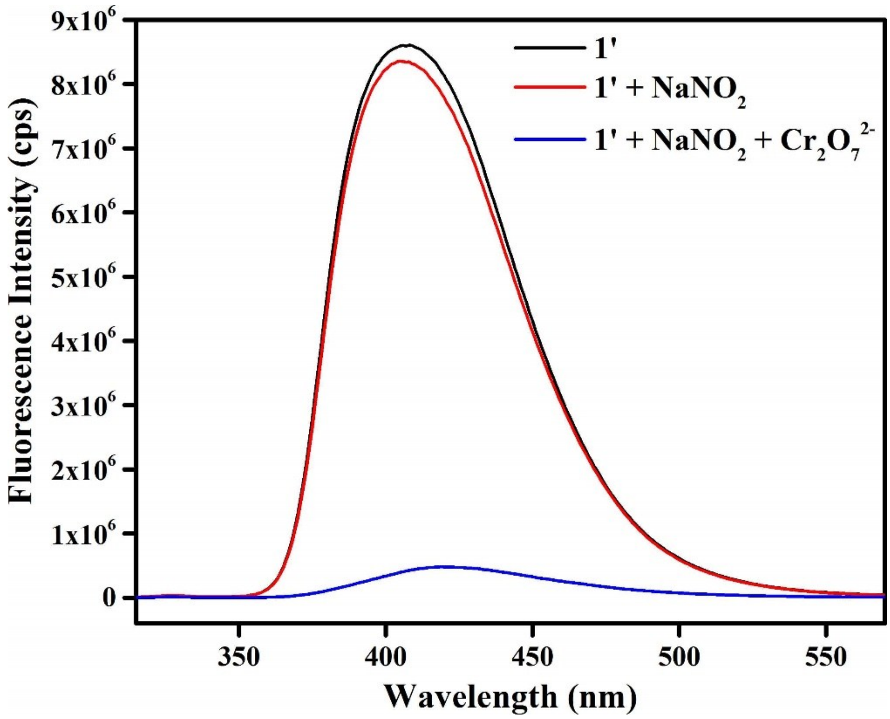

Figure S78. Luminescence quenching of **1'** dispersed in water after gradual addition of 3 mM solution of $NaNO_2$ in water (150 μL) in presence of 3 mM solution of $Cr_2O_7^{2-}$ in water (150 μL).

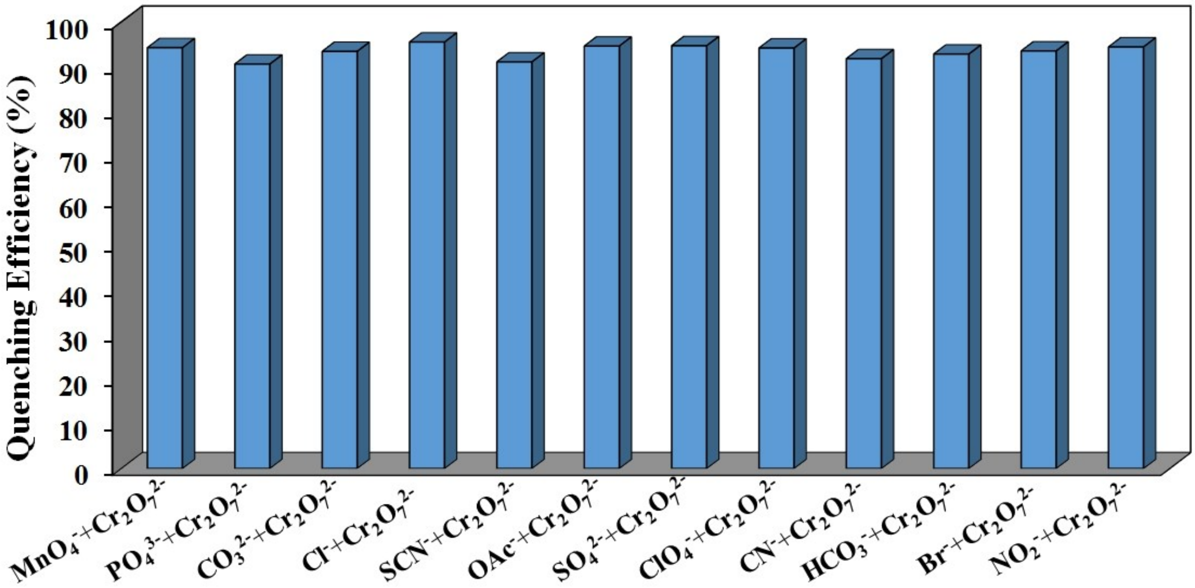

Figure S79. Quenching efficiencies of **1'** after addition of equal amounts of other anions and $Cr_2O_7^{2-}$ ion.

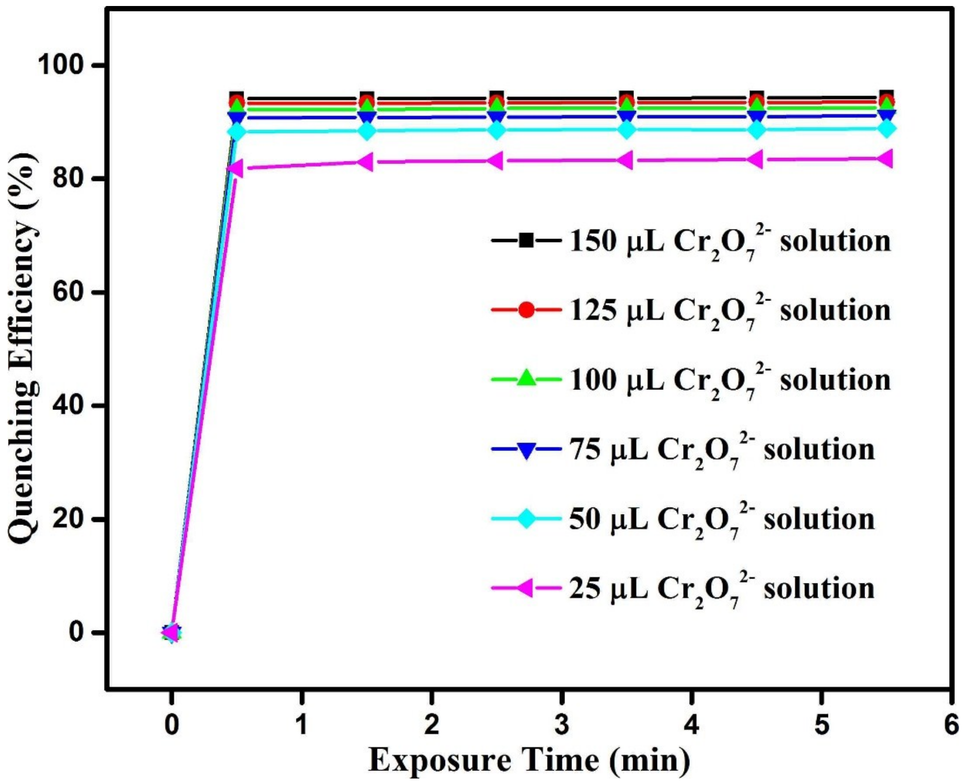

Figure S80. Quenching efficiencies of **1'** after addition of 3 mM $Cr_2O_2^{2-}$ as a function of exposure time in water.

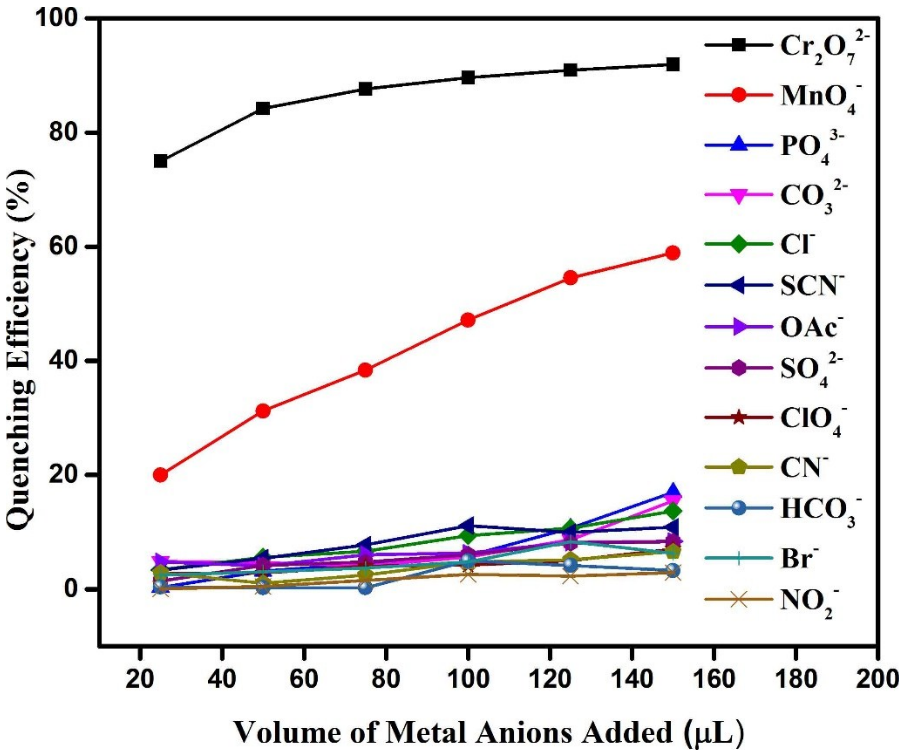

Figure S81. Change of quenching efficiency (%) after addition of different volumes of 3 mM different metal anions.

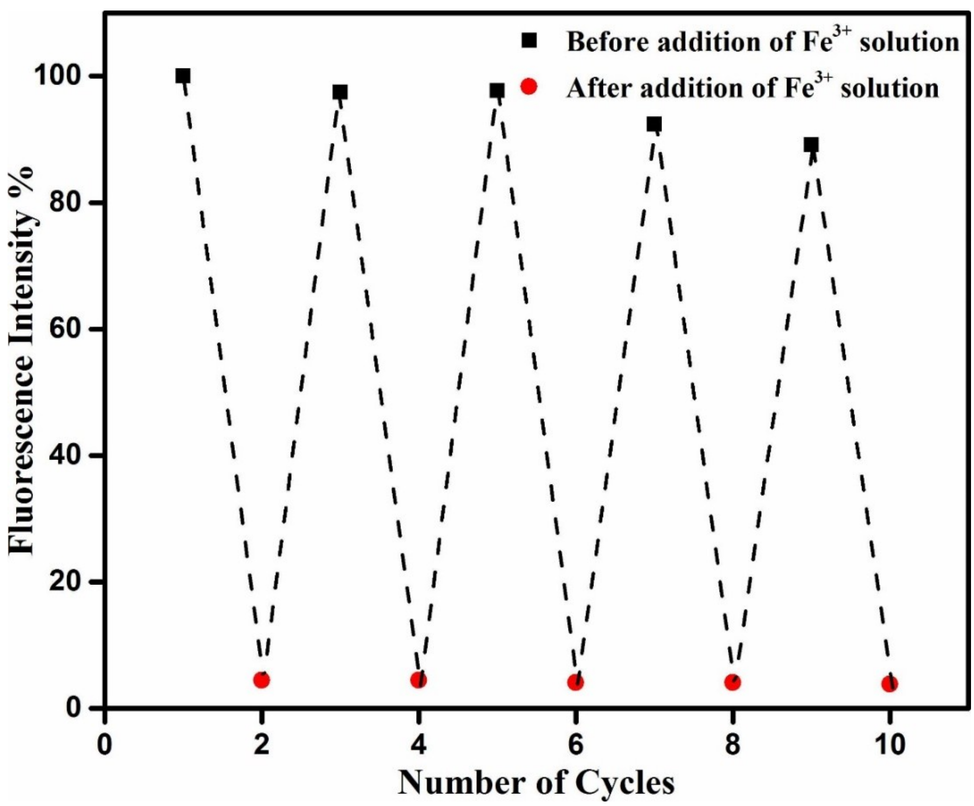

Figure S82. Reproducibility test for the aqueous suspension of **1'** towards sensing of Fe^{3+} ion.

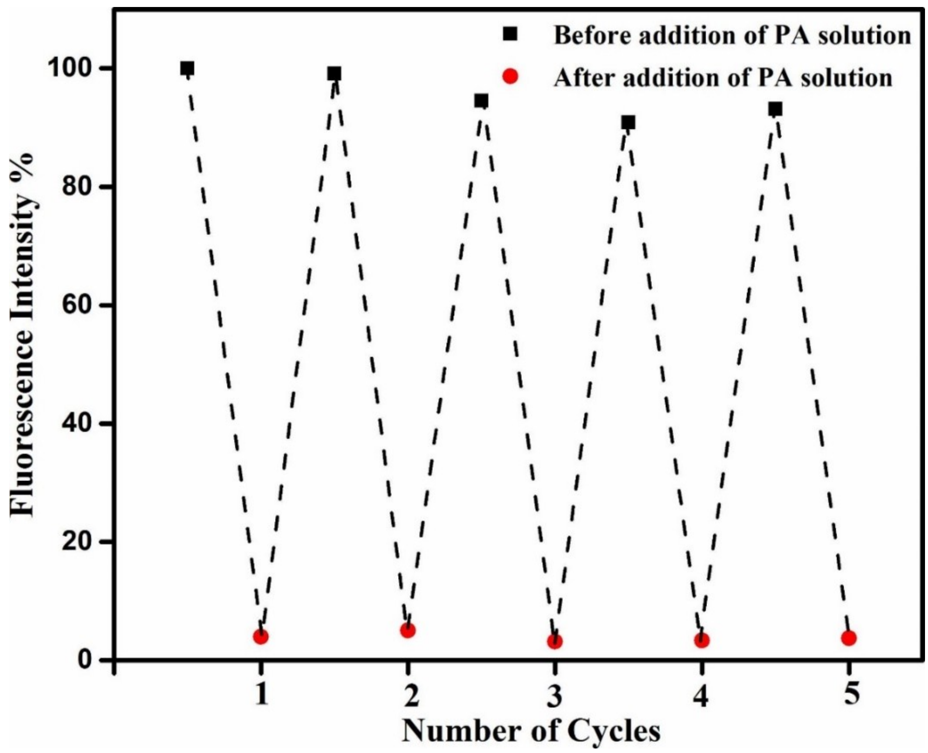

Figure S83. Reproducibility test for the aqueous suspension of **1'** towards sensing of PA.

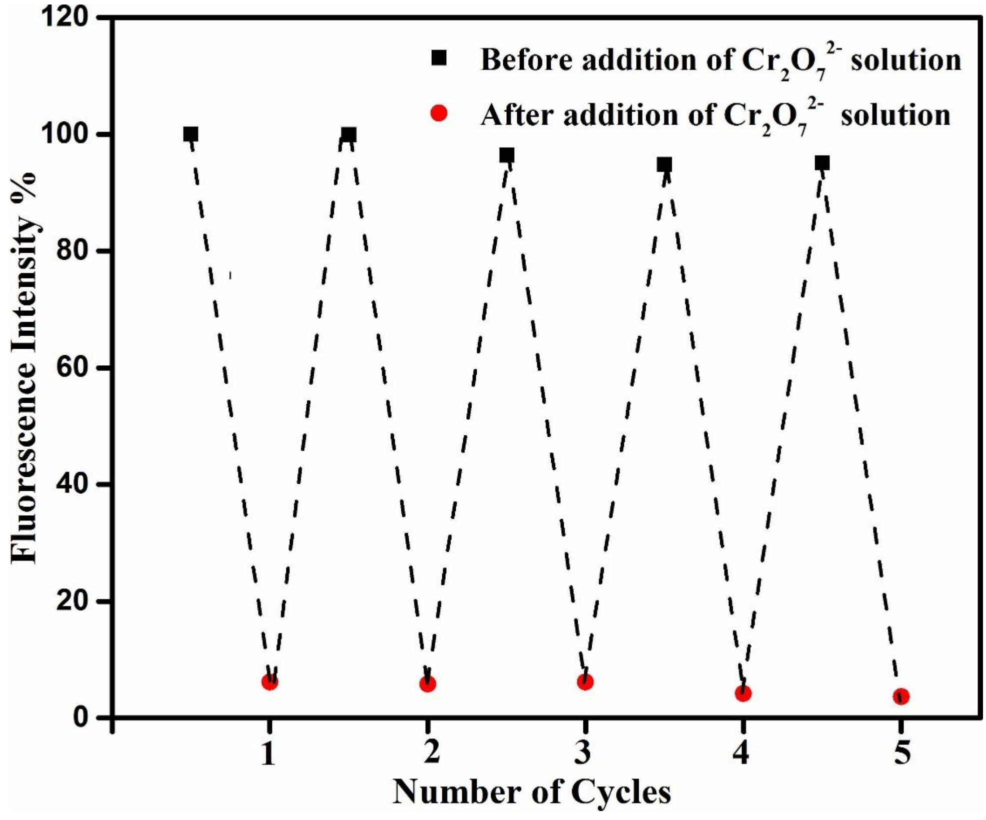

Figure S84. Reproducibility test for the aqueous suspension of **1'** towards sensing of $Cr_2O_7^{2-}$ ion.

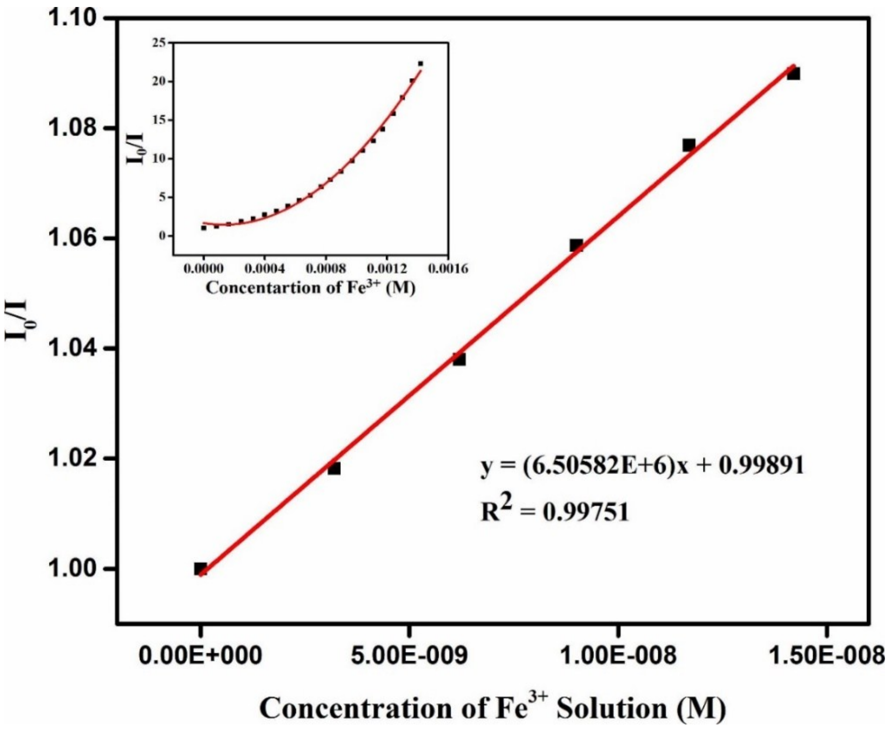

Figure S85. S-V plot for the quenching of **1'** at lower concentrations of Fe^{3+} ion in water. Inset: non linearity of the S-V plot at higher concentrations of Fe^{3+} ion.

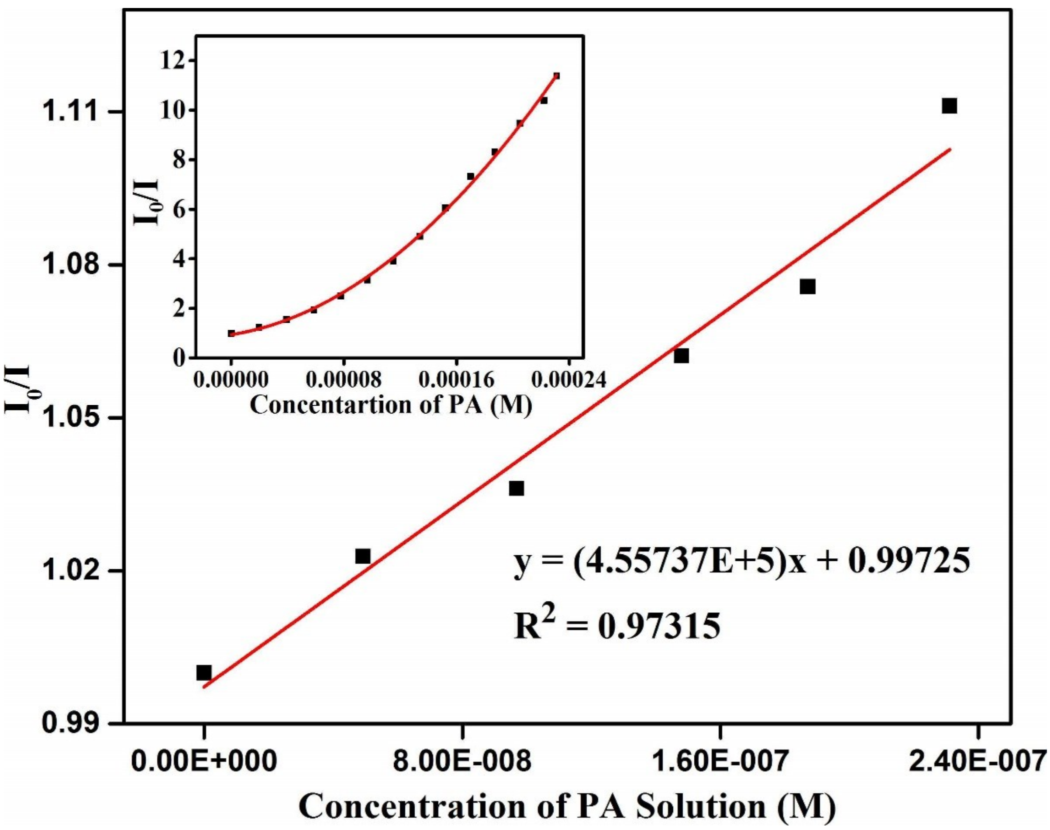

Figure S86. S-V plot for the quenching of **1'** at lower concentrations of PA in DMSO. Inset: non linearity of the S-V plot at higher concentrations of PA.

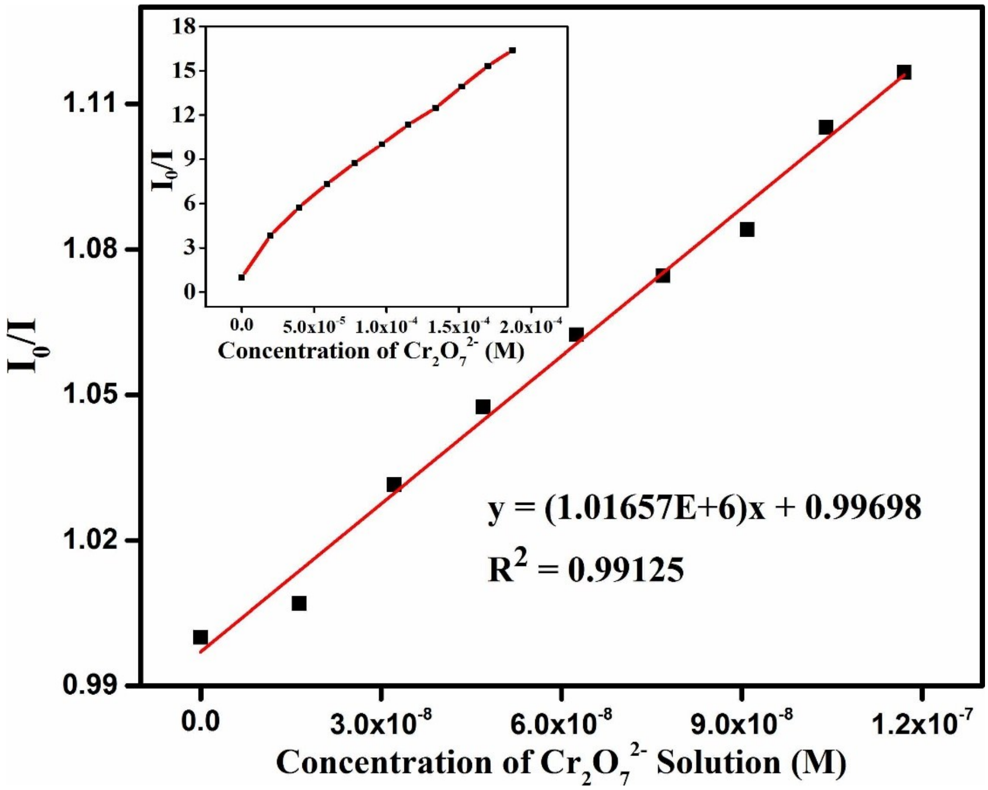

Figure S87. S-V plot for the quenching of **1'** at lower concentrations of $Cr_2O_7^{2-}$ ion in water. Inset: non linearity of the S-V plot at higher concentrations of $Cr_2O_7^{2-}$ ion.

Table S2. A comparison of the Stern-Volmer constant (K_{sv}), detection limit and medium used for Fe^{3+} detection for some MOFs already reported till date.

Sl. No.	MOF	K_{sv} (M^{-1})	Detection Limit	Medium Used	Ref.
1.	$[Zr_6(\mu_3\text{-}O)_4(\mu_3\text{-}OH)_4(OH)_4(H_2O)_4(L)_2]$	6.51×10^6	9.29×10^{-9} M	water	this work
2.	Eu^{3+}@MIL-124	3.87×10^4	0.28×10^{-6} M	water	2
3.	$[Zn(QDA)]\cdot0.3DMF\cdot0.2H_2O$	1.12×10^6	2.30×10^{-8} M	methanol	3
4.	$[(CH_3)_2NH_2]\cdot[Tb(bptc)]\cdot x$solvents	-	1.80×10^{-5} M	ethanol	4
5.	$(NH_2(CH_3)_2)[Zn_4(ddn)_2(COO)(H_2O)_4$	1.13×10^4	1.24 ppm	water	5
6.	$[La(TPT)(DMSO)_2]\cdot H_2O$	1.36×10^4	-	ethanol	6
7.	$[H(H_2O)_8][DyZn_4(imdc)_4(im)_4]$	2.88×10^4	-	DMSO	7
8.	$[Zr_6O_4(OH)_4(2,7\text{-}CDC)_6]\cdot 19H_2O\cdot2DMF$	5.5×10^3	9.10×10^{-7} M	water	8

9.	$[Zr_6O_6(OH)_2(CF_3COO)_2(C_{11}H_5NO_4)_4(H_2O)_4]$	2.25×10^7	1.7×10^{-9} M	water	9
10.	$[Zr_6O_6(OH)_2(CF_3COO)_2(C_{11}H_5NO_4)_4(H_2O)_4]$	1.91×10^7	2.7×10^{-9} M	HEPES buffer	9
11.	$[Al(OH)(BDC\text{-}N_3)]\cdot 1.2H_2O\cdot 0.3DMF$	6.13×10^3	3×10^{-8} M	water	10
12.	[Zn(*p*-CNPhHIDC)(4,4'-bipy)]	1.37×10^3	5×10^{-3} M	water	11
13.	EuL_3	4.1×10^3	10^{-4} M	ethanol	12
14.	$[Eu_2(MFDA)_2(HCOO)_2(H_2O)_6]\cdot H_2O$	-	3.3×10^{-7} M	DMF	13
15.	$[Cd(H_2La)0.5(H_2L_b)0.5(H_2O)]$	-	10^{-5} M	water	14
16.	$[Ln_2(Ccbp)_3\cdot 6H_2O]\cdot 3Cl^-\cdot 4H_2O$	1.143×10^5	-	ethanol	15
17.	[Cd(*p*-CNPhHIDC)(4,4'-bipy)$_{0.5}$]	1.99×10^3	5×10^{-3} M	water	11
18.	$[Tb(BTB)(DMF)]\cdot 1.5DMF\cdot 2.5H_2O$	-	10^{-5} M	ethanol	16
19.	$[Tb_4(OH)_4(DSOA)_2(H_2O)_8]\cdot(H_2O)_8$	3.5×10^4	-	water	17
20.	$[Ln(Hpzbc)_2(NO_3)]\cdot H_2O$	-	2.6×10^{-5} M	ethanol	18
21.	FJI-C8	8.245×10^3	0.0233 mM	DMF	19
22.	$[Eu_2L_3(DMF)]\cdot 2DMF$	6×10^5	0.793 µM	water	20
23.	$[Cd_2(L)(bimid)(DMF)_2]\cdot(DMF)$	3.75×10^4	3.70 × 10^{-7} M	DMF	21
24.	$[Zn_2(TCPP)(DMF)_2]$	1.08×10^4	-	ethanol	1

Table S3. A comparison of the Stern-Volmer constant (K_{sv}), detection limit and medium used for PA detection for some MOFs already reported till date.

Sl. No.	MOF	K_{sv} (M^{-1})	Detection Limit	Medium Used	Ref.
1.	$[Zr_6(\mu_3\text{-}O)_4(\mu_3\text{-}OH)_4(OH)_4(H_2O)_4(L)_2]$	4.56×10^5	5.72×10^{-8} M	DMSO	this work
2	$[[Cd(ATAIA)]\cdot 4H_2O]_n$	1.59×10^7	0.94×10^{-9} M	water	22
3.	EuNDC	3.22×10^4	1.64×10^{-7} M	water	23

4.	AHU-TW1 AHU-TW3 AHU-TW4 AHU-TW6	1.44×10^{4} 1.48×10^{4} 5.0×10^{4} 5.31×10^{4}	4.05×10^{-6} M 3.94×10^{-6} M 1.16×10^{-6} M 1.10×10^{-6} M	DMF	24
5.	$[Zr_6O_4(OH)_4(BTDB)_6]\cdot8H_2O\cdot$ 6DMF	2.49×10^{4}	1.63×10^{-6} M	methanol	25
6.	$[Cd_5Cl_6(L)(HL)_2]\cdot7H_2O$	4.05×10^{4}	1.87×10^{-7} M	ethanol	26
7.	[Tb(1,3,5-BTC)]	3.41×10^{4}	8.1×10^{-8} M	ethanol	27
8.	$Zr_6O_4(OH)_4(L)_6$	2.9×10^{4}	2.6×10^{-6} M	water	28
9.	$[Cd(NDC)_{0.5}(PCA)]_n$	3.5×10^{4}	-	acetonitrile	29
10.	$[La(TPT)(DMSO)_2]\cdot H_2O$	9.89×10^{4}	-	ethanol	6
11.	$[[CuL(I)].DMF.H_2O]_n$	1.51×10^{5}	215 ppb	acetonitrile	30
12.	BUT-12 BUT-13	3.1×10^{5} 5.1×10^{5}	23 ppb 10 ppb	water	31
13.	$[Zn_2(NDC)_2(bpy)].Gx$	0.4×10^{4}	-	ethanol	32
14.	$[Zn_8(ad)_4(BPDC)_6$ $(0.2Me_2NH_2)]\cdot G$	4.6×10^{4}	12.9×10^{-6} M	water	33
15.	$[Zr_6O_4(OH)_6(L)_6]n$	5.8×10^{4}	0.4 ppm	water	34
16.	$[Cd_3(TPT)_2(DMF)_2]$ $\cdot0.5H_2O]_n$	6.56×10^{4}	-	ethanol	35
17.	$[Zn_2(L)_2(dpyb)]_n$ $[Zn(L)(dipb)](H_2O)_2$	2.40×10^{4} 2.46×10^{4}	- -	DMA	36
18.	TB-Zn-CP	4.37×10^{4}	23 ppb	water	37
19.	$[Pr_2(TATMA)_2\cdot4DMF\cdot4H_2O]_n$	1.6×10^{4}	-	DMF	38
20.	$[[Zn(C_{34}H_{18}O_8)_{0.5}(C_{20}N_2H_{16})_{0.5}]$ $[0.5(C_{20}N_2H_{16})]]_n$	8.1×10^{4}	-	DMF	39
21.	$[Zn(NDC)H_2O)]_n$ $[Cd(NDC)(H_2O)]_n$	6×10^{4} 2.385×10^{4}	1×10^{-6} M 4×10^{-6} M	water	40
22.	$[Zn_4(DMF)(Ur)_2(2,6\text{-}NDC)_4]_n$	10.83×10^{4}	1.63 ppm	water	41

23.	H_2ATAIA $H_2AMTAIA$ $H_2DMTAIA$	1.759×10^5 9.875×10^4 1.646×10^4	120 ppb 0.8 ppm 1.2 ppm	water	42
24.	$[Zn_2(TCPP)(DMF)_2]$	3.59×10^4	-	ethanol	1

Table S4. A comparison of the Stern-Volmer constant (K_{sv}), detection limit and medium used for $Cr_2O_7^{2-}$ detection for some MOFs already reported till date

Sl. No	MOF	K_{sv} (M^{-1})	Detection Limit	Medium Used	Ref.
1.	$[Zr_6(\mu_3\text{-}O)_4(\mu_3\text{-}OH)_4(OH)_4(H_2O)_4(L)_2]$	1.02×10^6	2.88×10^{-8} M	water	this work
2.	JLU-MOF60	5.91×10^4	3.78×10^{-7} M	water	43
3.	JLU-MOF50	4.99×10^4	-	water	44
4.	$[(CH_3)_2NH_2]_6[Cd_3L(H_2O)_2]\cdot12H_2O$	9.19×10^5	-	water	45
5.	NUM-5	9.4×10^4	0.7 ppm	water	46
6.	$[Cd(TIPA)_2(ClO_4^-)_2]\cdot(DMF)_3(H_2O)$	7.15×10^4	8 ppb	water	47
7.	$[Cd(L)(TPOM)_{0.75}]$.xS	1.35×10^4	-	water	48
8.	$[Zn(L)(BBI)\cdot(H_2O)_2]$	1.17×10^4	-	water	48
9.	$[Zn_2(TPOM)(NDC)_2]\cdot3.5H_2O$	9.21×10^4	2.35×10^{-6} M	water	49
10.	BUT-28	1.02×10^5	36 ppb	water	50
11.	534-MOF-Tb	1.37×10^4	0.14×10^{-3} M	water	51
12.	$[Eu(ipbp)_2(H_2O)_3]Br_6H_2O$	8.98×10^3	5.16×10^{-6} M	water	52
13.	$[Zn_2(tpeb)_2(2,3\text{-}ndc)_2]\cdot H_2O\}_n$	-	2.531 ppb	water	53
14.	MOR-2	-	4 ppb	water	54
15.	Zn-MOF-1	2.07×10^4	3.53×10^{-6} M	water	55
16.	$\{[Zn(L)(bpp)]\cdot DMF\}_n$ $\{[Zn(L)(bpe)]\cdot DMF\}_n$	2.78×10^3 7.91×10^3	3.52×10^{-6} M 4.28×10^{-6} M	DMF	56
17.	$[Eu(L)(HCOO)(H_2O)]_n$	2.76×10^4	1.0×10^{-6} M	water	57

	$[Tb(L)(HCOO)(H_2O)]_n$	2.13×10^4	2.1×10^{-6} M		
18.	Eu-MOF	1.55×10^4	9.2×10^{-6} M	water	58
19.	Eu^{3+}@MIL-121	4.34×10^3	5.4×10^{-8} M	water	59
20.	$[Zn_7(TPPE)_2(SO_4^{2-})_7](DMF\cdot H_2O)$	1.09×10^4	26.98 ppb	water	60
21.	$[Tb(TATAB)(H_2O)_2]\cdot NMP$	1.11×10^4	-	water	61
22.	$[Zn_3(tza)_2(\mu_2\text{-}OH)_2(H_2O)_2]H_2O$	5.02×10^3	10^{-6} M	water	62
23.	$[Zn(btz)]_n$ $[Zn_2(ttz)H_2O]_n$	3.19×10^3 2.19×10^3	2×10^{-6} M 2×10^{-5} M	water	63
24.	$[Eu(Himdc)(ina)(H_2O)]_n$	2.46×10^3	-	water	64
25.	$[Eu_2(H_2O)(DCPA)_3]_n$	8.7×10^3	1.09×10^{-4} M	water	65
26.	BUT-39	1.57×10^3	1.5×10^{-6} M	water	66

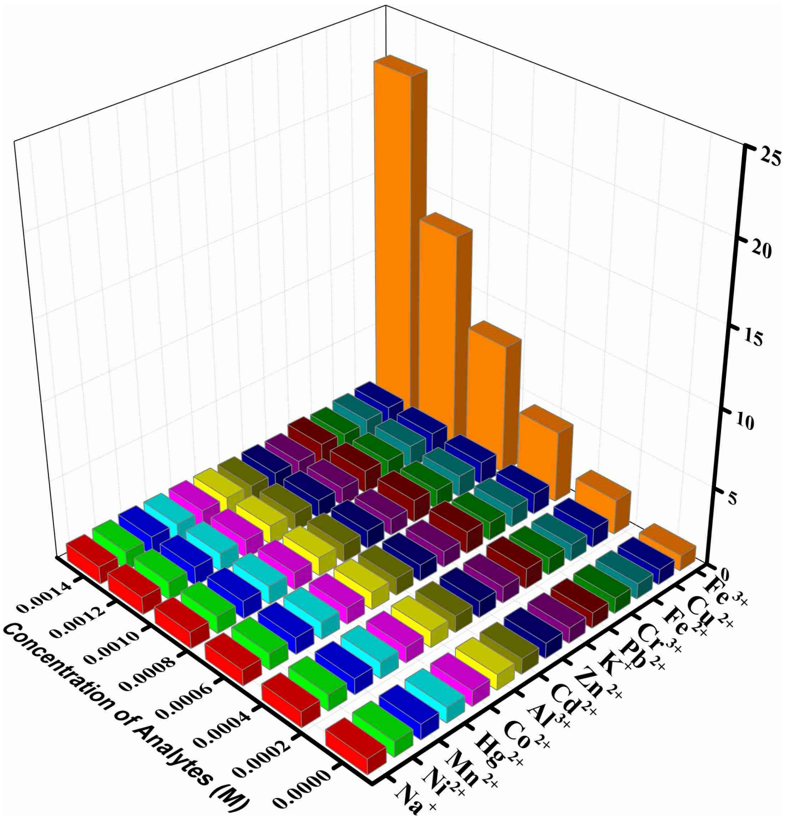

Figure S88. 3D S-V plots for the quenching of **1′** upon the addition of various concentrations of different metal cations.

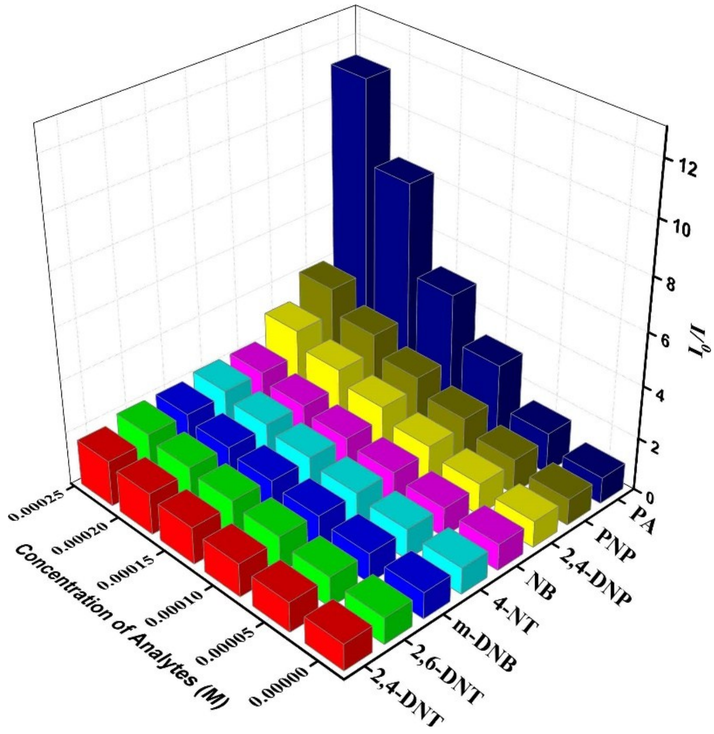

Figure S89. 3D S-V plots for the quenching of **1′** upon the addition of various concentrations of different NAEs.

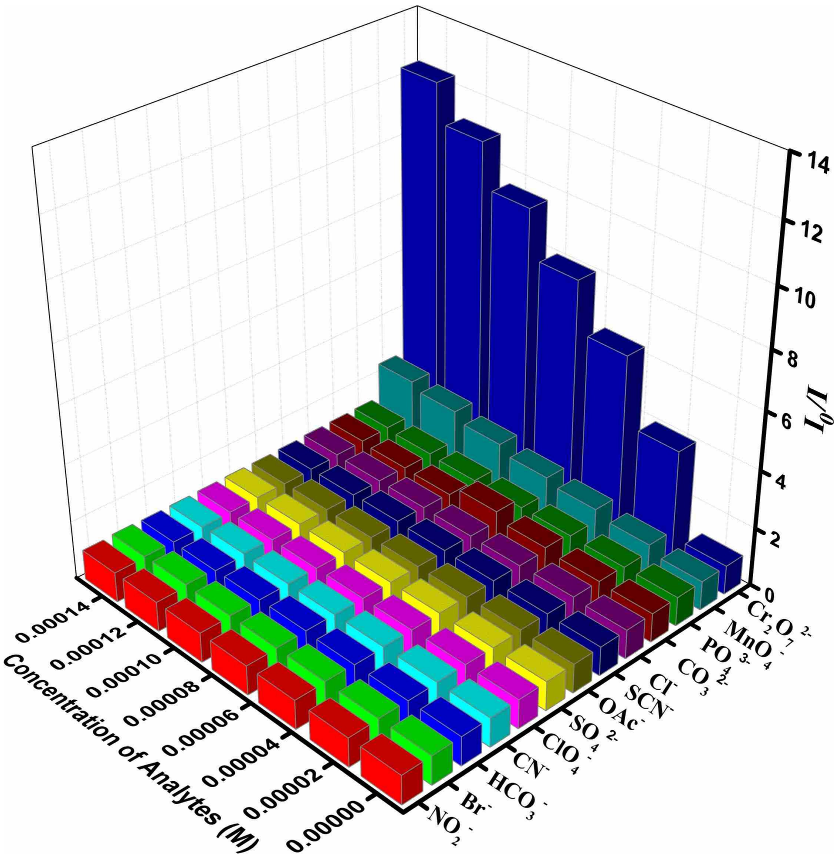

Figure S90. 3D S-V plots for the quenching of **1′** upon the addition of various concentrations of different metal anions.

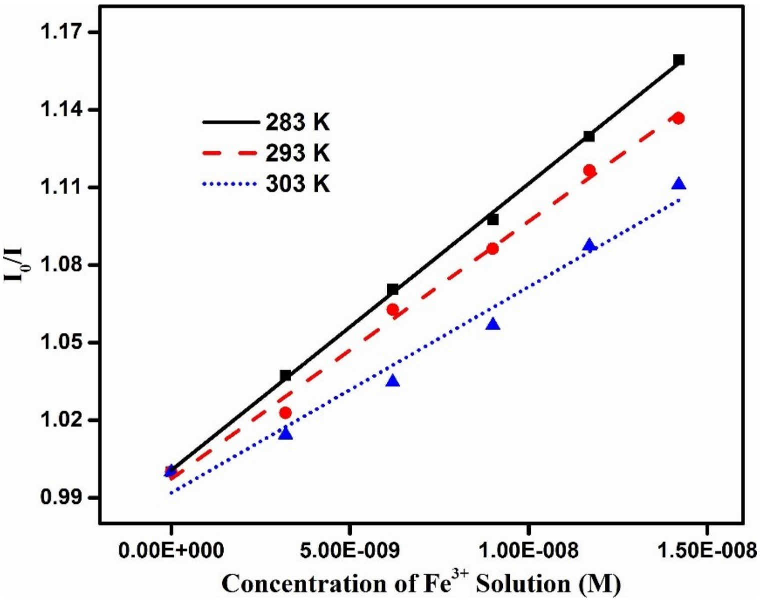

Figure S91. S-V plots at different temperatures for quenching of **1′** by Fe^{3+} solution.

Table S5. Liner regression analysis of the S-V plots (Figure S91) at different temperatures for quenching of **1′** by Fe^{3+} solution.

T (K)	K_{sv} (M^{-1}) ×10^6	R^2
283	11.083	0.99904
293	9.952	0.99342
303	7.967	0.97185

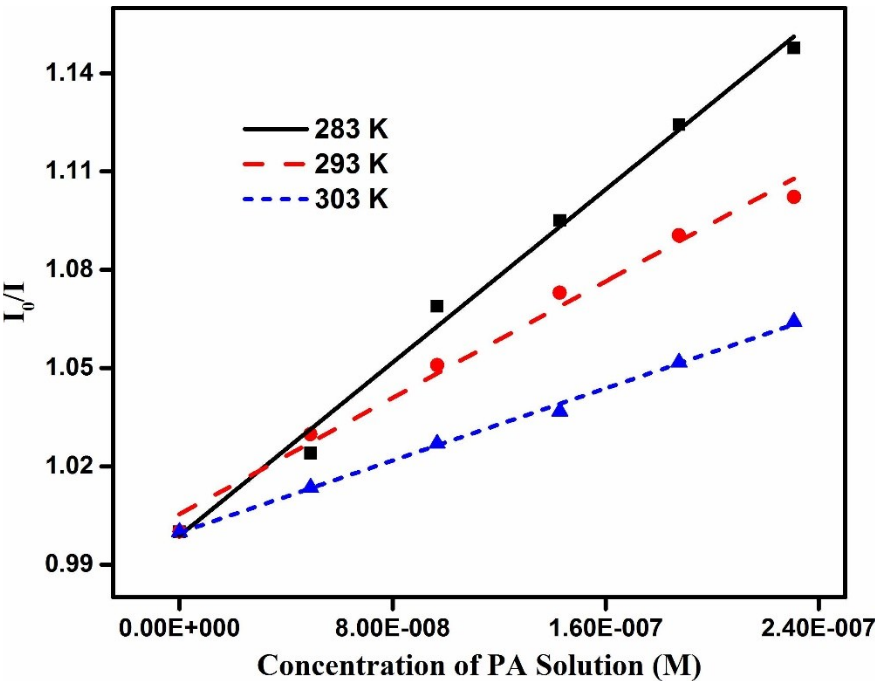

Figure S92. S-V plots at different temperatures for quenching of **1′** by PA solution.

Table S6. Liner regression analysis of the S-V plots (Figure S92) at different temperatures for quenching of **1′** by PA solution.

T (K)	K_{sv} (M^{-1})×10^5	R^2
283	6.606	0.99158
293	4.443	0.98416
303	2.756	0.99693

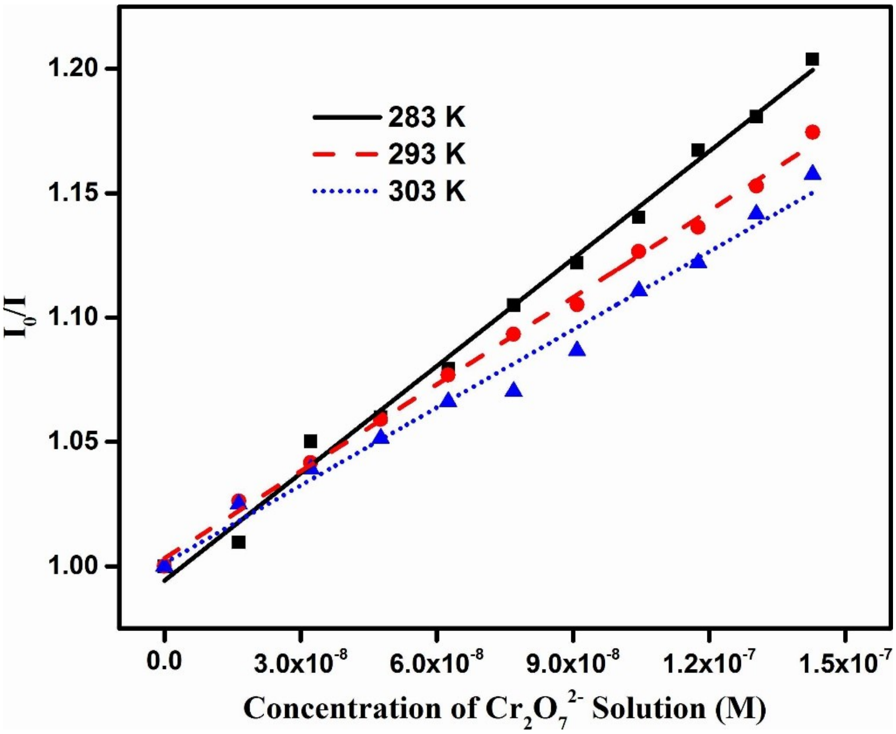

Figure S93. S-V plots at different temperatures for quenching of **1′** by $Cr_2O_7^{2-}$ solution.

Table S7. Liner regression analysis of the S-V plots (Figure S93) at different temperatures for quenching of **1′** by $Cr_2O_7^{2-}$ solution.

T (K)	K_{sv} (M^{-1})×10^6	R^2
283	1.438	0.99320
293	1.164	0.99669
303	1.044	0.98411

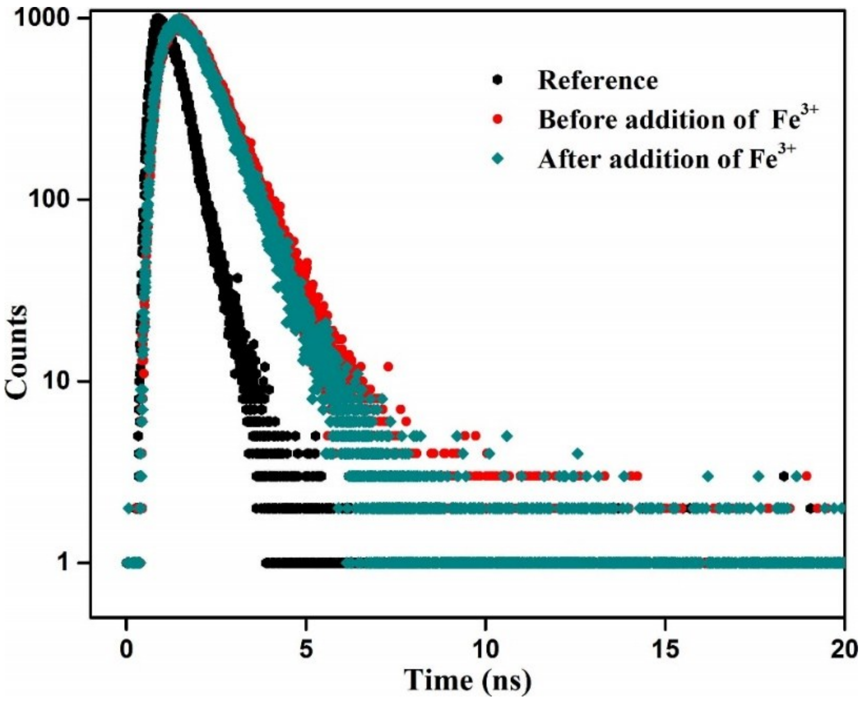

Figure S94. Lifetime decay profile of **1′** before and after addition of 200 µL of 10 mM Fe^{3+} solution in water.

Table S8. Average excited state lifetime (<τ>) values of **1'** before and after addition of 200 µL of 10 mM Fe^{3+} solution (λ_{ex} = 295 nm).

Volume Added (µL)	B_1	B_2	a_1	a_2	τ_1 (ns)	τ_1 (ns)	<τ>* (ns)	χ^2
0	0.006	0.006	32.61	62.39	0.48	0.92	0.78	1.00
200	0.008	0.004	54.66	45.34	0.53	0.93	0.71	1.01

* $<\tau> = a_1\tau_1 + a_2\tau_2$

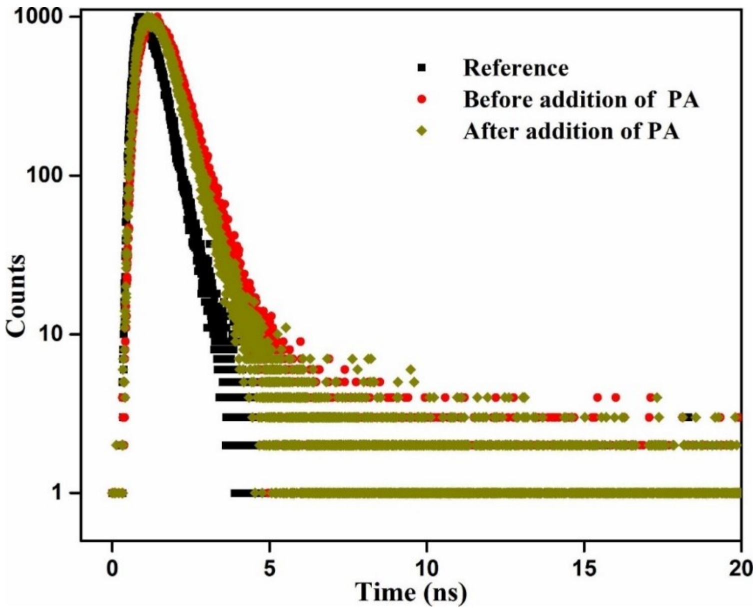

Figure S95. Lifetime decay profile of **1′** before and after addition of 200 μL of 10 mM PA in DMSO.

Table S9. Average excited state lifetime (<τ>) values of **1'** before and after addition of 200 μL of 10 mM PA solution in DMSO (λ_{ex} = 295 nm).

Volume Added (μL)	B_1	B_2	a_1	a_2	τ_1 (ns)	τ_1 (ns)	<τ>* (ns)	χ^2
0	0.016	0.001	88.52	11.48	0.36	1.06	0.44	1.01
200	0.021	0.001	99.90	9.91	0.28	1.10	0.38	1.03

* $\langle\tau\rangle = a_1\tau_1 + a_2\tau_2$

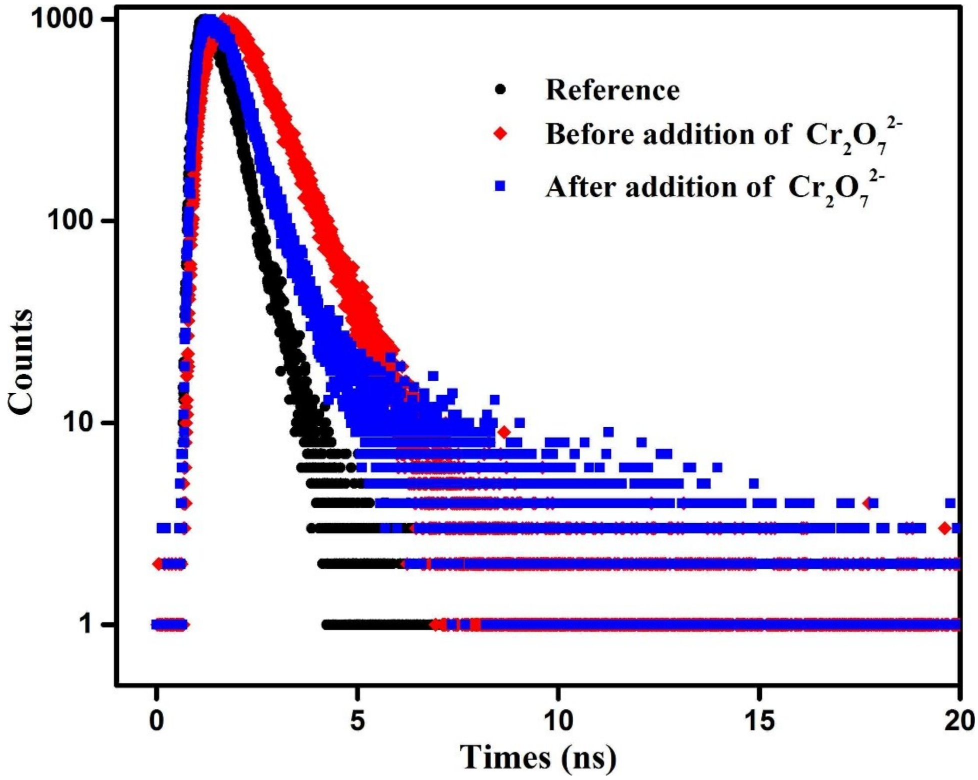

Figure S96. Lifetime decay profile of **1′** before and after addition of 150 μL of 3 mM $Cr_2O_7^{2-}$ solution in water.

Table S10. Average excited state lifetime (<τ>) values of **1'** before and after addition of 150 μL of 3 mM $Cr_2O_7^{2-}$ solution (λ_{ex} = 295 nm).

Volume Added (μL)	B_1	B_2	a_1	a_2	τ_1 (ns)	τ_1 (ns)	<τ>* (ns)	χ^2
0	0.012	0.001	90.32	9.67	0.69	1.40	0.76	1.01
150	0.020	0.001	92.13	7.66	0.35	2.73	0.53	1.01

* $<\tau> = a_1\tau_1 + a_2\tau_2$

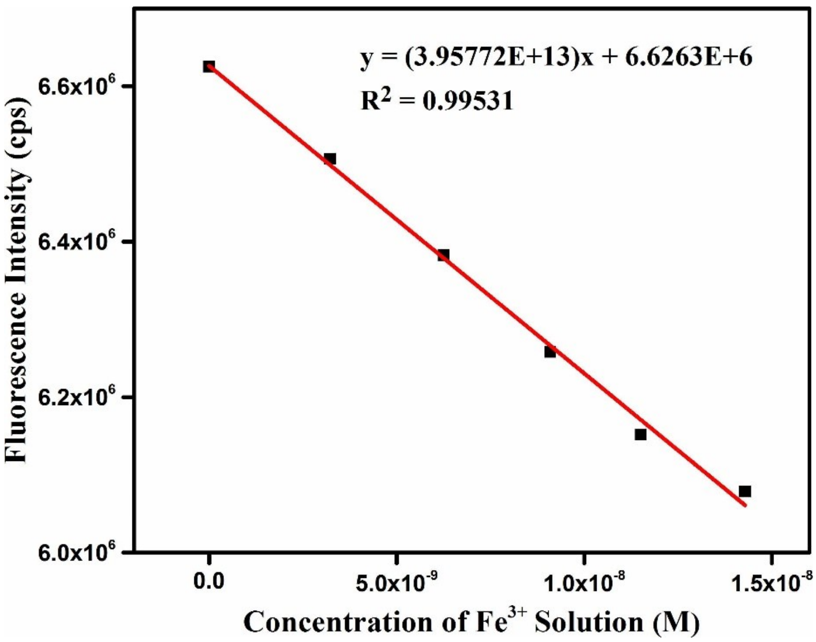

Figure S97. Change of fluorescence intensity of aqueous suspension of **1'** as a function of concentration of added Fe^{3+} solution in water.

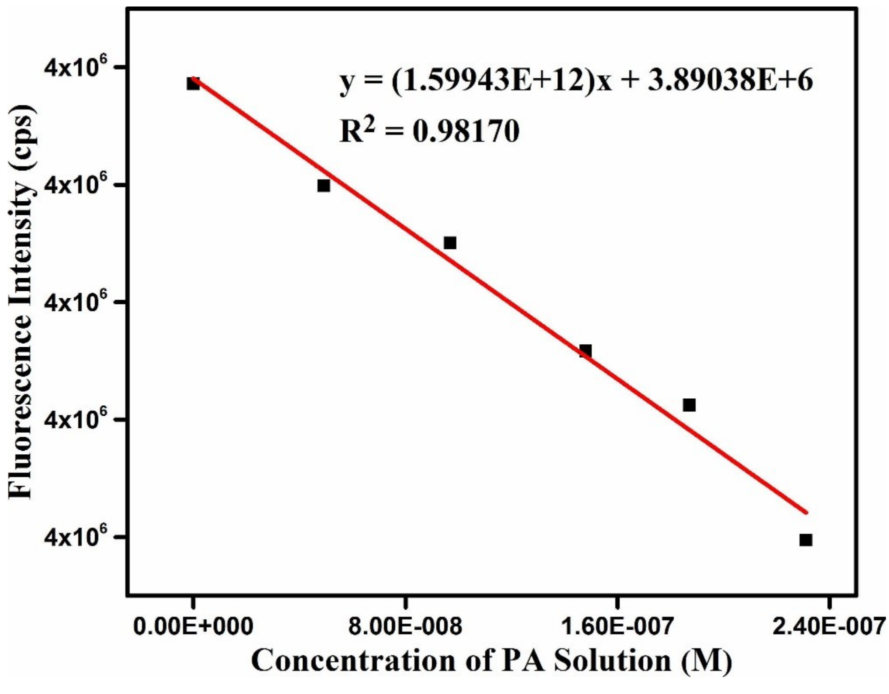

Figure S98. Change of fluorescence intensity of **1'** suspension in DMSO as a function of concentration of added PA solution in DMSO.

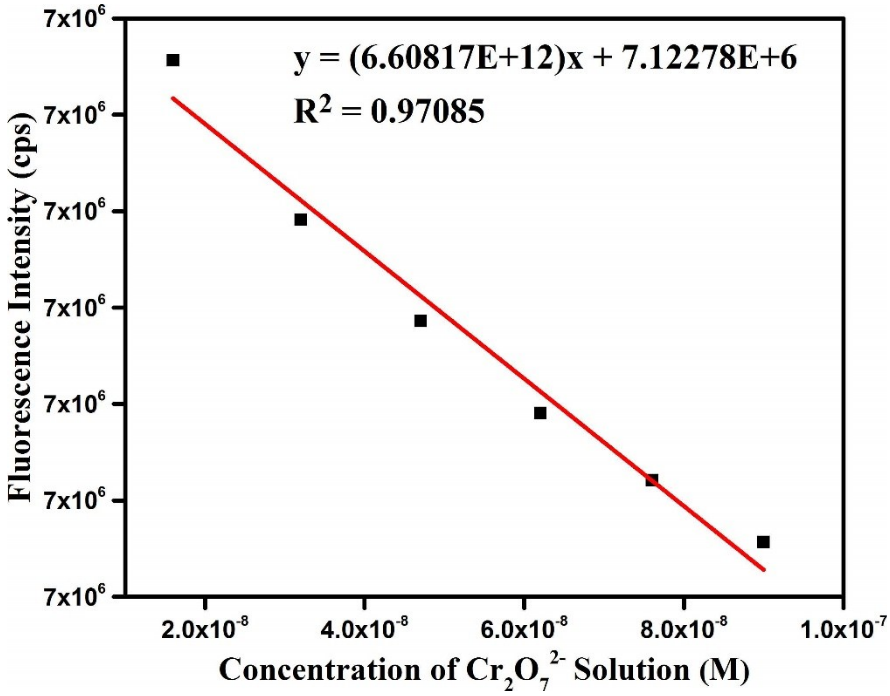

Figure S99. Change of fluorescence intensity of aqueous suspension of **1'** as a function of concentration of added $Cr_2O_7^{2-}$ solution in water.

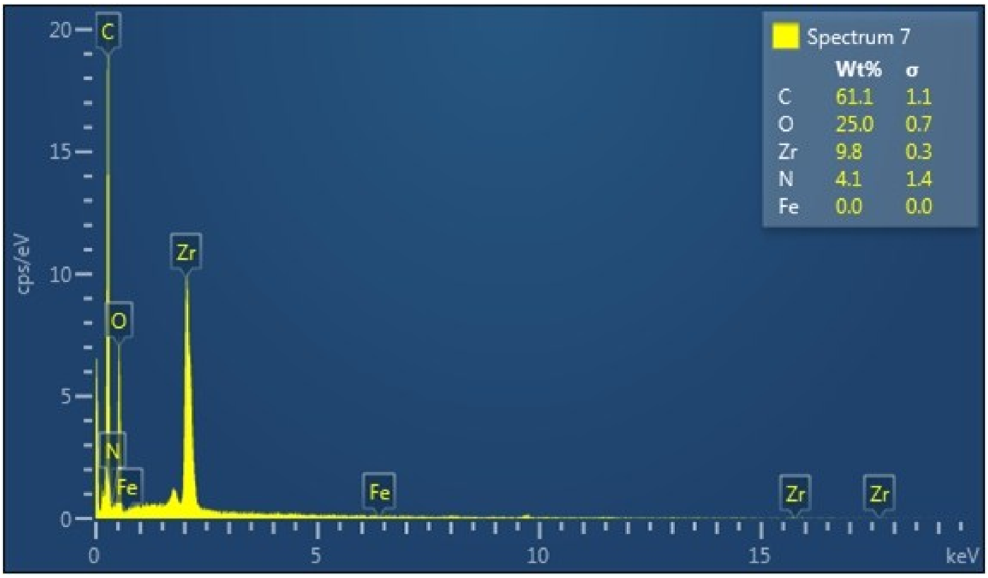

Figure S100. EDX analysis of **1′** after treatment of 10 mM Fe^{3+} aqueous solution.

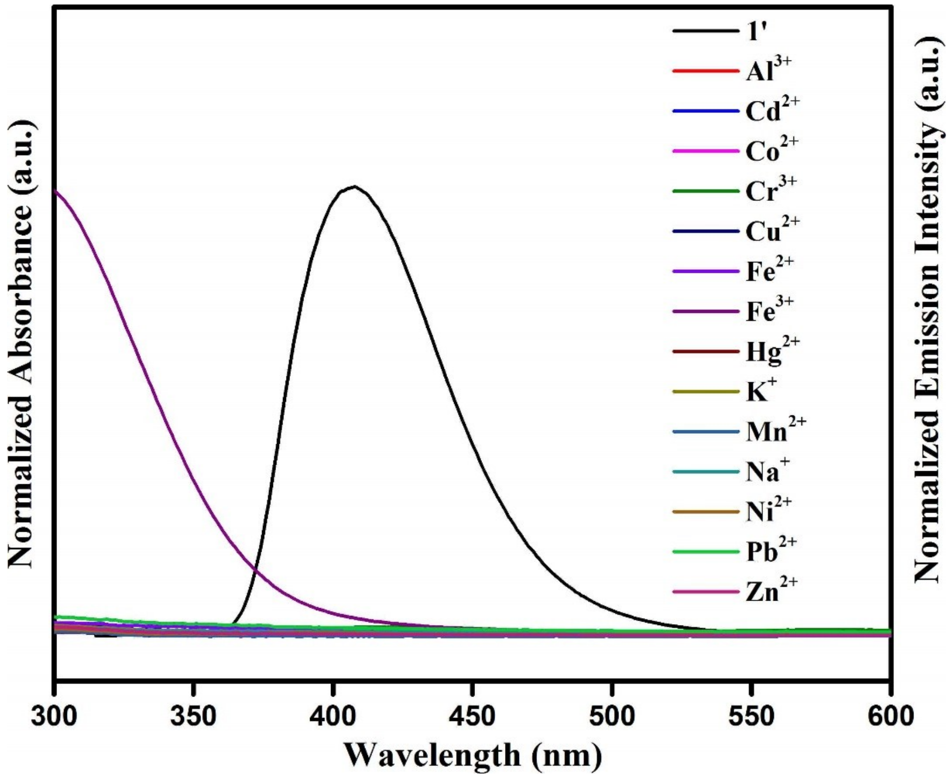

Figure S101. UV-Vis absorption spectra of the aqueous solutions containing different metal ions (10×10^{-3} M). The emission spectrum of **1'** (pink curve) (3 mg) dispersed in water (3 mL).

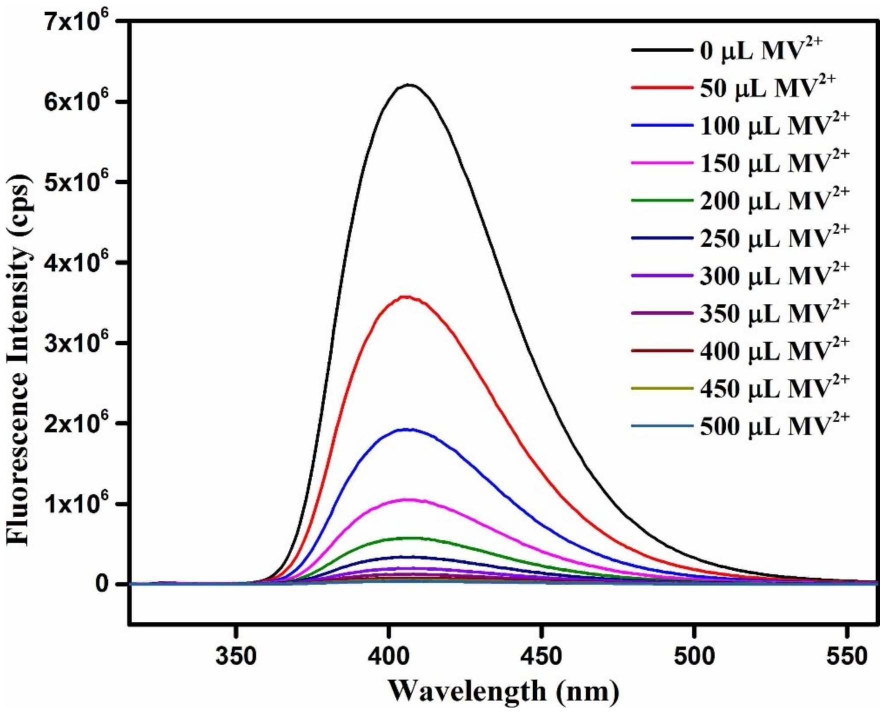

Figure S102. Quenching of the fluorescence intensity of **1′** with incremental addition of 10 mM MV^{2+} solution to a 3 mL stable aqueous suspension of **1′**.

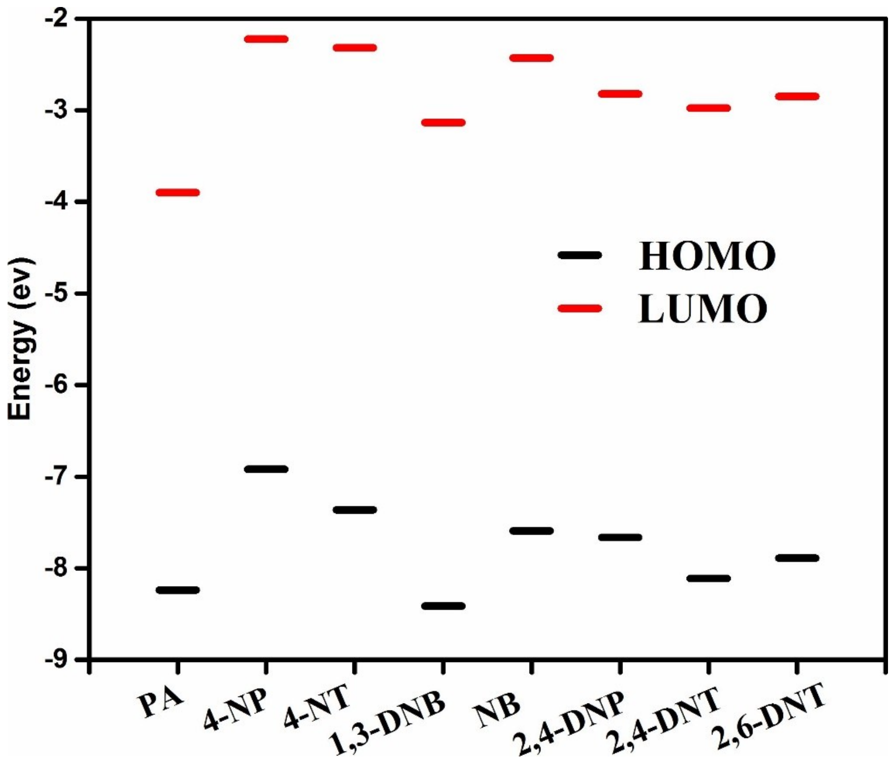

Figure S103. HOMO and LUMO energies of the selective NAEs.

Table S11. HOMO and LUMO energy levels of selected analytes calculated by density functional theory (DFT) at B3LYP/6-31G* accuracy level using Gaussian 09 package of program.[67]

Analyte	HOMO (eV)	LUMO (eV)	Band Gap (eV)
PA	-8.2374	-3.898	4.3394
4-NP	-6.9207	-2.2213	4.6994
2,4-DNP	-7.6644	-2.8202	4.8442
NB	-7.5917	-2.4294	5.1623
4-NT	-7.3626	-2.3171	5.0454
1,3-DNB	-8.4129	-3.1350	5.2779
2,6-DNT	-7.8913	-2.8501	5.0412
2,4-DNT	-8.1131	-2.9769	5.1362

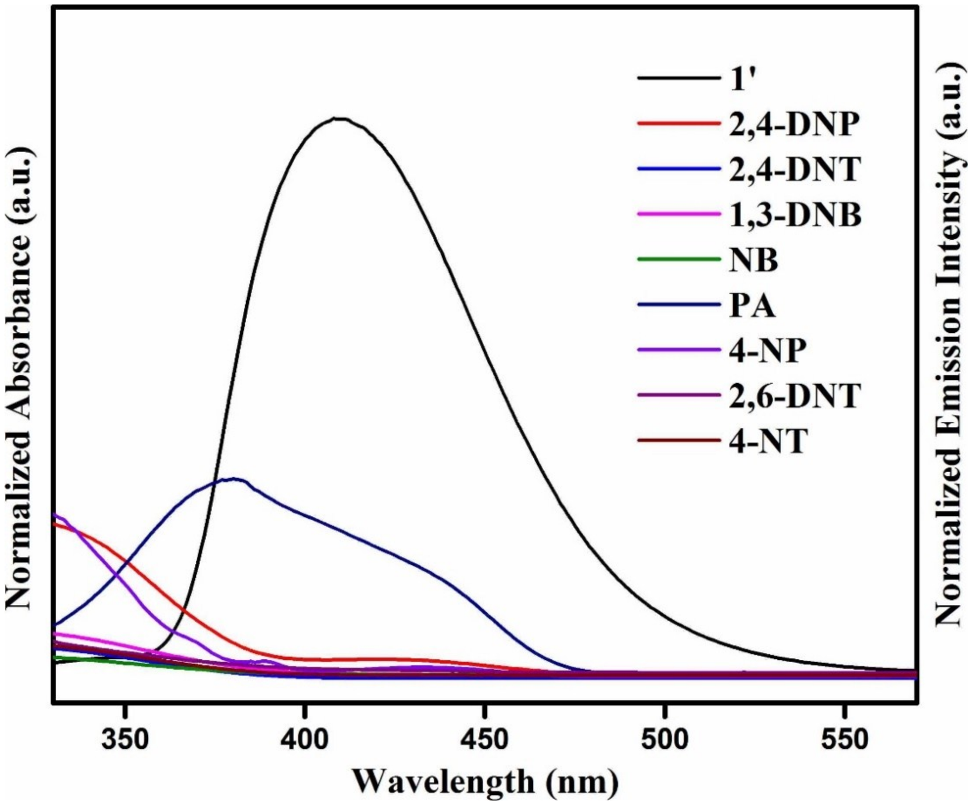

Figure S104. UV-Vis absorption spectra of the NAEs in DMSO (3×10^{-3} M). The emission spectrum of **1'** (black curve) (3 mg) dispersed in DMSO (3 mL).

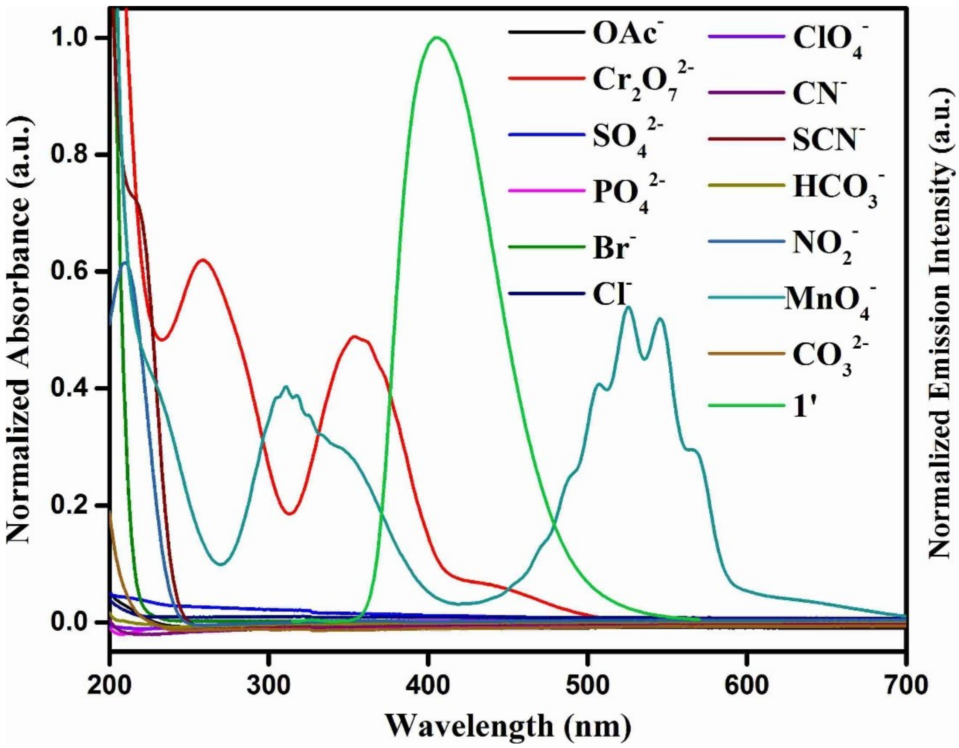

Figure S105. UV-Vis absorption spectra of the aqueous solutions (3×10^{-3} M) containing different metal anions. The emission spectrum of **1'** (green curve) (3 mg) dispersed in water (3 mL).

Calculated Crystallographic Information File (CIF) for compound 1.

```
data_compound 1

_audit_creation_method            'Materials Studio'
_symmetry_space_group_name_H-M    'CMMM'
_symmetry_Int_Tables_number       65
_symmetry_cell_setting            orthorhombic
loop_
_symmetry_equiv_pos_as_xyz
  x,y,z
  -x,-y,z
  -x,y,-z
  x,-y,-z
  -x,-y,-z
  x,y,-z
  x,-y,z
  -x,y,z
  x+1/2,y+1/2,z
  -x+1/2,-y+1/2,z
  -x+1/2,y+1/2,-z
  x+1/2,-y+1/2,-z
  -x+1/2,-y+1/2,-z
  x+1/2,y+1/2,-z
  x+1/2,-y+1/2,z
  -x+1/2,y+1/2,z
_cell_length_a                    19.4920
_cell_length_b                    33.4890
_cell_length_c                    12.6080
_cell_angle_alpha                 90.0000
_cell_angle_beta                  90.0000
_cell_angle_gamma                 90.0000
loop_
_atom_site_label
_atom_site_type_symbol
_atom_site_fract_x
_atom_site_fract_y
_atom_site_fract_z
_atom_site_U_iso_or_equiv
_atom_site_adp_type
_atom_site_occupancy
Zr1    Zr   -0.09026   0.00000    0.12976   0.10132  Uiso   1.00
Zr2    Zr    0.00000  -0.07076    0.00000   0.10132  Uiso   1.00
O1     O     0.00000  -0.03598    0.14402   0.10132  Uiso   1.00
O2     O    -0.09777  -0.04057    0.00000   0.10132  Uiso   1.00
O3     O    -0.19988   0.00000    0.16079   0.10132  Uiso   1.00
O4     O    -0.06992  -0.00000   0.29906   0.10132  Uiso   1.00
O5     O    -0.06274  -0.10550    0.10695   0.10132  Uiso   1.00
O6     O    -0.12725  -0.05748   0.18972   0.10132  Uiso   1.00
C1     C    -0.10823  -0.09418   0.17507   0.10132  Uiso   1.00
C2     C    -0.13960  -0.12564   0.24312   0.10132  Uiso   1.00
C3     C    -0.19932  -0.11810   0.30267   0.10132  Uiso   1.00
C4     C    -0.22714  -0.14769   0.36870   0.10132  Uiso   1.00
C5     C    -0.19466  -0.18491   0.37919   0.10132  Uiso   1.00
C6     C    -0.13569  -0.19267   0.31903   0.10132  Uiso   1.00
C7     C    -0.10852  -0.16347   0.25170   0.10132  Uiso   1.00
```

C8	C	-0.22506	-0.21734	0.44392	0.10132	Uiso	1.00
N1	N	-0.25000	-0.25000	0.39241	0.10132	Uiso	1.00

References:

1. Jiang, Y.; Sun, L.; Du, J.; Liu, Y.; Shi, H.; Liang, Z.; Li, J. Multifunctional zinc metal−organic framework based on designed H_4TCPP ligand with aggregation-induced emission effect: CO_2 adsorption, luminescence, and sensing property. *Cryst. Growth Des.* **2017,** 17, 2090−2096.
2. Xu, X.-Y.; Yan, B. Eu(III)-Functionalized MIL-124 as Fluorescent Probe for Highly Selectively Sensing Ions and Organic Small Molecules Especially for Fe(III) and Fe(II). *ACS Appl. Mater. Interfaces* **2015,** 7, 721-729.
3. Gogoi, C.; Yousufuddin, M.; Biswas, S. A new 3D luminescent Zn(II)–organic framework containing a quinoline-2,6-dicarboxylate linker for the highly selective sensing of Fe(III) ions. *Dalton Trans.* **2019,** 48, 1766-1773.
4. Zhao, X.-L.; Tian, D.; Gao, Q.; Sun, H.-W.; Xu, J.; X.-H. Bu. A chiral lanthanide metal–organic framework for selective sensing of Fe(III) ions. *Dalton Trans.* **2016,** 45, 1040-1046.
5. Ma, A.; Wu, J.; Han, Y.; Chen, F.; Li, B.; Cai, S.; Huang, H.; Singh, A.; Kumar, A.; Liu, J. Rational synthesis of a luminescent uncommon (3,4,6)-c connected Zn(II) MOF: a dual channel sensor for the detection of nitroaromatics and ferric ions. *Dalton Trans.* **2018,** 47, 9627–9633.
6. Zhang, C.; Yan, Y.; Pan, Q.; Sun, L.; He, H.; Liu, Y.; Liang, Z.; Li, J. A microporous lanthanum metal–organic framework as a bi-functional chemosensor for the detection of picric acid and Fe3+ ions. *Dalton Trans.* **2015,** 44, 13340-13346.
7. Li, Y.-F.; Wang, D.; Liao, Z.; Kang, Y.; Ding, W.-H.; Zheng, X.-J.; Jin, L.-P. Luminescence tuning of the Dy–Zn metal–organic framework and its application in the detection of Fe(III) ions. *J. Mater. Chem. C* **2016,** 4, 4211-4217.
8. Das, A.; Biswas, S. A multi-responsive carbazole-functionalized Zr(IV)-based metal-organic framework for selective sensing of Fe(III), cyanide and p-nitrophenol. *Sens. Actuator B-Chem.* **2017,** 250, 121-131.
9. Gogoi, C.; Biswas, S. A new quinoline based luminescent Zr(IV) metal–organic framework for the ultrasensitive recognition of 4-nitrophenol and Fe(III) ions. *Dalton Trans.* **2018,** 48, 14696-14705.
10. Das, A.; Banesh, S.; Trivedi, V.; Biswas, S. Extraordinary sensitivity for H_2S and Fe(III) sensing in aqueous medium by Al-MIL-53-N_3 metal–organic framework: in vitro and in vivo applications of H_2S sensing. *Dalton Trans.* **2018,** 47, 2690–2700.
11. Zhang, J.; Zhao, L.; Liu, Y.; Li, M.; Li, G.; Meng, X. Two luminescent transition-metal–organic frameworks with a predesigned ligand as highly sensitive and selective iron(III) sensors. *New J.Chem.* **2018,** 42, 6839-6847.
12. Zheng, M.; Tan, H.; Xie, Z.; Zhang, L.; Jing, X.; Sun, Z. Fast response and high sensitivity europium metal organic framework fluorescent probe with chelating terpyridine sites for Fe^{3+}. *ACS Appl. Mater. Interfaces* **2013,** 5, 1078–1083.
13. Zhou, X.-H.; Li, L.; Li, H.-H.; Li, A.; Yanga, T.; Huang, W. A flexible Eu(III)-based metal–organic framework: turn-off luminescent sensor for the detection of Fe(III) and picric acid. *Dalton Trans.* **2013,** 42, 12403-12409.
14. Wu, Y.; Yang, G.-P.; Zhang, Y.; Shi, N.; Han, J.; Wang, Y.-Y. A new luminescent Cd(II)-MOF as a highly selective chemical probe for Fe^{3+} in aqueous solution with mixed metal ions. *RSC Adv.* **2015,** 5, 90772-90777.

15. Wang, K.-M.; Du, L.; Ma, Y.-L.; Zhao, J.-S.; Wang, Q.; Yan, T.; Zhao, Q.-H. Multifunctional chemical sensors and luminescent thermometers based on lanthanide metal–organic framework materials. *CrystEngComm* **2016,** 18, 2690-2700.
16. Xu, H.; Hu, H.-C.; Cao, C.-S.; Zhao, B. Lanthanide organic framework as a regenerable luminescent probe for Fe^{3+}. *Inorg. Chem.* **2015,** 54, 4585-4587.
17. Dong, X.-Y.; Wang, R.; Wang, J.-Z.; Wang, S.-Q.; Mak, T. C. W. Highly selective Fe^{3+} sensing and proton conduction in a water-stable sulfonate–carboxylate Tb–organic-framework. *J. Mater. Chem. A* **2015,** 3, 641–647.
18. Li, G.-P.; Liu, G.; Li, Y.-Z.; Hou, L.; Wang, Y.-Y.; Zhu, Z. Uncommon pyrazoyl-carboxyl bifunctional ligand-based microporous lanthanide systems: sorption and luminescent sensing properties. *Inorg. Chem.* **2016,** 55, 3952-3959.
19. Chen, C.-H.; Wang, X.-S.; Li, L.; Huang, Y.-B.; Cao, R. Highly selective sensing of Fe3+ by an anionic metal–organic framework containing uncoordinated nitrogen and carboxylate oxygen sites. *Dalton Trans.* **2018,** 47, 3452–3458.
20. Rao, P. C.; Mandal, S. Europium-based metal−organic framework as a dual luminescence sensor for the selective detection of the phosphate anion and Fe^{3+} ion in aqueous media. *Inorg. Chem.* **2018,** 57, 11855-11858.
21. Zhou, L.; Zhao, K.; Hu, Y.-J.; Feng, X.-C.; Shi, P.-D.; Zheng, H.-G. A bifunctional photoluminescent metal-organic framework for detection of Fe^{3+} ion and nitroaromatics. *Inorg. Chem. Commun.* **2018,** 89, 68-72.
22. Das, P.; Mandal, S. K. Strategic design and functionalization of an amine-decorated luminescent metal organic framework for selective gas/vapor sorption and nanomolar sensing of 2,4,6-trinitrophenol in water. *ACS Appl. Mater. Interfaces* **2018,** 10, 25360−25371.
23. Xia, T.; Zhu, F.; Cui, Y.; Yang, Y.; Wang, Z.; Qian, G. Highly selective luminescent sensing of picric acid based on a water-stable europium metal-organic framework. *J. Solid State Chem.* **2017,** 245, 127–131.
24. Wang, D.; Hu, Z.; Xu, S.; Li, D.; Zhang, Q.; Ma, W.; Zhou, H.; Wu, J.; Tian, Y. Fluorescent metal–organic frameworks based on mixed organic ligands: new candidates for highly sensitive detection of TNP. *Dalton Trans.* **2019,** 48, 1900–1905.
25. SK, M.; Biswas, S. A thiadiazole-functionalized Zr(IV)-based metal–organic framework as a highly fluorescent probe for the selective detection of picric acid. *CrystEngComm* **2016,** 18, 3104-3113.
26. Buragohain, A.; Yousufuddin, M.; Sarma, M.; Biswas, S. 3D luminescent amide-functionalized cadmium tetrazolate framework for selective detection of 2,4,6-trinitrophenol. *Cryst. Growth Des.* **2016,** 16, 842−851.
27. Xiao, J.-D.; Qiu, L.-G.; Ke, F.; Yuan, Y.-P.; Xu, G.-S.; Wang, Y.-M.; Jiang, X. Rapid synthesis of nanoscale terbium-based metal–organic frameworks by a combined ultrasound-vapour phase diffusion method for highly selective sensing of picric acid. *J. Mater. Chem. A* **2013,** 1, 8745-8752.
28. Nagarkar, S. S.; Desai, A. V.; Ghosh, S. K. A fluorescent metal–organic framework for highly selective detection of nitro explosives in the aqueous phase. *Chem. Commun.* **2014,** 50, 8915-8918.
29. Nagarkar, S. S.; Joarder, B.; Chaudhari, A. K.; Mukherjee, S.; Ghosh, S. K. Highly selective detection of nitro explosives by a luminescent metal–organic framework. *Angew. Chem. Int. Ed* **2013,** 52, 2881–2885.
30. Santra, A.; Francis, M.; Parshamoni, S.; Konar, S. Nanoporous Cu(I) metal–organic framework: selective adsorption of benzene and luminescence sensing of nitroaromatics. *ChemistrySelect* **2017,** 2, 3200-3206.

31. Wang, B.; Lv, X.-L.; Feng, D.; Xie, L.-H.; Zhang, J.; Li, M.; Xie, Y.; Li, J.-R.; Zhou, H.-C. Highly stable Zr(IV)-based metal-organic frameworks for the detection and removal of antibiotics and organic explosives in water. *J. Am. Chem. Soc.* **2016,** 138, 6204-6216.
32. Asha, K. S.; Bhattacharyya, K.; Mandal, S. Discriminative detection of nitro aromatic explosives by a luminescent metal–organic framework. *J. Mater. Chem. C* **2014,** 2, 10073-10081.
33. Joarder, B.; Desai, A. V.; Samanta, P.; Mukherjee, S.; Ghosh, S. K. Selective and sensitive aqueous-phase detection of 2,4,6-trinitrophenol (TNP) by an amine-functionalized metal–organic framework. *J. Mater. Chem. C* **2014,** 2, 10073-10081.
34. Nagarkar, S. S.; Desai, A. V.; Samanta, P.; Ghosh, S. K. Aqueous phase selective detection of 2,4,6-trinitrophenol using a fluorescent metal–organic framework with a pendant recognition site. *Dalton Trans.* **2015,** 44, 15175-15180.
35. Zhang, C.; Sun, L.; Yan, Y.; Li, J.; Song, X.; Liu, Y.; Liang, Z. A luminescent cadmium metal–organic framework for sensing of nitroaromatic explosives. *Dalton Trans.* **2015,** 44, 230-236.
36. Shi, Z.-Q.; Guo, Z.-J.; Zheng, H.-G. Two luminescent Zn(II) metal–organic frameworks for exceptionally selective detection of picric acid explosives. *Chem. Commun.* **2015,** 51, 8300-8303.
37. Shanmugaraju, S.; Dabadie, C.; Byrne, K.; Savyasachi, A. J.; Umadevi, D.; Schmitt, W.; Kitchen, J. A.; Gunnlaugsson, T. A supramolecular Troger's base derived coordination zinc polymer for fluorescent sensing of phenolic-nitroaromatic explosives in wate. *Chem. Sci.* **2017,** 8, 1535-1546.
38. He, H.; Chen, S.-H.; Zhang, D.-Y.; Yang, E.-C.; Zhao, X.-J. A luminescent metal–organic framework as an ideal chemosensor for nitroaromatic compounds. *RSC Adv.* **2017,** 7, 38871-38876.
39. Sanda, S.; Parshamoni, S.; Biswas, S.; Konar, S. Highly selective detection of palladium and picric acid by a luminescent MOF: a dual functional fluorescent sensor. *Chem. Commun.* **2015,** 51, 6576-6579.
40. Ghosh, P.; Saha, S. K.; Roychowdhury, A.; Banerjee, P. Recognition of an explosive and mutagenic water pollutant, 2,4,6-Trinitrophenol, by cost-effective luminescent MOFs. *Eur. J. Inorg. Chem.* **2015**.
41. Mukherjee, S.; Desai, A. V.; Manna, B.; Inamdar, A. I.; Ghosh, S. K. Exploitation of guest accessible aliphatic amine functionality of a metal−organic framework for selective detection of 2,4,6-trinitrophenol (TNP) in water. *Cryst. Growth Des.* **2015,** 15, 4627-4634.
42. Das, P.; Mandal, S. K. Understanding the effect of an amino group on the selective and ultrafast detection of TNP in water using fluorescent organic probes. *J. Mater. Chem. C* **2018,** 6, 3288-3297.
43. Liu, J.; Ye, Y.; Sun, X.; Liu, B.; Li, G.; Liang, Z.; Liu, Y. A multifunctional Zr(IV)-based metal–organic framework for highly efficient elimination of Cr(VI) from the aqueous phase. *J. Mater. Chem. A* **2019,** 7, 16833-16841.
44. Sun, X.; Yao, S.; Yu, C.; Li, G.; Liu, C.; Huo, Q.; Liu, Y. An ultrastable Zr-MOF for fast capture and highly luminescence detection of $Cr_2O_7^{2-}$ simultaneously in an aqueous phase. *J. Mater. Chem. A* **2018,** 6, 6363-6369.
45. Lu, B.-B.; Jiang, W.; Yang, J.; Liu, Y.-Y.; Ma, J.-F. Resorcin[4]arene-based microporous metal-organic framework as an efficient catalyst for CO_2 cycloaddition with epoxides and highly selective luminescent sensing of $Cr_2O_7^{2-}$. *ACS Appl. Mater. Interfaces* **2017,** 9, 39441-39449.
46. Yao, Z.-Q.; Li, G.-Y.; Xu, J.; Hu, T.-L.; Bu, X.-H. A water-stable luminescent Zn^{II} metal-organic framework as chemosensor for high-efficiency detection of Cr^{VI}-anions ($Cr_2O_7^{2-}$ and CrO_4^{2-}) in aqueous solution. *Chem. Eur. J.* **2018,** 24, 3192-3198.

47. Fu, H.-R.; Zhao, Y.; Zhou, Z.; Yang, X.-G.; Ma, L.-F. Neutral ligand TIPA-based two 2D metal–organic frameworks: ultrahigh selectivity of C_2H_2/CH_4 and efficient sensing and sorption of Cr(VI). *Dalton Trans.* **2018,** 47, 3725-3732.
48. Zhao, Y.; Xu, X.; Qiu, L.; Kang, X.; Wen, L.; Zhang, B. Metal-organic frameworks constructed from a new thiophene functionalized dicarboxylate: luminescence sensing and pesticide removal. *ACS Appl. Mater. Interfaces* **2017,** 9, 15164-15175.
49. Lv, R.; Li, H.; Su, J.; Fu, X.; Yang, B.; Gu, W.; Liu, X. Zinc metal-organic framework for selective detection and differentiation of Fe(III) and Cr(VI) ions in aqueous solution. *Inorg. Chem.* **2017,** 56, 12348-12356.
50. Xu, M.-M.; Kong, X.-J.; He, T.; Wu, X.-Q.; Xie, L.-H.; Li, J.-R. A stable Zr(IV)-based metal-organic framework constructed from C=C bridged di-isophthalate ligand for sensitive detection of $Cr_2O_7^{2-}$ in water. *Inorg. Chem.* **2018,** 57, 14260-14268.
51. Chen, M.; Xu, W.-M.; Tian, J.-Y.; Cui, H.; Zhang, J.-X.; Liu, C.-S.; Du, M. A terbium(III) lanthanide–organic framework as a platform for a recyclable multi-responsive luminescent sensor. *J. Mater. Chem. C* **2017,** 5, 2015-2021.
52. Zhang, C.; Sun, L.; Yan, Y.; Shi, H.; Wang, B.; Liang, Z.; Li, J. A novel photo- and hydrochromic europium metal–organic framework with good anion sensing properties. *J. Mater. Chem. C* **2017,** 5, 8999-9004.
53. Gu, T.-Y.; Dai, M.; Young, D. J.; Ren, Z.-G.; Lang, J.-P. Luminescent Zn(ii) coordination polymers for highly selective sensing of Cr(III) and Cr(VI) in water. *Inorg. Chem.* **2017,** 56, 4668-4678.
54. Rapti, S.; Sarma, D.; Diamantis, S. A.; Skliri, E.; Armatas, G. S.; Tsipis, A. C.; Hassan, Y. S.; Alkordi, M.; Malliakas, C. D.; Kanatzidis, M. G.; Lazarides, T.; Plakatouras, J. C.; Manos, M. J. All in one porous material: exceptional sorption and selective sensing of hexavalent chromium by using a Zr^{4+} MOF. *J. Mater. Chem. A* **2017,** 5, 14707-14719.
55. Guo, X.-Y.; Zhao, F.; Liu, J.-J.; Liu, Z.-L.; Wang, Y.-Q. An ultrastable zinc(II)–organic framework as a recyclable multi-responsive luminescent sensor for Cr(III), Cr(VI) and 4-nitrophenol in the aqueous phase with high selectivity and sensitivity. *J. Mater. Chem. A* **2017,** 5, 20035-20043.
56. Chen, Z. W.; Mi, X. N.; Wang, S. N.; Lu, J.; Li, Y. W.; Li, D. C.; Dou, J. M. Two novel penetrating coordination polymers based on flexible S-containing dicarboxylate acid with sensing properties towards Fe^{3+} and Cr^2O^{72-} ions. *J. Solid State Chem.* **2018,** 261, 75-85.
57. Sun, Z.; Yang, M.; Ma, Y.; Li, L. C. Multi-responsive luminescent sensors based on two-dimensional lanthanide-metal organic frameworks for highly selective and sensitive detection of Cr(III) and Cr(VI) ions and benzaldehyde. *Cryst. Growth Des.* **2017,** 17, 4326-4335.
58. Gai, Y.-L.; Guo, Q.; Zhao, X.-Y.; Chen, Y.; Liu, S.; Zhang, Y.; Zhuo, C.-X.; Yao, C.; Xiong, K.-C. Extremely stable europium-organic framework for luminescent sensing of $Cr_2O_7^{2-}$ and Fe^{3+} in aqueous systems. *Dalton Trans.* **2018,** 47, 12051-12055.
59. Hao, J.-N.; Yan, B. Ln^{3+} post-functionalized metal–organic frameworks for color tunable emission and highly sensitive sensing of toxic anions and small molecules. *New J. Chem.* **2016,** 40, 4654-4661.
60. Wu, X.-X.; Fu, H.-R.; Han, M.-L.; Zhou, Z.; Ma, L.-F. Tetraphenylethylene immobilized metal-organic frameworks: highly sensitive fluorescent sensor for the detection of $Cr_2O_7^{2-}$ and nitroaromatic explosives. *Cryst.Growth Des* **2017,** 17, 6041-6048.
61. Wen, G.-X.; Han, M.-L.; Wu, X.-Q.; Wu, Y.-P.; Dong, W.-W.; Zhao, J.; Li, D.-S.; Ma, L.-F. A multi-responsive luminescent sensor based on a super-stable sandwich-type terbium(III)–organic framework. *Dalton Trans.* **2016,** 45, 15492-15499.
62. Song, T.-Q.; Dong, J.; Gao, H.-L.; Cui, J.-Z.; Zhao, B. A unique zinc-organic framework constructed through in situ ligand synthesis for conversion of CO_2 under mild

conditions and as a luminescence sensor for $Cr_2O_7^{2-}$/CrO_4^{2-}. *Dalton Trans.* **2017,** 46, 13862-13868.
63. Cao, C.-S.; Hu, H.-C.; Xu, H.; Qiao, W.-Z.; Zhao, B. Two solvent-stable MOFs as a recyclable luminescent probe for detecting dichromate or chromate anions. *CrystEngComm* **2016,** 18, 4445-4451.
64. Liu, L.-H.; Qiu, X.-T.; Wang, Y.-J.; Shi, Q.; Sun, Y.-Q.; Chen, Y.-P. NIR emission and luminescent sensing of a lanthanide–organic framework with Lewis basic imidazole and pyridyl sites. *Dalton Trans.* **2017,** 46, 12106-12113.
65. He, H. M.; Chen, S.-H.; Zhang, D.-Y.; Hao, R.; Zhang, C.; Yang, E.-C.; Zhao, X.-J. A micrometer-sized europium(III)–organic framework for selective sensing of the $Cr_2O_7^{2-}$ anion and picric acid in water systems. *Dalton Trans.* **2017,** 46, 13502-13509.
66. He, T.; Zhang, Y.-Z.; Kong, X.-J.; Yu, J. M.; Lv, X.-L.; Wu, Y. F.; Guo, Z.-J.; Li, J.-R. Zr(IV)-based metal-organic framework with T-shaped ligand: unique structure, high stability, selective detection, and rapid adsorption of $Cr_2O_7^{2-}$ in water. *ACS Appl. Mater. Interfaces* **2018,** 10, 16650-16659.
67. Frisch, M. J.; Trucks, G. W.; Schlegel, H. B.; Scuseria, G. E.; Robb, M. A.; Cheeseman, J. R.; Scalmani, G.; Barone, V.; Mennucci, B.; Petersson, G. A.; Nakatsuji, H.; Caricato, M.; Li, X.; Hratchian, H. P.; Izmaylov, A. F.; Bloino, J.; Zheng, G.; Sonnenberg, J. L.; Hada, M.; Ehara, M.; Toyota, K.; Fukuda, R.; Hasegawa, J.; Ishida, M.; Nakajima, T.; Honda, Y.; Kitao, O.; Nakai, H.; Vreven, T.; Montgomery, J. A.; Peralta, J. E.; Ogliaro, F.; Bearpark, M.; Heyd, J. J.; Brothers, E.; Kudin, K. N.; Staroverov, V. N.; Kobayashi, R.; Normand, J.; Raghavachari, K.; Rendell, A.; Burant, J. C.; Iyengar, S. S.; Tomasi, J.; Cossi, M.; Rega, N.; Millam, J. M.; Klene, M.; Knox, J. E.; Cross, J. B.; Bakken, V.; Adamo, C.; Jaramillo, J.; Gomperts, R.; Stratmann, R. E.; Yazyev, O.; Austin, A. J.; Cammi, R.; Pomelli, C.; Ochterski, J. W.; Martin, R. L.; Morokuma, K.; Zakrzewski, V. G.; Voth, G. A.; Salvador, P.; Dannenberg, J. J.; Dapprich, S.; Daniels, A. D.; Farkas, O.; Foresman, J. B.; Ortiz, J. V.; Cioslowski, J.; Fox, D. J. *Gaussian 09, Gaussian, Inc., Wallingford CT* **2009**.